CIVIL ENGINEERING STUDIES
Illinois Center for Transportation Series No. 16-023
UILU-ENG-2016-2023
ISSN: 0197-9191

IMPROVING THE EFFECTIVENESS OF SMART WORK ZONE TECHNOLOGIES

Prepared By
Yanning Li
Juan Carlos Martinez Mori
Daniel Work
University of Illinois at Urbana-Champaign

Research Report No. FHWA-ICT-16-021

A report of the findings of

ICT PROJECT R27-155
Improving the Effectiveness of Smart Work Zone Technologies

Illinois Center for Transportation

November 2016

ILLINOIS CENTER FOR TRANSPORTATION

TECHNICAL REPORT DOCUMENTATION PAGE

1. Report No. FHWA-ICT-16-021	**2. Government Accession No.** N/A	**3. Recipient's Catalog No.** N/A
4. Title and Subtitle Improving the Effectiveness of Smart Work Zone Technologies		**5. Report Date** November 2016 **6. Performing Organization Code** N/A
7. Author(s) Yanning Li, Juan Carlos Martinez Mori, and Daniel B. Work		**8. Performing Organization Report No.** ICT-16-023 UILU-ENG-2016-2023
9. Performing Organization Name and Address Illinois Center for Transportation Department of Civil and Environmental Engineering University of Illinois at Urbana-Champaign 205 North Mathews Avenue, MC-250 Urbana, IL 61801		**10. Work Unit No.** N/A **11. Contract or Grant No.** R27-155
12. Sponsoring Agency Name and Address Illinois Department of Transportation (SPR) Bureau of Material and Physical Research 126 East Ash Street Springfield, IL 62704		**13. Type of Report and Period Covered** Final report, October 15, 2014, through November 30, 2016 **14. Sponsoring Agency Code** FHWA

15. Supplementary Notes

Conducted in cooperation with the U.S. Department of Transportation, Federal Highway Administration.

16. Abstract

This project evaluates the effectiveness of sensor network systems for work zone traffic estimation. The comparative analysis is performed on a work zone modeled in microsimulation and calibrated with field data from two Illinois work zones. Realistic error models are used to generate noisy measurements corresponding to Doppler radar sensors, remote traffic microwave sensors (RTMS), and low-energy radar (LER). The velocity, queue length, and travel time are estimated with three algorithms based on (1) interpolation, (2) spatio-temporal smoothing, and a (3) flow model–based Kalman filter. More than 700 sensor and algorithm configurations are evaluated, and the accuracy of the resulting traffic estimates are compared with the true traffic state from the microsimulation. The nonlinear Kalman filter provides up to 30% error reduction over other velocity estimators when the RTMS spacing exceeds 2 miles and generally offers the best performance for queue and travel time estimation.

17. Key Words Smart work zone systems; traffic estimation; microsimulation	**18. Distribution Statement** No restrictions. This document is available through the National Technical Information Service, Springfield, VA 22161.

19. Security Classif. (of this report) Unclassified	**20. Security Classif. (of this page)** Unclassified	**21. No. of Pages** 60 plus appendices	**22. Price** N/A

Form DOT F 1700.7 (8-72) **Reproduction of completed page authorized**

ACKNOWLEDGMENT, DISCLAIMER, MANUFACTURERS' NAMES

This publication is based on the results of **ICT-R27-155, Improving Effectiveness of Smart Work Zone Technologies**. ICT-R27-155 was conducted in cooperation with the Illinois Center for Transportation; the Illinois Department of Transportation; and the U.S. Department of Transportation, Federal Highway Administration.

Members of the Technical Review panel were the following:

- Paul Lorton, IDOT, TRP Chair
- Michael Wiater, IDOT, TRP Co-Chair
- Kyle Armstrong, IDOT, TRP Member
- Matthew Daeda, IDOT, TRP Member
- Bernard Griffin, IDOT, TRP Member
- Herbert Jung, IDOT, TRP Member
- Randy Laninga, IDOT, TRP Member
- Dean Mentjes, FHWA, TRP Member
- Marshall Metcalf, IDOT, TRP Member
- Ted Nemsky, IDOT, TRP Member
- Juan Pava, IDOT, TRP Member
- Keith Roberts, IDOT, TRP Member
- Ryan Sheley, IDOT, TRP Member
- Gary Sims, IDOT, TRP Member

The contents of this report reflect the view of the authors, who are responsible for the facts and the accuracy of the data presented herein. The contents do not necessarily reflect the official views or policies of the Illinois Center for Transportation, the Illinois Department of Transportation, or the Federal Highway Administration. This report does not constitute a standard, specification, or regulation.

Trademark or manufacturers' names appear in this report only because they are considered essential to the object of this document and do not constitute an endorsement of product by the Federal Highway Administration, the Illinois Department of Transportation, or the Illinois Center for Transportation.

EXECUTIVE SUMMARY

Federal regulations (23 CFR 630 Subpart J, 23 CFR 630 Subpart K) place emphasis on smart work zone technologies within and around work zones to improve safety and mobility. Given the increasing number of smart work zone deployments, cross-studies have been performed to summarize the lessons learned, and work zone implementation guidelines were recently published by the Federal Highway Administration (FHWA) to assist departments of transportation (DOTs) in determining the feasibility and design of smart work zones for a given application.

Two critical components for the success of a smart work zone deployment are the quality of the traffic data collected by sensor networks and the algorithms used for data processing, which, when combined, provide real-time traffic information in the work zone. Accurate and reliable traffic estimation is the basis for many smart work zone systems regardless of the specific application. For example, the effectiveness of a portable changeable message sign (PCMS) is reduced if the message does not accurately correspond to current traffic conditions. Therefore, the accuracy of the traffic estimation can be regarded as a critical metric for the potential effectiveness of smart work zones.

Using the estimation accuracy as a metric of the potential effectiveness of work zones, this study focuses on quantitatively evaluating a large variety of sensor network configurations and traffic estimation algorithms in microsimulation to obtain insights on best practices for designing smart work zone systems. Two work zones located on I-80 in Will County and I-57 in Jefferson County were modeled and calibrated with field data in the microsimulation environment. Dedicated sensor error models were developed to generate realistic measurements corresponding to Doppler radar sensors (radar), remote traffic microwave sensors (RTMS), and low-energy radar (LER).

To assess the importance of algorithms for the estimation accuracy of the velocity, queue length, and travel time, three algorithms with different levels of sophistication were implemented: (1) spatial interpolation used in practice, (2) spatio-temporal filtering, which integrated a smoothing component in the temporal horizon, (3) and a traffic flow model–based nonlinear Kalman filter. To identify the critical factors on the sensor network design in a smart work zone, 242 different configurations of sensor networks were quantitatively assessed, each with three algorithms that varied in the number and spacing of sensors, the type of sensors, and the accuracy of individual sensors.

In summary, this study assessed 726 combinations of sensor network configurations and traffic estimation algorithms. The main findings are as follows:

- The spacing of sensors is an important factor for improving the accuracy of traffic estimation, especially at a large sensor spacing (e.g., 1 mile). When the sensor spacing is smaller than 0.5 mile, the benefit of additional sensors or the choice of algorithm is marginal (i.e., less than 5% improvement per sensor).
- The nonlinear Kalman filter generally provides significantly more-accurate estimation of the velocity, the queue length, and the travel time compared with other algorithms when the spacing of sensors exceeds 1 mile. It has the potential to reduce the cost of the existing sensors by approximately 50% while achieving the same level of traffic estimation accuracy. However,

the performance of the nonlinear Kalman filter relies on the appropriate selection of algorithmic parameters, which requires field data collection and expertise to apply the technique.

- The RTMS provides more-accurate flow measurements than radar and LER because of its less prominent occlusion issue. The accurate flow measurement can significantly improve the estimation accuracy of the nonlinear Kalman filtering algorithm. The spatial interpolation and the spatio-temporal filtering algorithms use velocity measurements only; hence, they have less accuracy variation across three types of sensors. In the cost accuracy analysis, the radar sensors are the most cost effective for estimating the velocity and queue length. At the same system cost, the additional number of radar sensors (a lower unit price allows more to be installed) provides higher improvement of the estimation accuracy than using more-accurate but fewer RTMS. It should be noted that the cost accuracy analysis was conducted based on limited cost data. It is recommended that the cost accuracy be re-assessed, given the updated cost data for each specific deployment.
- Existing sensor technologies are sufficient for good performance across all algorithms considered, and little additional benefit can be expected from improvements of the quality of individual sensors because measurement error is dominated by the quantization error and errors related to occlusion (for radar and LER). This finding is based on the assumption that all sensors are properly calibrated to achieve the error magnitudes as specified by the sensor manufacturer specification and operate reliably. More benefit can be achieved by improving the reliability of sensors instead of increasing individual sensor accuracy. This conclusion is made based on the rate of significant missing data during congestion in the field dataset in a work zone where no traffic estimation algorithm can produce accurate traffic estimates.
- All classes of implemented algorithms perform relatively poorly on travel time estimation owing to the use of the instantaneous travel time estimation scheme. The use of Bluetooth sensors will not improve travel time estimation accuracy when the travel times are quickly changing. This is because the sensors only record the travel time of the vehicle that just completed the trip, which may no longer be a good estimate of the travel time of the vehicle just entering the stretch of roadway. Analytics with the capability of travel time prediction for smart work zone monitoring systems are recommended to obtain a better travel time estimation.

The findings in this study are intended to

- Help DOTs in their decision-making process regarding the acquisition of smart work zone systems.
- Assist vendors working with state DOTs on the development of improved systems for smart work zones.

All source code developed in this study can be found at https://github.com/Lab-Work/ IDOT-SmartWorkzone.

CONTENTS

CHAPTER 1: INTRODUCTION 1
1.1 OBJECTIVE OF THE STUDY 1
1.2 METHODOLOGY 2
1.3 ORGANIZATION OF THE REPORT 3
CHAPTER 2: LITERATURE REVIEW OF SMART WORK ZONES 5
2.1 REPRESENTATIVE SMART WORK ZONE DEPLOYMENTS 5
2.1.1 Real-Time Traveler Information System 5
2.1.2 Queue Warning and Detection System 6
2.1.3 Dynamic Lane Merge System 7
2.1.4 Incident Management System 8
2.1.5 Variable Speed Limit System 8
2.1.6 Automated Speed Enforcement System 9
2.1.7 Performance Measurement System 9
2.2 ASSESSMENTS AND GUIDELINES OF SMART WORK ZONES 10
2.3 SUMMARY OF LITERATURE REVIEW 11
CHAPTER 3: CONSTRUCTION OF A VIRTUAL TESTBED IN MICROSIMULATION 13
3.1 SELECTION OF WORK ZONE SITES 13
3.2 ANALYSIS OF FIELD DATA 16
3.2.1 Data Description 16
3.2.2 Data Analysis Findings 17
3.2.3 Summary of Data Analysis 20
3.3 MODELING OF WORK ZONES 21
3.4 CALIBRATION OF WORK ZONES 24
3.4.1 Literature Review on Calibration of Microsimulation Models 24
3.4.2 Automated Calibration Framework 26
3.4.3 Calibration Results of Two Work Zones 27
3.5 SENSOR MODELS 28
3.5.1 Overview of Sensor Types 28
3.5.2 Generation of Noisy Measurements 29
CHAPTER 4: TRAFFIC ESTIMATION ALGORITHMS 31
4.1 SPATIAL INTERPOLATION 31
4.2 SPATIO-TEMPORAL FILTERING 31
4.3 KALMAN FILTER 32
4.4 BACK OF QUEUE AND TRAVEL TIME ESTIMATION 33

CHAPTER 5: COMPARATIVE ANALYSIS 35
5.1 TRAFFIC ESTIMATION ERROR METRICS 35
5.2 ALGORITHMS AND SENSOR SPACINGS 37
5.3 TYPE OF SENSORS 39
5.4 ACCURACY OF SENSORS 40
5.5 COST ACCURACY ANALYSIS 43
CHAPTER 6: SUMMARY AND CONCLUSIONS 47
REFERENCES 52
APPENDIX A: CALIBRATION PROCEDURE 61
APPENDIX B: DATA QUALITY ANALYSIS 69
APPENDIX C: IMPLEMENTATION OF ALGORITHMS 77
APPENDIX D: COMPLETE EVALUATION RESULTS 83

CHAPTER 1: INTRODUCTION

1.1 OBJECTIVE OF THE STUDY

Smart work zones aim to improve work zone safety and mobility through the integration of traffic sensors, estimation algorithms, and traffic management strategies. As illustrated in Figure 1.1, a smart work zone [1] normally consists of (1) a sensor network to measure current traffic conditions in and around the work zone; (2) a data processing algorithm to process the raw data and estimate work zone quantities of interest (e.g., the back of the queue, the average velocity in the work zone); (3) output devices that disseminate traffic information to the appropriate consumer (e.g., drivers or departments of transportation) depending on the application; and (4) a communication network that connects the individual components.

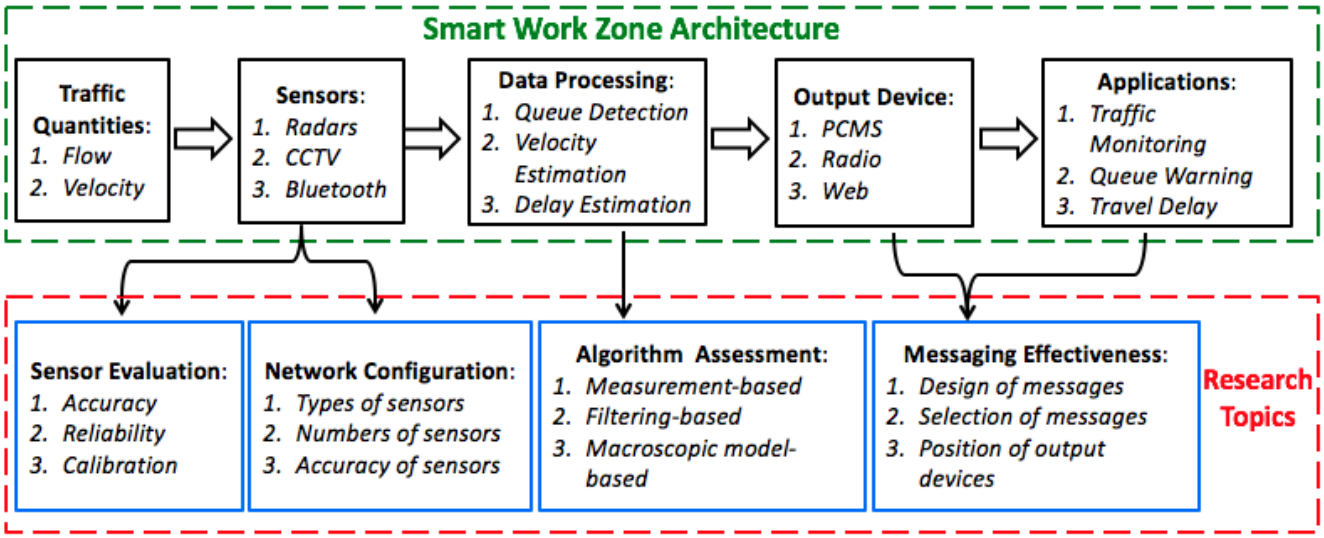

Figure 1.1: Architecture of smart work zones. This study focuses on the assessment of network configurations and data processing algorithms for estimating velocity, queue length, and travel time.

Smart work zones have been deployed in a variety of applications, such as the provision of real-time traveler information [2, 3, 4], back-of-queue warnings [5, 6], and traffic management [7, 8, 9]. Many qualitative and quantitative benefits of smart work zones are reported from field deployments, such as a reduction in aggressive maneuvers and crashes [3, 10, 11], smoothed merging activities [7, 12], reduced speeding [7, 13], increased throughput [7], and reduced delay [14, 15].

Given the increasing number of smart work zone deployments, cross-studies have been performed to summarize the lessons learned and the benefits of each smart work zone [10, 11, 16, 17]. Recently, the Federal Highway Administration (FHWA) published work zone implementation guidelines [1] to determine the feasibility and design of a work zone intelligent transportation system (ITS) for a given

application. The guidelines also report that trade-offs typically exist between the number and type of work zone components, but the guidelines lack a quantitative assessment of the trade-offs. A main reason for the knowledge gap is the difficulty of collecting detailed performance data from a large number of configurations in an active work zone.

Regardless of the application, the effectiveness of smart work zones relies on accurate and reliable estimates of traffic conditions (e.g., traffic velocity, the back of queue, and the travel time). For example, the estimated traffic conditions that are used to produce safety-critical messages on portable changeable message signs (PCMS) must be accurate and credible to be effective [18]. Therefore, the estimation accuracy of the traffic condition can be used as a metric for the potential effectiveness of smart work zones, which circumvents the time-consuming collection of performance data for mobility and safety.

The main objective of this study is to identify the key factors for improving the estimation accuracy, by evaluating a large number of smart work zone configurations in a microsimulation environment. Specifically, the objectives are as follows:

- To develop and calibrate a microsimulation environment for the simulation of a large number of smart work zone configurations, which vary in the number and spacing of sensors, types of sensors, and accuracy of individual sensors.
- To review and implement a variety of algorithms for estimating the traffic velocity, queue length, and travel time, including a spatial interpolation algorithm, a spatio-temporal filter that incorporates the temporal dynamics of traffic, and a state-of-the-art nonlinear Kalman filter.
- To quantitatively assess the influence of the number and spacing of sensors, the type of sensors, the accuracy of sensors, and the traffic estimation algorithms on traffic estimation accuracy to help determine the potential effectiveness of smart work zones.

1.2 METHODOLOGY

This study uses a microsimulation environment to simulate a large number of smart work zone configurations and traffic estimation algorithms. The developed framework is illustrated in Figure 1.2. The framework consists of the following key components:

- A microscopic traffic simulation software, AIMSUN, is used to model the work zones, simulate the traffic at the level of individual vehicle movements, and generate detailed trajectory data at a 0.2 second granularity for each vehicle. The microsimulation model is calibrated using field data to reproduce similar traffic statistic as observed in the field.
- To investigate the influence of types of sensors and the accuracy of individual sensors, dedicated sensor error models are developed that can generate realistic sensor measurements from the trajectory data. Three types of commonly used sensors are modeled in this study, namely, remote traffic microwave sensor (RTMS), Doppler radar (radar), and low-energy radar (LER, an example of which is iCone®).

- Three algorithms are implemented to estimate the traffic condition. The algorithms are representative of the (1) spatial interpolation approaches often used in practice by state departments of transportation (DOTs), (2) spatial-temporal filtering algorithms that can incorporate the temporal dynamics of traffic, and (3) nonlinear Kalman filtering methods conventionally applied on highways outside of work zone environments [19, 20] by the research community. The algorithms directly estimate the traffic velocity, from which the length of the queue and the travel time could be computed.
- Finally, true states are obtained from the trajectory data for computing the estimation error of the velocity, queue length, and travel time.

In total, more than 700 smart work zone deployments were simulated for assessing the importance of the number and spacing of sensors, the types of sensors, the accuracy of individual sensors, and the estimation algorithms.

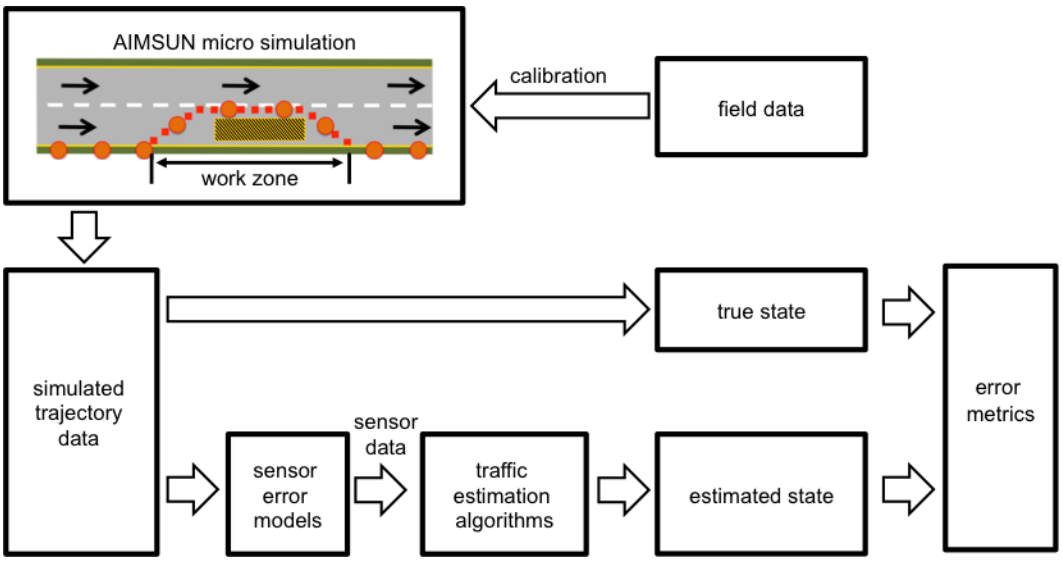

Figure 1.2: Framework for the evaluation of various sensor network configurations and algorithms.

1.3 ORGANIZATION OF THE REPORT

The remainder of this report is organized as follows.

Chapter 2 summarizes representative smart work zone deployments, existing work zone summary reports, and guidelines for smart work zones. The literature review identifies a lack of a comprehensive, quantitative, and comparative analysis on the design of smart work zones, which motivates this study.

Chapter 3 documents the development of a virtual testbed in the microsimulation environment. Two work zones in Illinois, on I-80 and I-57, were modeled and calibrated in the microsimulation environment. Prior to the calibration of work zones, an analysis of the field data was conducted. The data quality analysis revealed data incompleteness and inconsistency issues, which presented challenges for the calibration of the two work zones. The developed sensor models for RTMS, radar, and LER are described in the last subsection.

Chapter 4 reviews the traffic estimation algorithms and describes the implementation of representative algorithms in three categories with different levels of sophistication. The algorithms are based on spatial interpolation, spatio-temporal filtering, and a nonlinear Kalman filter.

Chapter 5 presents the evaluation results and summarizes the impact of each factor on estimation accuracy of traffic conditions. Based on the analysis results, a cost-effectiveness analysis was conducted.

Chapter 6 summarizes the main findings of this study on the design of smart work zones.

CHAPTER 2: LITERATURE REVIEW OF SMART WORK ZONES

A large number of studies have been conducted to summarize the benefits, lessons learned, and guidelines for implementing smart work zones. The objective of the literature review in this study is to summarize a list of available resources that can be used as references in the strategic design of smart work zones. The literature review places more emphasis on the detailed configuration of the deployed sensor network, as opposed to system-level implementation strategies. Section 2.1 focuses on representative smart work zone deployments and summarizes the lessons learned in case studies. Section 2.2 reviews existing works on the cross-cutting assessment and summarizes existing meta-studies for smart work zones.

2.1 REPRESENTATIVE SMART WORK ZONE DEPLOYMENTS

Smart work zone technologies can be applied to achieve a variety of goals. According to the work zone implementation guide [21] by FHWA, smart work zones can be classified as follows:

- Real-time traveler information systems that provide congestion, delay, and alternative route information to motorists.
- Queue warning systems, which provide warnings to motorists about stopped or slow traffic to reduce the risk of rear-end collisions.
- Dynamic lane merge systems, which dynamically instruct the motorists' merge actions to smooth merge maneuvers based on the traffic condition.
- Incident management systems, which detect the occurrences of incidents for quick response.
- Variable speed limit systems, which dynamically adjust the speed limit to smooth traffic through work zones. They aim to improve mobility and/or safety.
- Automated enforcement systems, which detect speeding vehicles and enforce the speed compliance of motorists.
- Performance measurement systems, which evaluate the impact of the work zone based on quantitative measures, such as the induced travel delay and the length of developed queues.

This section summarizes a representative subset of smart work zone deployments in each of the above categories.

2.1.1 Real-Time Traveler Information System

A real-time traveler information system provides traffic information to motorists, which may include the travel time or delay, the queue length, or reroute information. Two representative real-time traveler information systems are summarized next. A comprehensive review of real-time traveler information systems can be found in [22].

Automated Portable Real-Time Traffic Control Systems, Illinois, 2001–2002 [4]

- Objective: The primary goal of the deployed system was to estimate and disseminate the travel delay time to motorists via portable dynamic message signs (PDMS) and the Illinois Department of Transportation (IDOT) website. The secondary goal of the system was to provide congestion and incident detection alerts to IDOT staff.
- System configuration: The system was deployed on both the northbound and southbound approaches to the work zone, covering approximately 40 miles of I-55. Eight portable X-Band radar units were used to measure the vehicle speed and presence data. Four portable closed circuit television (CCTV) cameras were deployed to identify possible incidents detected by the radar sensors. Seventeen remotely controlled PDMS were used to disseminate delay and lane closure advisories.
- Reported benefits: Overall, no significant traffic backups occurred while the system was in place. IDOT officials "were satisfied with the performance." However, owing to the lack of "before" and "after" data, no quantitative benefit of the system was reported.

Automated Work Zone Information System, Arkansas, 2000 [3]

- Objective: The main objective of the system was to provide traffic information regarding the length of the queue to assist travelers in making routing decisions. The delay time was not provided to travelers because of the potential for inaccurate estimates. However, the system could provide faster incident response.
- System configuration: Twelve RTMS were deployed over 7 miles to measure the traffic speed, volume, and occupancy. The traffic information was disseminated by five PDMS covering 9 miles, three highway advisory radios (HARs) covering 23 miles, and the project website.
- Reported benefits: The system was reported to have improved construction project productivity by adjusting construction activity schedules to avoid the identified peak traffic periods. Improved incident response was also noted. It was observed that 90% of the PDMS messages matched the actual conditions. The field engineer stated, "The system worked well and appeared to be effective in preventing and reducing rear-end collisions and enhancing congestion management" [3].

2.1.2 Queue Warning and Detection System

Queue warning and detection systems estimate the location of the back of the queue and disseminate warning messages to approaching motorists. A comprehensive review on the practices of queue warning systems is available in [5], which found that the most notable benefit of the deployment of queue warning systems is the reduction of rear-end crashes. This section summarizes two representative deployments of queue warning systems. More deployments of queue warning systems can be found in [23, 24, 25].

I-57/I-64 Queue Warning System, Illinois, 2011–2013 [6]

- Objective: The main goal of the system was to detect and warn approaching traffic about slow-moving or stopped traffic.

- System configuration: Thirty-two LER-based iCone® devices were deployed at approximately 1 mile spacings to measure the speed of traffic. Fifteen PCMS were used to disseminate the queue information.
- Reported benefits: No quantitative benefits were reported owing to the lack of data before deployment of the system. It was reported, however, that "project staff ... believed the system was helpful in reducing queues and managing traffic" [6].

I-35 End-of-Queue Warning System, Texas, 2013 [26, 27]

- Objective: The main goal of this system, which is currently in operation, is to detect and predict the formation of queues and warn motorists of slow and stopped traffic ahead [28].
- System configuration: The project is expected to be completed in 2018. Currently, the system consists of 17 RTMS for measuring the traffic speed, volume, and vehicle classification; 40 pairs of Bluetooth sensors for detecting the travel time; six CCTV cameras for traffic surveillance; and 10 PCMS for disseminating traffic information [29].
- Reported benefits: No quantitative benefit is currently reported.

2.1.3 Dynamic Lane Merge System

Dynamic lane merge systems aim to smooth the flow of traffic through the work zone by regulating merge movements based on traffic conditions. The effectiveness of dynamic lane merge system was evaluated in [8]. It was reported that the average delay per vehicle to pass through the work zone and the number of aggressive driving maneuvers decreased with the deployment of a dynamic lane merge system. Two representative dynamic lane merge systems are summarized below.

Dynamic Lane Merge System, Michigan, 2002–2003 [7]

- Objective: The goals of the system included reducing aggressive driving at the merge point, maximizing available capacity, and enhancing traveler safety.
- System configuration: Five dynamic lane merge trailers were deployed upstream of the work zone at a spacing of 1,500 feet. Each trailer consisted of an RTMS for measuring the traffic speed, volume, and occupancy, and a dynamic sign for posting merge instructions to travelers.
- Reported benefits: Quantitative benefits were presented in a Michigan DOT report [30]. The average number of stops in the work zone decreased from 1.75 to 0.96, and the travel time delay decreased from 95 seconds to 69 seconds during the morning peak period. The average travel speed increased from 40 mph to 46 mph during the morning peak period. In addition, the average number of aggressive driving maneuvers decreased from 2.88 to 0.55 during the afternoon peak period, which consequently improved the safety.

Simplified Dynamic Lane Merge System (SDLMS), Florida, 2008 [8]

- Objective: The primary goal was to regulate the merge movements depending on the traffic conditions to increase capacity and safety using a simplified lane merge system for short-term

movable work zones. A secondary goal was to quantitatively assess the effectiveness of simplified dynamic lane merge system using field data.

- System configuration: RTMS were used to collect the volume, speed, occupancy, and vehicle classification data at the merging points, while PCMS were used to display proper merging instructions.
- Reported benefits: A significant increase of the work zone capacity from 881 vehicles/hour to 970 vehicles/hour using the early-merge system SDLMS was observed. Using the late-merge strategy, the capacity increased from 881 vehicles/hour to 896 vehicles/hour, which was not statistically significant. In general, the early-merge SDLMS performs better at low traffic volume and worse at high traffic volume than the late-merge SDLMS.

2.1.4 Incident Management System

Incident management systems automatically detect the occurrence and location of the incidents for quick traffic control response to mitigate the safety and congestion issues caused by the incidents. Typically, traffic sensors are deployed to automatically detect abnormal traffic conditions and CCTV videos are used to visually inspect and assess the incidents. Once incidents are confirmed, PCMS are used to warn and reroute travelers to mitigate potential safety issues and prevent severe backups.

Incident management can be the primary goal of a smart work zone deployment, or it can be integrated into smart work zones with other primary goals such as in [2, 4]. A typical incident management is described as follows.

Incident Management System, New Mexico, 2000 [31]

- Objective: The primary goal of the system was to quickly identify incidents for an effective response to clear the roadway and enhance traveler safety.
- System configuration: Eight CCTV were installed at key locations and the videos were inspected manually in real-time to detect incidents. Eight DMS, four HAR, and the project website were used to disseminate the incident and rerouting information to travelers.
- Reported benefits: The response time to incidents reduced from 45 minutes to 25 minutes with the deployment of the incident management system. More than 60% of respondents in a survey reported the disseminated traffic information was accurate and timely [2].

2.1.5 Variable Speed Limit System

The variable speed limit systems aim to increase the throughput and enhance safety by providing travelers a speed limit derived based on the current traffic conditions. The effectiveness of variable speed limit systems was evaluated in [32, 33, 34, 35], which report increased throughput, reduced travel time, and an increase in speed limit compliance. A typical variable speed limit system deployed in Utah [39] is summarized below, and more examples of variable speed limit systems can be found in [36, 37, 38].

Variable Advisory Speed System, Utah, 2010 [39]

- Objective: The goal of the system was to provide drivers with an advised traffic speed based on the measured traffic conditions in the work zone.
- System configuration: Five RTMS were deployed to measure the traffic speed, volume, and occupancy at spacings ranging from 0.17 to 0.4 mile. Two variable message signs were used to display the advisory speed.
- Reported benefits: Statistical analysis showed the system was in general effective at increasing mean speed and decreasing speed variance, thus providing smooth traffic flow when there was a slowdown during the weekend evening peak period.

2.1.6 Automated Speed Enforcement System

Automated speed enforcement systems are commonly used to improve the speed compliance of motorists. These systems can be deployed as a stand-alone device equipped with a speed sensor, a PCMS, and an optional camera. The effectiveness of the system varies based on the operational strategies used [40]. In general, the system is reported to decrease the average speed of traffic, resulting in fewer speed limit violations and improved safety. A typical stand-alone speed enforcement system is summarized below, while more deployments and evaluations of speed enforcement systems can be found in [41, 42, 43, 44].

Photo Radar Speed Enforcement System, Oregon, 2008–2009 [45]

- Objective: The system was deployed as a demonstration project to evaluate the effectiveness of the photo speed enforcement system.
- System configuration: An RTMS was used to measure the traffic speed and volume. A camera was used to take photos of the license plates as the primary enforcement strategy.
- Reported benefits: On average, the speed was reduced by 23.7% while the photo radar speed enforcement system was active.

2.1.7 Performance Measurement System

Performance measurement systems use traffic data to quantitatively measure the impact of the work zone project on safety and mobility, such as induced travel delay and the queue length [46, 47]. Such quantitative assessments can be used as incentives or disincentives for the work zone project contractors.

A synthesis of work zone performance measures was reported in [48]. A performance measurement system using license plate recognition technology is summarized below. The operational impact of the I-35 reconstruction project in Texas in 2012 (ongoing) was quantified in the travel delay using Bluetooth sensors [26]. The experience of using probe vehicle data (e.g., vehicles equipped with GPS, Bluetooth, or Electronic Toll Collection devices) for evaluating work zone performance is described in [49, 50]. A more comprehensive review of mobility-based performance measures using seven different technologies can be found in [51].

Work Zone Travel Time System, Arizona, 2002 [9]

- Objective: The main goal of the system was to measure travel time through the work zone, which was used to provide incentives to the contractors if the traffic delay was less than a specified threshold.
- System configuration: Two inductive loop detectors at both ends of the work zones were used to detect the presence of vehicles, which triggered digital cameras to take photos of the license plates. A license plate recognition algorithm was used to identify vehicles for measuring the travel time.
- Reported benefits: The system was able to read 60% of the license plates and match approximately 11% of the license plates. The travel time measure helped the contractor adjust work operations to reduce congestion.

2.2 ASSESSMENTS AND GUIDELINES OF SMART WORK ZONES

This section reviews the existing works summarizing the collective experiences from work zone case studies, including evaluations of smart work zone systems, assessments of the benefits of smart work zone deployments, and guidelines for implementing smart work zone technologies.

A continuing effort has been devoted to the development of a knowledge database (http://www.itskr.its.dot.gov) for documenting the ITS benefits, costs, and lessons learned [11, 52, 53]. More than 1,600 summaries of ITS deployments across 16 taxonomy areas have been archived through 2014, including more than 130 summaries for ITS deployments in work zones. Twenty fact sheets were developed to summarize the benefits, costs, and lessons learned in ITS deployments, including one fact sheet focusing specifically on smart work zones. The primary lessons learned across smart work zone deployments were generally operations oriented (e.g., planning for sufficient testing time during the deployment of the smart work zone), allowing an adjustment period for travelers for higher effectiveness of the smart work zone.

A detailed literature review [5] of 94 smart work zone deployments including queue warning systems, dynamic merge systems, alternate routes, and variable speed limits was conducted to summarize the benefits and typical uses of smart work zone technologies. It concludes that when more sensors are deployed, the systems provide faster notification of changes of the traffic conditions and increase the estimation accuracy of the traffic conditions.

A cross-cutting study report [2] summarizes lessons learned from four smart work zone deployments and identifies key lessons learned for the success of a smart work zone system. For example, it is concluded that is vital to deliver accurate information to the public. However, no analysis of the detailed design of sensor networks of smart work zones is included.

The best practices and lessons learned for the ITS strategic planning are documented in [16]. The emphasis is placed on the decision-making processes, including agency interactions, processes and procedures, organizational structures, and institutional involvement.

The current practices for queue warning used by international agencies and state DOTs are identified in [54] based on a literature review of more than 40 practices and techniques. One of the reported

difficulties of queue warning systems is the selection of locations for deployment of sensors, which may rely on the field engineers' expertise and knowledge to estimate where the end of the queue is likely to be located.

A quantitative assessment of the mobility and safety benefits of smart work zones is conducted using a "before" and "after" analysis in [17]. The requirements of the "before" and "after" performance data constrained the scope of the study to consider only five work zone deployments.

In addition to summaries of smart work zone deployments, assessments of commercial smart work zone systems for specific applications have been conducted. Four different smart work zone configurations were evaluated for the accuracy of queue detection [25]. The LER solution iCone®, designed for work zones, was evaluated in [55]. A comprehensive study [22] compared 16 different commercially available advanced traveler information systems (ATIS) in 27 separate deployments throughout the United States. An 11-step procedure was developed to assist DOTs in choosing the most appropriate ATIS configuration for any given work zone. However, more emphasis was placed on the selection of generic systems, and little information was provided on the detailed design of the system (e.g., the number and type of sensors). Overall, it was concluded that more-advanced real-time systems (consisting of multiple detectors and PCMS) have the greatest potential benefits in general, but they offered few advantages over stand-alone systems (consisting of one detector and one PCMS) when traffic is light and free flowing.

Because of the distinct specifications and goals in each work zone, existing studies commonly summarize the collective experiences of smart work zone deployments into guidelines for future implementation via a systems engineering approach. Two representative implementation guidelines are summarized next.

An intelligent work zone toolbox [56] was developed by Minnesota DOT, which contains guidelines for selecting an appropriate smart work zone system for different applications. The toolbox was intended as "brainstorming material" and therefore did not include detailed designs of the smart work zone systems.

Recently, a smart work zone implementation guide [1] was developed by FHWA, which summarizes key steps for successfully implementing smart work zones via a systems engineering process. The guidelines report that trade-offs typically exist between the desired system features and components, which, however, lacks quantitative assessment to understand the implications of different designs and work zone sensor configurations.

2.3 SUMMARY OF LITERATURE REVIEW

In general, the benefits of smart work zones have been widely reported. However, to quantify the effectiveness of smart work zones, measurement data before and after the deployment of the system is required, which is often unavailable in most case studies. In addition, based on the review of reports, the data collection process for quantifying the impact of smart work zones on mobility and safety was confirmed to be time consuming and often impractical.

Based on the large number of smart work zone deployments, efforts have been devoted to summarize the collective experiences from a variety of perspectives, ranging from the evaluation of off-the-shelf commercial systems for a specific application and assessment of operational strategies, to the development of a generic implementation guidelines via systems engineering approaches. However, very limited attention is given to subsystem-level analysis on the configuration of traffic monitoring component of smart work zones (e.g., the number and type of sensors used). The primary reason is that traffic monitoring system configurations vary significantly across smart work zone deployments and are typically developed for each specific deployment in collaboration with professional vendors. Moreover, collection of true traffic conditions (informally referred to as ground truth) is extremely difficult in the field. The deployment expense of the systems makes comparisons of various system configurations costly.

The goal of this study is to fill a knowledge gap in the configuration of work zone systems via the evaluation of a large number of traffic monitoring configurations, which vary in the number and spacing of sensors, the type of sensors, the accuracy of individual sensors, and traffic estimation algorithms. For a quantitative comparison, the accuracy of the estimate of the traffic condition is used as the performance measure because of its importance in effectively enabling a variety of smart work zone systems such as back-of-queue warning, travel time estimation, and traffic advisory information.

CHAPTER 3: CONSTRUCTION OF A VIRTUAL TESTBED IN MICROSIMULATION

This study proposes to use a microsimulation environment to assess a variety of smart work zone configurations and traffic estimation algorithms. This chapter describes the development of the microsimulation environment, including modeling and calibration of two work zones selected in Illinois, the quality analysis of field data, and the development of sensor error models.

This chapter is organized as follows. Section 3.1 describes the selection of two work zones in Illinois for modeling in the microsimulation environment. Section 3.2 evaluates the field sensor data available for selecting the simulation period and the work zone model calibration. Section 3.3 introduces a microsimulation software (AIMSUN) and the modeling procedure of the selected work zones. Section 3.4 documents the calibration procedure performed for the modeled work zones and the calibration results. Finally, the development of dedicated sensor models is presented in Section 3.5, which completes the setup of the microsimulation environment.

3.1 SELECTION OF WORK ZONE SITES

A microsimulation environment can simulate traffic flows at the microscopic level. To enhance the validity of the findings in this study, a microsimulation that resembles realistic traffic conditions is highly desirable. Specifically, the traffic in the microsimulation should replicate traffic conditions in the selected work zones. Two work zones were selected in collaboration with IDOT: one with moderate average daily traffic (ADT) and one with high ADT.

The selection criteria are summarized in Table 3.1. For modeling a work zone in the microsimulation software AIMSUN, detailed work zone geometry from the construction plan is required. Meanwhile, field sensor data is required for calibration of microsimulation models. In consultation with IDOT, several candidate work zones were reviewed, and the following two work zones with existing field deployed smart work zone systems were selected:

- I-80 bridge repair project (IDOT Contract No. 60Y64) over the Des Plaines River in Will County, Illinois, with an ADT of 82,000 with 27% trucks. This project started in January 2015 and was ongoing at the time of the analysis. A smart work zone system was deployed, consisting of 18 radar sensors and 12 RTMS. For the purpose of this research, Stage I of the work zone was modeled, shown in Figure 3.1. In the remainder of this report, this work zone is referred to as the I-80 work zone.
- I-57/I-64 freeway interchange pavement resurfacing project (IDOT Contract No. 78276) near Mt. Vernon in Jefferson County, Illinois, with an ADT of 33,620 with 32% trucks (2014). This project started in April 2014 and is ongoing at the time of this report. A smart work zone system was deployed, consisting of 22 radar sensors and three RTMS. For the purpose of this research, Stage IV of the work zone was modeled, shown in Figure 3.2. In the remainder of this report, this work zone is referred to as the I-57 work zone.

Table 3.1: Criteria Used for Selection of Work Zones to Be Modeled in Microsimulation Software

Purpose	Doc/Data		Comments
Modeling	Required	Basic geometry	• Length of the closed lane (taper, transition area, buffer space, construction zone). • Width of lanes. • Number of lanes.
		Typical daily construction activity	Construction hours on weekdays and weekends. Lane closure information if not closed all day.
		Speed limit	Changes of speed limits throughout the work zone and the location of the speed limit signs.
		Typical hourly traffic volume	The traffic volume in the work zone with a granularity of 1 hour or higher.
		Percentage of trucks	A rough estimation of the percentage of trucks.
	Desired	Curvature, grade, geometry of merges/diverges	The curvature and grade may help improve the soundness of the model; the geometry of the merge and diverge points may not be modeled depending on its complexity.
Calibration	Required	Entering/exiting traffic volume data	• On a typical construction day. • With a granularity of 1 hour or higher.
	Desired	Traffic speed data	• On a typical construction day. • With a granularity of 1 hour or higher.
		Travel time data	• On a typical construction day. • With a granularity of 1 hour or higher.
		Queue length data	On a typical construction day (see Chapter 4 for more discussion on how queue length is quantified).
		Sign placements	The location and types of traffic signs placed before and through the work zone, including speed limit signs, work zone warning signs, and lane merging signs.

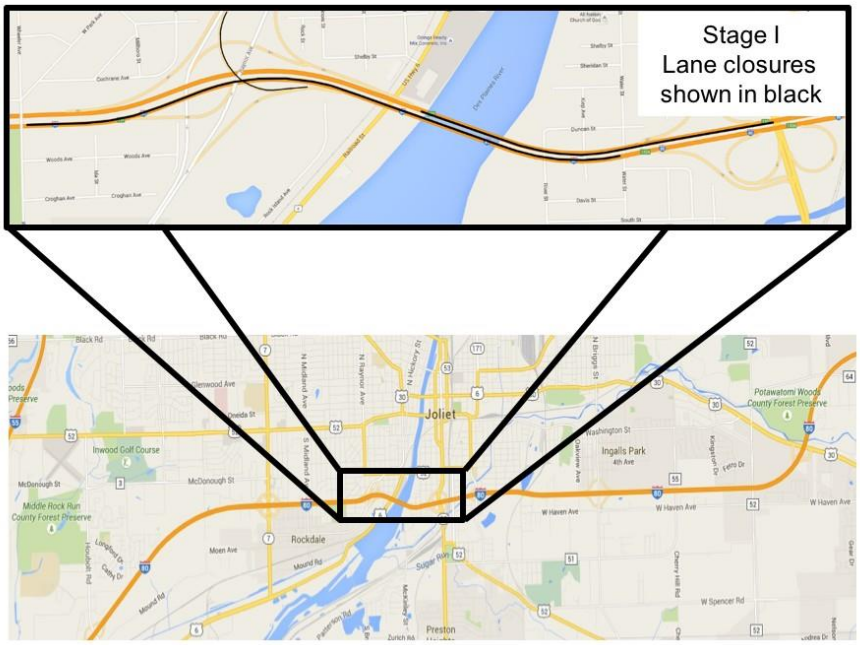

Figure 3.1: Stage I of the I-80 work zone.

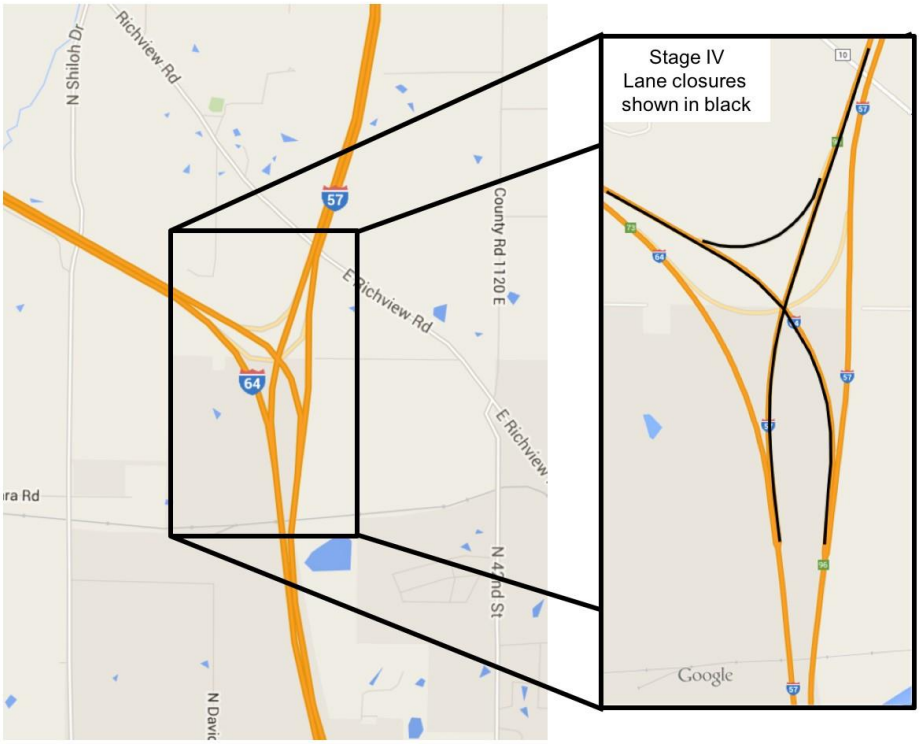

Figure 3.2: Stage IV of the I-57 work zone.

3.2 ANALYSIS OF FIELD DATA

The most safety-critical period in work zones is when severe congestion occurs. In addition, the period of severe traffic congestion provides varying traffic conditions, such as queue formation and dissipation, and is suitable for testing the performance of various sensor network configurations and traffic estimation algorithms. This study proposes to reproduce the traffic conditions in severe congestion periods in each of the work zones. For this purpose, the field data was investigated to select the most congested period for modeling in each work zone. During the process of analyzing the field data, degradation of the data quality was observed during congested periods. This subsection documents the main findings during the analysis of the field data and also incorporates additional information based on a discussion with the vendor of the smart work zone systems, Ver-Mac, held on June 8, 2016. The methodology adopted in the data quality analysis is described in Appendix B.1. The draft report submitted to IDOT on December 26, 2015, and forwarded to Ver-Mac is found in Appendix B.2.

This section reports on two data quality measures: (1) missing data rates, and (2) sensor measurement inconsistencies. The dataset used in this section was obtained through the software JamLogic, provided by Ver-Mac. The dataset includes the velocity and count data aggregated in user-defined intervals. In this project, 5 minute intervals were considered to provide a good balance between data granularity and quantization error.

This section is organized as follows. Section 3.2.1 describes the scope of the field data analyzed in this study. The main findings are summarized in Section 3.2.2. Finally, Section 3.2.3 remarks on the limitation of the data quality analysis and selects the congested periods to be modeled based on the data analysis findings.

3.2.1 Data Description

The data quality analysis was limited to the time and sensors that were considered for simulation. Specifically, the analysis was limited to the following periods and sensors:

- **Eastbound direction of the I-80 work zone between May 1, 2015, and May 31, 2015.** This month was selected because the project started in April, 2015 and the modeling of this work zone in the microsimulation environment was conducted in June, 2015. The missing data percentage and the sensor measurement inconsistencies were computed under different scenarios to better understand the potential issues:
    - The entire month of May 2015.
    - An estimated peak hour between 1630 and 1730 hours for the entire month in May 2015, based on visual inspection of the speed data patterns.
    - Three time intervals with apparent congestion (May 1 from 1530 to 1800 hours, May 3 from 1100 to 1630 hours, and May 7 from 0700 to 1630 hours), based on visual inspection of the speed data patterns.
    - A typical free-flow time interval (May 1, 2015, from 1300 to 1530 hours).

- **Southbound direction of the I-57 work zone between November 1, 2014, and November 30, 2014**. This dataset was of interest for modeling because of the occurrence of severe congestion. For the data quality assessment, the missing data percentage and the sensor measurement inconsistencies were computed in the following scenarios:
  - The entire month of November 2014.
  - An estimated peak hour between 1630 and 1730 hours for the entire month of November 2014, based on visual inspection of the speed data patterns from the RTMS.
  - Three time intervals with apparent congestion (i.e., November 26 from 1600 to 1800 hours, November 26 from 2100 to 2300 hours, and November 16 from 1700 to 1830 hours), based on visual inspection of the speed data patterns.
  - A typical free-flow time interval (November 18, 2014, from 0600 to 1100 hours).

3.2.2 Data Analysis Findings

This section presents the numerical results of the data quality assessment performed on the datasets in each of the work zones.

I-80 Work Zone Data Analysis

The missing data rates for the I-80 data during the analyzed periods for sensors installed in the eastbound direction are summarized in Table 3.2.

The following observations can be made:

- EB9* had a large number of missing speed records and count records, and was identified as problematic.
- EB11 also had a large number of missing speed records and no count records. Ver-Mac clarified that EB11 was a standard radar unit installed on a distinct hardware platform (a portable changeable message sign) that was not designed to capture count data. Other radar units were installed on the stand-alone JamLogic platform and consequently recorded speed and count data.
- During the congested intervals, EB10, EB14, EB15, and EB16 each had missing data rates above 10%, but they had lower missing data rates averaged over the month.
- The RTMS EB12* had a higher missing data rate over the entire month compared to other intervals considered. Ver-Mac provided additional analysis that indicated the causes of the missing data included a sensor malfunction from May 5 0400 to May 6 1322. The additional analysis also identified that from 0550 to 0725 on May 28, the sensor did not report any data, and an adjacent sensor also did not report data during the interval. This localized failure is consistent with a problem occurring at the nearest cellular tower (e.g., tower maintenance).
- Sensors EB16 through EB8 experienced significant issues during the congestion intervals. Sensors EB7 through EB3 had less significant missing data issues, presumably because the queue did not extend to their location.

- Overall, the missing data rate in the entire period was 3% over all sensors deployed, and less than 1% when excluding EB9* and EB11. The missing data rate in congested intervals was several times higher, especially for radar sensors. Ver-Mac provided additional analysis that indicated the missing data is more prominent between 0500 to 0700 and 1200 to 1500. Ver-Mac indicated one cause could be due to prioritization of voice communications over data communications by the cellular provider during high communication traffic on the cellular network. In heavily congested road traffic conditions, the missing data rate is also influenced by the fact that the radar units have reduced performance at speeds less than 20 mph, and do not record data at speeds less than 10 mph. When the communication network and the road network are both congested, both may influence the missing data rate.
- The quantitative data inconsistency results between sample pairs of sensors on I-80 for all of May 2015 and a typical free-flow interval are shown in Table 3.3 and Table 3.4, respectively. The notation $i \rightarrow i + 1$ refers to the data percent change from sensor i to $i + 1$.

The following findings were obtained based on the statistical analysis:

- As seen in Table 3.3 and Table 3.4, the RTMS provided higher values for speed and count measurements than the radar sensors.
- The measurement inconsistencies occurred across two types of sensors, as well as among radar sensors. The largest inconsistency for speed (10% to 17%) and counts (73% to 93%) was observed between RTMS and radar sensors.

Table 3.2: May 2015 I-80 Eastbound Percent Missing Data Rate

	Entire Period		Peak Hours		Congested Intervals		Free-Flow Interval	
Sensor	**Speed**	**Count**	**Speed**	**Count**	**Speed**	**Count**	**Speed**	**Count**
EB3	0.41%	0.41%	0.00%	0.00%	1.99%	1.99%	0.00%	0.00%
EB4	0.44%	0.44%	0.00%	0.00%	3.28%	3.28%	0.00%	0.00%
EB5*	0.27%	0.27%	0.00%	0.00%	2.99%	2.99%	0.00%	0.00%
EB6	0.53%	0.53%	0.00%	0.00%	2.99%	2.99%	0.00%	0.00%
EB7*	0.24%	0.24%	0.00%	0.00%	2.99%	2.99%	0.00%	0.00%
EB8	0.46%	0.46%	0.00%	0.00%	6.47%	6.47%	0.00%	0.00%
EB9*	27.40%	27.40%	25.81%	25.81%	34.83%	34.83%	0.00%	0.00%
EB10	0.52%	0.52%	0.00%	0.00%	10.45%	10.45%	0.00%	0.00%
EB11	0.84%	N/A	0.00%	N/A	0.00%	N/A	0.00%	N/A
EB12*	4.84%	4.84%	3.23%	3.23%	2.99%	2.99%	0.00%	0.00%
EB14	0.85%	0.85%	0.00%	0.00%	15.92%	15.92%	0.00%	0.00%
EB15	0.74%	0.74%	0.00%	0.00%	16.92%	16.92%	0.00%	0.00%
EB16	0.75%	0.75%	0.00%	0.00%	19.90%	19.90%	0.00%	0.00%
Average	2.95%	3.12%	2.23%	2.42%	9.36%	10.14%	0.00%	0.00%
Average excluding EB9*, EB11	0.91%	0.91%	0.29%	0.29%	7.90%	7.90%	0.00%	0.00%

Note: the symbol * denotes an RTMS.

Table 3.3: May 2015
Data Percent Change on I-80

	Percent Change	
Sensor Pair	**Speed**	**Count**
EB4→EB5*	17.08%	73.79%
EB4→EB6	3.12%	22.58%
EB8→EB9*	14.23%	84.49%
EB8→EB10	8.29%	26.35%

Note: The symbol * denotes an RTMS.

Table 3.4: May 1, 2015
(1300–1530 hours)
Data Percent Change on I-80

	Percent Change	
Sensor Pair	**Speed**	**Count**
EB4→EB5*	16.31%	79.85%
EB4→EB6	1.73%	10.35%
EB8→EB9*	10.81%	93.73%
EB8→EB10	6.93%	13.68%

I-57 Work Zone Data Analysis

The missing data rates for sensors installed in the I-57 southbound lane during November 2014 are presented in Table 3.5.

The following observations were made:

- The dataset was largely complete when the traffic was in free flow.
- The radar sensors had around a tenfold increase in the missing speed data rate during congested periods compared with the monthly average. One primary cause was the slow traffic speed where radar sensors failed to detect the traffic. An illustrative figure plotting the missing data from radar sensors in severe congestion can be found in Appendix B.2 Figure 1.
- The rate of missing data during congestion was significantly higher than the rate of missing count data during the same time interval. This may be explained by the operational principle of sensors (i.e., if no speed data is recorded, the vehicle counts are set to zero).
- The RTMS did not have any missing speed or count records during the congested intervals, but it had higher than average missing data rates over the entire month compared with the radar sensors. As reported in JamLogic, SB7* had low battery and communication timeout issues between November 1 and November 4, which resulted in missing 34.98% of the speed data and 34.38% of the count data.

Table 3.5: November 2014 I-57 Southbound Percent Missing Data

	Entire Period		Peak Hours		Congested Intervals		Free-Flow Interval	
Sensor	**Speed**	**Count**	**Speed**	**Count**	**Speed**	**Count**	**Speed**	**Count**
SB1	1.33%	1.20%	1.54%	0.77%	10.67%	0.00%	1.64%	1.64%
SB2	1.15%	0.75%	3.59%	0.26%	44.00%	0.00%	0.00%	0.00%
SB3	0.83%	0.44%	3.59%	0.26%	33.00%	0.00%	0.00%	0.00%
SB4	0.54%	0.38%	1.79%	0.26%	16.00%	0.00%	0.00%	0.00%
SB5	7.14%	6.91%	10.51%	8.72%	21.33%	0.00%	0.00%	0.00%
SB6	3.68%	3.02%	7.18%	3.85%	58.67%	0.00%	0.00%	0.00%
SB7*	5.19%	5.00%	7.18%	7.18%	0.00%	0.00%	0.00%	0.00%
SB8	1.52%	1.01%	4.36%	1.03%	49.33%	0.00%	0.00%	0.00%
SB9	0.31%	0.08%	2.82%	0.00%	25.33%	0.00%	0.00%	0.00%
Average	2.41%	2.09%	4.73%	2.48%	28.74%	0.00%	0.18%	0.18%

Note: The symbol * denotes an RTMS.

The inconsistency assessment statistics between samples of neighboring sensors are presented in Table 3.6 and Table 3.7. The following findings were summarized from Table 3.6 and Table 3.7:

- The count inconsistencies between sensor pairs were large regardless of the sensor types. The inconsistency can be caused by measurement error from sensors, occlusion (i.e., the vehicle on the closer lane blocking the vehicle on the further lane from the view of the sensor) in heavy traffic, and the location of sensors (e.g., downstream sensors close to the work zone bottleneck may experience slower traffic with daily queues).
- The inconsistency of speed readings between radar and RTMS pairs was relatively larger compared to that of radar–radar sensor pairs.

Table 3.6: November 2014 Data Percent Change on I-57

	Percent Change	
Sensor Pair	**Speed**	**Count**
SB5→SB6	1.64%	23.49%
SB6→SB7*	12.45%	39.64%
SB7*→SB8	10.06%	39.37%
SB8→SB9	6.06%	46.15%

Note: The symbol * denotes an RTMS.

Table 3.7: November 18, 2014 (0600–1100 hours) Data Percent Change on I-57

	Percent Change	
Sensor Pair	**Speed**	**Count**
SB5→SB6	1.19%	28.39%
SB6→SB7*	10.38%	27.94%
SB7*→SB8	5.26%	24.24%
SB8→SB9	6.93%	19.85%

3.2.3 Summary of Data Analysis

Based on the analysis of data in limited time periods and a subset of sensors in two work zones, the following findings were discovered:

- The missing data and inconsistency issues are common in field data, especially if collected in noisy environments (i.e., characterized by large sensor measurement error) such as work zones. These issues were found in the data of both work zones. An additional analysis by Ver-Mac shared with the research team showed that the average missing data rate on I-57 decreased from 4% in 2014 to 1.3% in 2016.
- The I-57 work zone had severe (28%) missing data issues for radar sensors during the congested intervals. The I-80 work zone had a lower missing data rate (< 8%) during congestion, except for specific sensors that malfunctioned (EB9*).
- Both work zones presented data inconsistency issues. Inconsistencies were largest between RTMS and radar sensor pairs, where speed and count errors exceeded 10% and 70%, respectively, in the I-80 work zone.

A preliminary data analysis report was submitted to IDOT and forwarded to the vendor, Ver-Mac. In a follow-up meeting that was held between the research team and Ver-Mac, Ver-Mac provided valuable information on practical deployment considerations and additional data analysis. This

helped the research team analyze the source of sensor measurement errors. For example, the RTMS are often calibrated using radar sensors and can have larger speed measurement errors than radar does if they are not properly calibrated. Owing to calibration difficulty, RTMS are typically placed in locations where they are not expected to move (and therefore require recalibration). These constraints are not considered in the present study; however, they are practical considerations when designing work zone systems.

It is important to note that the missing data or inconsistent data causes challenges for the calibration of microsimulation models in this study, as summarized in Section 3.4. The influence of missing data and inconsistent data on the smart work zone application is algorithm and application dependent. For example, Ver-Mac system produced "slow traffic" and "prepare to stop" messages on the portable changeable message signs on November 26 during the period when congestion was confirmed to be present by field engineers. These messages occurred even in the presence of the high missing data rates. In addition, as demonstrated in the results of Section 4.3, low-quality count data provided by LER does not influence velocity estimates when simple algorithms are used. On the other hand, it can have a much larger influence on back-of-queue estimation when used with a more sophisticated estimation algorithm such as the nonlinear Kalman filter (see Section 4.3)

It is also worth noting that the data analysis findings in this report were limited to one month of data collected by a subset of sensors. A comprehensive, long-term study is required for a more thorough understanding of the expected data quality in work zones across the state of Illinois.

In summary, two occurrences of severe congestion in two work zones were identified from the data analysis and confirmed by field engineers:

- I-80 eastbound direction between 1530 and 1800 hours on May 1, 2015.
- I-57 southbound direction between 1530 and 1800 hours on November 26, 2014.

3.3 MODELING OF WORK ZONES

Two documents provided by IDOT primarily used for the work zone modeling: (1) construction plans, and (2) IDOT design standards. The construction plans were used to identify details of the existing road network such as road geometric design, topography, number of lanes, location of ramps, and speed limit. Further, the construction documents detail the work zone geometry based on the project stage, including location of tapers, closed lanes, and closed ramps. Additional details about work zone designs were found in the IDOT design standards, including taper lengths and work zone speed limits. In summary, the material rendered in both documents was studied to obtain the precise work zone geometry.

The commercial simulation software selected for this project was AIMSUN, which uses a modified Gipps' car-following model [57]. AIMSUN is a traffic simulation software developed by the company Transport Simulation Systems (TSS). The work zones were modeled in AIMSUN in a two-step process.

The first step was to model the existing road network. AIMSUN provides basic tools for manually modeling the road network. Alternatively, it also supports importing the online OpenStreet Map (OSM) file, which provides topological data, containing road network information of user-specified

areas. The models loaded from the OSM files need to be pre-processed because they may contain an inconsistent number of lanes, lane widths, intersection design, road types, and speed limits.

The second step was to model the work zone based on the documentation provided by IDOT. This included activating traffic management strategies such as changes in speed limits and lane closures. The geographical coordinates and topographic features of the OSM models were used to estimate the location of the work zone design elements such as tapers, start of lane closures, and end of lane closures.

One difficulty of this step was that AIMSUN did not formally support tapers such as those found in work zone environments. One solution was to drop a lane at the work zone location and connect it to the upstream road segment using a connecting node that narrowed smoothly, as shown in Figure 3.3a. However, it was found that this approach produced unrealistic merging behavior because the narrowed node did not provide warning of the reduction of lanes to upstream vehicles. Consequently, all vehicles merged to the open lane right before the work zone. The approach adopted in this study was to model work zones as lane closures as shown in black in Figure 3.3b, where the sight-distance of lane closures was set to be the same as the taper length.

(a) Model the work zone by reduction of lanes. (b) Model the work zone as a lane closure.

Figure 3.3: Two approaches for modeling work zones in microsimulation.

The modeled eastbound freeway road section near the I-80 work zone is shown in Figure 3.4. According to the design standards followed in the work zone project, the speed limits in work zones are 45 mph, which, however, is inconsistent with the speed data recorded by the deployed smart work zone system on I-80. This is likely due to drivers exceeding the posted speed limit and not because of measurement error. To capture this behavior in the work zone model, the speed limit in the simulation software was at 65 mph to reflect observations from the field data.

The modeled southbound freeway road section near the I-57 work zone is shown in Figure 3.5. No field speed data was available in the work zone, and consequently the speed limit in the I-57 work zone was set to the posted work zone speed limit value of 45 mph.

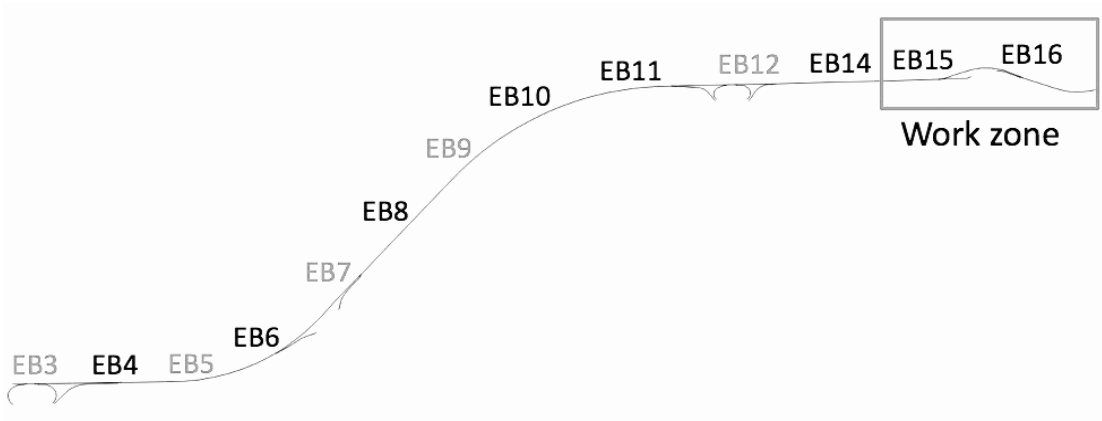

Figure 3.4: Eastbound road network near the I-80 work zone.
The deployed RTMS are labeled in light gray; radar sensors are in black.

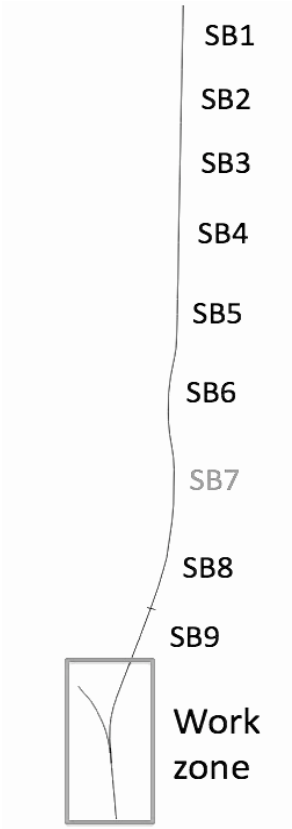

Figure 3.5: Southbound road network near the I-57 work zone.
The deployed RTMS are labeled in light gray; radar sensors are in black.

3.4 CALIBRATION OF WORK ZONES

The simulated microscopic traffic behavior is influenced by a large number of adjustable microscopic parameters. Calibration of a microsimulation model is the selection of a set of values for parameters such that the simulated microscopic traffic exhibits similar macroscopic traffic characteristics as observed in the field (e.g., similar queue propagation speed).

The objective of this study is to reproduce severe traffic congestion in selected periods in two work zones. Therefore, a calibration step was conducted to properly select a set of microscopic parameters.

This section summarizes the calibration process in this study. First, a literature review was conducted to identify the standard procedure and available tools for the calibration of a microsimulation model. Then an automated calibration framework was developed following the standard calibration procedure and using a nonlinear simulation-based optimization program. A sensitivity analysis for identifying the critical parameters to be calibrated and a validation of the developed automated calibration framework can be found in Appendix A. Finally, the calibration results are summarized for each work zone.

3.4.1 Literature Review on Calibration of Microsimulation Models

The standard procedure for the calibration of a microsimulation model can be found in [58]. In general, the calibration procedure consists of five steps, as illustrated in Figure 3.6:

1. Identify a set of sensitive microscopic parameters to be calibrated. Though a large number of microscopic parameters are adjustable, only a subset of parameters is very sensitive in terms of influencing the traffic behavior in a specific simulation setup. In addition, calibrating all microscopic parameters is extremely time consuming and unrealistic in practice. Therefore, it is highly recommended to first identify a small set of sensitive parameters based on the literature review, prior knowledge, and sensitivity analysis techniques [59, 60].
2. Evaluate the default values for the parameters. The simulation outputs using the default values (e.g., velocity or flow measurements) are compared with the field data to compute a measure of goodness of fit. The default parameters can be used as the benchmark for assessing the effectiveness of the calibration.
3. Adjust the values of the selected sensitive parameters. Depending on the initial evaluation result, a subset of the sensitive parameters is adjusted to achieve better goodness of fit. These values can be manually adjusted, which, however, relies strongly on the analyst's prior knowledge. Alternatively, an optimization program can be employed to automate the adjustment of the parameter values, which will be discussed shortly.
4. Simulate the work zone traffic in the microsimulation using the new set of parameters. The microscopic simulation is a stochastic process, and consequently multiple runs (typically ten replications) are required to minimize the dependency of the simulated traffic on the random number generator used in the simulator. Commonly, the microsimulation is the most time-consuming step.

5. Evaluate the simulated traffic using a selected metric that quantifies the goodness of fit to the field data.

Calibration of a microsimulation model is generally a challenging problem owing to the large number of correlated microscopic parameters. The combination of the parameters can explode to millions, which makes an exhaustive search time consuming and impossible in practice.

Earlier attempts are commonly based on trial-and-error manner to manually adjust the parameters that could reproduce the traffic condition as observed in the field. The effectiveness of the manual calibration relies strongly on the analyst's knowledge and can be extremely time consuming, even for a small-scale network and a few parameters [61].

Alternatively, automated calibration has been explored in recent years. The calibration of a microsimulation model is essentially an optimization problem (i.e., maximizing the goodness of fit of the simulated traffic to the field observation data, by adjusting the microscopic parameters). Automatic calibration is a procedure that employs an optimization program in the step for searching potentially better values for the parameters. Compared with manual calibration, automatic calibration has been shown to be capable of significantly reducing the calibration time (from months to hours) while achieving similar calibration accuracy [62].

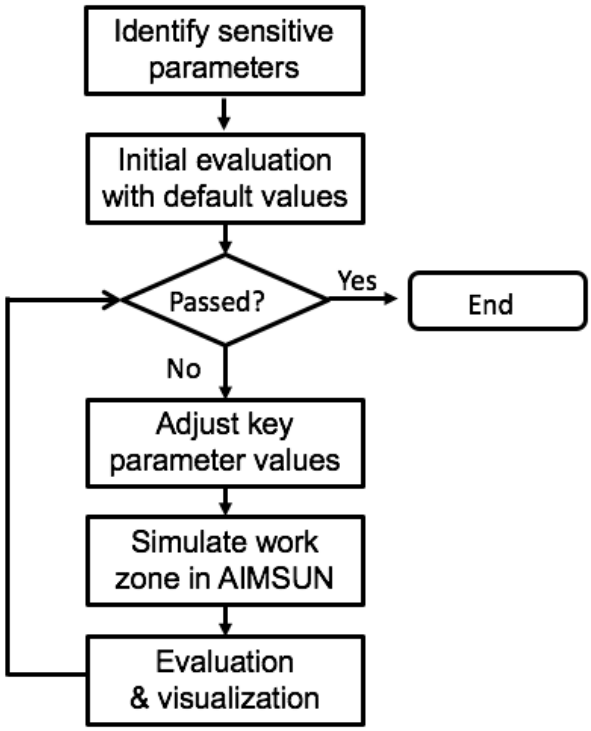

Figure 3.6: Procedure for calibrating a microsimulation model.

A variety of nonlinear optimization programs and commercial software have been previously proposed for the calibration of microsimulation models. Representative algorithms include Simplex [63], simultaneous perturbation stochastic approximation (SPSA) [64, 65], genetic algorithm [64], and OptQuest [66]. A comprehensive comparison of these nonlinear optimization programs on the effectiveness of calibrating microscopic model parameters was reported in the MULTITUDE project [66]. Recently, an advanced nonlinear optimization by mesh adaptive direct search (NOMAD) [67] software was also used for the calibration of microscopic traffic models [68]. Considering the software availability and the implementation effort, this study adopts NOMAD as the nonlinear optimization software in the calibration process.

3.4.2 Automated Calibration Framework

This study adopted the automated calibration approach following the standard procedure shown in Figure 3.6. The nonlinear optimization program NOMAD was integrated with AIMSUN for adjusting the microscopic parameters.

Based on an extensive literature review [58, 60, 62, 63, 69, 70, 71, 72, 73], empirical knowledge, and a sensitivity analysis (which is described in Appendix A), eight parameters were identified as sensitive and associated with two types of vehicles:

- Speed acceptance (*speedAcceptance*). This parameter multiplied by the speed limit on the road section determines the desired speed of vehicles. This parameter was found to be sensitive only for passenger cars.
- Maximum acceleration (*maxAccel*). This parameter was found to be sensitive only for trucks in stop-and-go traffic.
- Sensitivity factor (*sensitivityFactor*). This parameter represents the estimation of a vehicle on the deceleration rate of its leading vehicle. By setting this parameter below or above 1, the following vehicle underestimates or overestimates the deceleration rate of the leading vehicle, hence being more or less aggressive. This parameter was found to be sensitive for both car and truck types.
- Reaction time (*reactionTime*). This parameter is the time for a driver to react to speed changes in the preceding vehicle. This parameter was found to be sensitive for both car and truck types.
- Minimum headway (*minHeadway*). This parameter determines the minimum headway (i.e., the time difference of two consecutive vehicles passing the same location) of a vehicle to its preceding vehicle. This parameter was found to be sensitive for both car and truck types.

The objective of the calibration in this study is to reproduce the severe traffic congestion in a specific period in the work zones, instead of developing a general microsimulation model. Therefore, considering the significant amount of time required in the simulation step, only one replication was simulated for each set of parameters.

The root-mean-square error (RMSE) was selected as the error metric considering its reliable performance for measuring the goodness of fit [66]. Because there was a lack of high-quality flow data from the deployed work zone sensors as reported in Section 3.2, only the velocity data was used in the error metric to calibrate the microsimulation.

The inflow to the modeled freeway section was manually calibrated based on the flow measurement from the first sensor in each work zone. The truck ratio, the on-ramp and off-ramp flows were determined using the Illinois online database http://www.gettingaroundillinois.com/gai.htm?mt=aadt, and http://idot.ms2soft.com/tcds/tsearch.asp?loc=Idot&mod=.

The developed automated calibration framework was validated in a synthetic work zone described in Appendix A.2, where the true values of the calibrated parameters were known. The validation results showed the developed framework could effectively improve the goodness of fit of the simulated traffic to the field data. Meanwhile, the validation results confirmed the difficulty of the calibration of microsimulation models. Owing to the nonlinear correlation between parameters, different combinations of parameter values can achieve similar goodness of fit, which had been previously identified [66]. As a result, the combination of extreme values for two parameters may produce reasonable macroscopic traffic characteristics. However, such extreme values are less desirable, though the corresponding goodness of fit may be optimal. Therefore, after the automated calibration, a final selection step should be performed among the best auto-calibrated parameter values to select a set of plausible parameters based on empirical knowledge.

3.4.3 Calibration Results of Two Work Zones

The calibrated values for the parameters in the I-80 work zone after approximately 1,000 iterations and the final selection are summarized in Table 3.8. The calibrated values achieved an approximately 40% reduction in the speed RMSE compared with the default values.

Table 3.8: Calibrated Values for the I-80 Work Zone

Parameter	Default Value	Calibrated Value
car *speedAcceptance*	1	1.09
truck *maxAccel* (m/s^2)	1	0.82
car *sensitivityFactor*	1	0.5
truck *sensitivityFactor*	1	1.02
car *reactionTime* (s)	0.8	0.6
truck *reactionTime* (s)	0.8	0.8
car *minHeadway* (s)	0	1.5
truck *minHeadway* (s)	0	2.5
speed RMSE	283.2	168.3

m: meter; s: second

The calibrated values for the parameters on I-57 after approximately 800 iterations and the final selection are summarized in Table 3.9. The speed RMSE for the calibrated value decreased by only 8% compared with the default value. The main reason for the insignificant reduction of the RMSE was the high percentage of missing data during the congested period as identified in Section 3.2.

Table 3.9: Calibrated Values for the I-57 Work Zone

Parameter	Default Value	Calibrated Value
car *speedAcceptance*	1	1.1
truck *maxAccel* (m/s^2)	1	0.9
car *sensitivityFactor*	1	1.0
truck *sensitivityFactor*	1	1.0
car *reactionTime* (s)	0.8	0.6
truck *reactionTime* (s)	0.8	0.8
car *minHeadway* (s)	0	2.0
truck *minHeadway* (s)	0	2.0
speed RMSE	337.8	310.4

m: meter; s: second

3.5 SENSOR MODELS

The microsimulation software AIMSUN allows error-free sensors to be placed in the simulation environment, but it lacks realistic traffic sensor error models representative of sensors deployed in work zone environments. Alternatively, AIMSUN can export the trajectory data at a fine granularity for each vehicle, which allows the development of customized sensors. This section presents how microsimulation trajectories are used to generate noisy traffic sensor data that reflects the true errors observed in the field.

3.5.1 Overview of Sensor Types

To better assess how different types of sensors featuring distinct measurement errors affect the traffic estimation accuracy, realistic sensor models were developed to degrade the simulated traffic measurements to be consistent with the data quality observed in practical field deployments. A large variety of sensor technologies have been applied to traffic monitoring. Interested readers are referred to the *Traffic Detector Handbook* [74, 75] for the comprehensive description and evaluation of traffic sensor technologies. In this study, three types of sensors commonly used in work zones were modeled: Doppler radar, LER units (e.g., iCone® sensor), and RTMS.

Doppler radar (heretofore referred to as radar) is widely used in traffic sensing because the technology is mature and the cost is low. Doppler radar relies on the Doppler effect for measuring the velocity of vehicles, and it provides accurate velocity measurement for vehicles (less than 1 mph [76]), although performance degrades at lower velocities, where the Doppler shift is not as prominent. The traffic flow data is obtained by counting the number of velocity measurements recorded during each detection cycle. For best performance, Doppler radar units are commonly

mounted relatively low to the ground (a minimum 3 feet [76]). Consequently, the sensor is prone to occlusion issues (e.g., where one vehicle blocks another vehicle in an adjacent lane from being detected by the sensor), which may result in biased velocity and flow measurements when deployed on multi-lane freeways.

LER units are deployed in traffic control drums for ease of deployment, but they have limited battery capacity available for detection. For long-term deployments, a basic operational mode of sensors consists of the sensor operating for only part of each detection cycle (typically 30 seconds of detection in a 60 second detection cycle, per a 2010 technical report [55]). Consequently, these sensors have measurement errors similar to those found with radar units for velocity and count data, as well as an additional sampling error related to the discontinuous operation.

The RTMS measures the distance to objects in the path of its microwave beam; hence, it is able to detect moving and stationary vehicles in multiple detection zones (lanes). The RTMS is commonly mounted in an elevated position (at least 17 feet [77]), which reduces the occlusion potential and increases the counting accuracy compared with lower positioned sensors. With proper field calibration, the RTMS produces velocity measurements with 10% error, with larger velocity errors in heavy congestion [77].

3.5.2 Generation of Noisy Measurements

A multistep process is used to convert the detailed trajectory data from AIMSUN into noisy sensor data to mimic the field data collected from the sensors described above. The first step is to determine which vehicles pass through the detection zone of a given sensor. The detection zones for each sensor are modeled based on the recommended installation guidelines [76] and the reported field of view. For example, the radar and LER sensors are aimed at oncoming traffic, resulting in a detection zone approximately 140 feet upstream of the sensor, as shown in Figure 3.7. The detection zone of the LER is assumed active for only the first half of the detection cycle, resulting in the detection of only a subset of vehicles. The RTMS detection zone is located at the installation point. For a given detection cycle, the vehicles that pass through the detection zone are potentially available to contribute to the average velocity or count measurements.

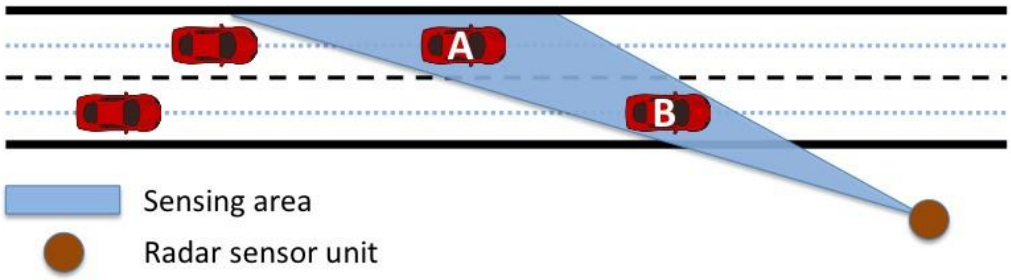

Figure 3.7: Illustration of an occluded vehicle A caused by the presence of vehicle B in the detection zone.

The next step is to discard any vehicle that passes through the detection zone whose trajectory is occluded by another vehicle. As illustrated in Figure 3.7, two vehicles, labeled A and B, travel through the sensing area in the outside lane and inside lane, respectively. Vehicle A is considered occluded if more than p_o percent of the trajectory of vehicle A overlaps with the trajectory of B in the detection zone. The parameter p_o is selected as p_o = 30% which results in the occlusion of approximately 40% of vehicles in heavy congestion. Occluded vehicles are removed for radar and LER sensors, while RTMS are assumed to be mounted in a position to prevent occlusion, but the count is still perturbed by a counting error consistent with the reported accuracy [77].

After occluded vehicles are removed, any vehicle with a velocity outside the measurement range of the sensor is also discarded. The radar and LER sensors have a measurement range of 5~99 mph [76], while the RTMS has a range of 0~110 mph [77].

For vehicles that remain, the measured velocity is assumed to be a reading of the true vehicle velocity perturbed by measurement error. Measured velocities are constructed by adding a measurement error generated from $N\ (0, \sigma)$ to the true velocity, where σ takes two distinct values in free-flow and congested traffic. For the radar and LER sensors, σ is chosen such that the true vehicles are measured with an accuracy of 1 mph, while the RTMS velocities are measured to within 10%. At low vehicle velocities, the errors are increased to 2 mph for radar and LER, and 15% for the RTMS devices. Note that although the measurement error is assumed unbiased, the average velocities and counts are biased because of the sample set (i.e., removing occluded vehicles, which are predominantly from the faster lane of traffic). Finally, the harmonic mean of the noisy velocity measurements is taken as the average velocity reported by the sensor, and the number of measurements is the count.

To model the realistic missing data rates that occur in field deployments, a subset of measurement detection cycles is also discarded, resulting in no data available for estimation during the cycle. Up to 15% of the data from the radar and LER sensors and 3% of the data from RTMS are dropped in during congested conditions, based on the missing data rates observed from work zone field data in Illinois.

CHAPTER 4: TRAFFIC ESTIMATION ALGORITHMS

This chapter is devoted to the description of the traffic estimation algorithms implemented for estimating the velocity, queue length, and travel time. Consider a segment of roadway of length L containing a work zone, observed over a period of time T. The velocity along the roadway is denoted $v\ (t, x)$, where $t \in\ [0, T]$ and $x \in\ [0, L]$. If a queue develops on the segment because of a bottleneck created by the work zone, the length of the queue is denoted $l(t) \geq 0$. Finally, the travel time of a vehicle entering the roadway at time t traveling the length of the road segment L is denoted $\tau\ (t)$. In this study, the velocity along the roadway is directly estimated, which is then used to estimate the travel time and the length of the queue when it occurs. The evaluated traffic estimation algorithms are described next. More technical details can be found in Appendix C.

4.1 SPATIAL INTERPOLATION

A common class of algorithms infer the traffic conditions along the roadway by spatially interpolating the measurement data obtained from sensors. Such strategies include constant interpolation [78], min interpolation [79] adopted by the Texas DOT, averaging interpolation [80], the mid-point algorithm adopted by the Chicago DOT [81] and Wisconsin DOT [81], and the three-segment algorithm [82]. More sophisticated interpolation strategies, such as linear interpolation [83] and quadratic interpolation [84] have also been proposed.

Considering the performance and ease of implementation, the linear spatial interpolation was selected as a representative interpolation algorithm for further evaluation. To estimate the velocity $v(t, x)$ between a pair of sensors located at x_1 and $x_2\ (> x_1)$ with corresponding measured velocities $\tilde{v}_1$ and $\tilde{v}_2$, the estimated velocity $\hat{v}(x, t)$ for $x \in [x_1, x_2]$ is computed as follows:

$$\hat{v}(t, x) = \frac{x_2 - x}{x_2 - x_1}\tilde{v}_1(t) + \left(1 - \frac{x_2 - x}{x_2 - x_1}\right)\tilde{v}_2(t). \tag{4.1}$$

The same process is repeated for each pair of adjacent sensors to obtain the estimated velocity field throughout the spatial domain.

4.2 SPATIO-TEMPORAL FILTERING

One criticism of spatial interpolation algorithms is that they do not directly account for the spatio-temporal dynamics of traffic. A number of research articles have developed algorithms that attempt to circumvent these limitations.

A two-dimensional interpolation algorithm for speed-map reconstruction and travel time estimation was proposed in [85]. This algorithm produces speed estimates at any point (t, x) as a weighted average of four neighboring sensor measurements in the time-space domain; that is, a point of estimation between two sensor deployments (in space) and two sensor reports (in time). The weight

of each measurement is a function of the distance to the point of estimation. This results in a smooth speed surface that is then used to reconstruct vehicle trajectories.

A trajectory reconstruction–based method was explored in [86]. That algorithm relies on first-order traffic flow theory to extrapolate traffic states at sensor locations to an extended segment of road. The general idea is to reconstruct vehicle trajectories using discrete speed observations of vehicles as they cross the sensor location. Each observation is assumed representative of the speed state in a subset of the time-space domain, with a width delimited by the headway between vehicles and projected in time and space (upstream or downstream of the sensor location) based on wave propagation speeds. Once a new observation arrives, the next subset of the time-space domain is determined and the speed state is updated. The vehicle trajectories are reconstructed by concatenating the projected traffic states.

A kernel smoothing technique that incorporates traffic dynamics was developed in [87]. This type of algorithm was further adapted to the context of heterogeneous data sources [88, 89]. More importantly, it was improved in [81] to avoid structural bias in travel time estimation.

The main idea of this family of spatio-temporal estimators is to estimate traffic speed (which is equal to the inverse of the traffic pace) using a weighted average of the available sensor measurements. The weight of each measurement is given by an exponential decay function that penalizes measurements that are distant to the point of estimation. This distance, however, is offset in the time dimension to account for the propagation of traffic waves. An underlying assumption is that the traffic wave propagation velocity is constant for a given traffic state. Because the traffic wave propagation velocities in congestion and free flow differ, two estimates are produced: one assuming free flow and one assuming congestion. The final estimate is obtained as a convex combination of the free-flowing and congested estimates.

Considering the scalability, robustness and ease of online implementation required for this research, the filtered inverse speed-based estimation algorithm proposed by Van Lint [81] was selected as representative of the spatio-temporal estimation algorithms.

The selected parameter values for the implemented spatio-temporal algorithm can be found in Appendix C.1.

4.3 KALMAN FILTER

The Kalman filter [92] is an algorithm used to estimate the state of a linear system by correcting a model-based prediction with measurement data. The Kalman filter and its nonlinear extensions necessary for traffic estimation can be understood by posing the model and sensor measurement processes in state space form as follows:

$$\begin{cases} x^n = \mathcal{F}(x^n) + \eta^n, \\ \tilde{y}^n = \mathcal{H}(x^n) + \epsilon^n. \end{cases} \tag{4.2}$$

The first line in Equation 4.2 is known as the evolution equation, where x^n is the traffic state vector at time step n to be estimated, $\mathcal{F}$ denotes the traffic flow model used to predict the traffic state at time

n given the traffic state at time $n - 1$, and $\eta^n \sim (0, \boldsymbol{Q})$ is a white noise process with covariance $\boldsymbol{Q}$. The second line in Equation 4.7 is the observation equation that relates the vector of measurements $\tilde{y}^n$ received at time n with the traffic state variables x^n through the measurement model $\mathcal{H}$. The random variable $\epsilon^n \sim (0, \boldsymbol{R})$ denotes the measurement error distribution and is modeled as white noise with covariance $\boldsymbol{R}$. The Kalman filter and its nonlinear variants are sequential-state estimators that are optimal estimators (in the best linear unbiased sense) of the state x^n given a sequence of measurements $\tilde{y}^0, \cdots, \tilde{y}^n$.

Considering the nonlinearity of the traffic models, a number of variations of Kalman filter have been explored for estimation of the traffic conditions, including the extended Kalman filter (EKF) [19], the unscented Kalman filter (UKF) [93], the mixture Kalman filter (MKF) [94, 95], the particle filter (PF) [96, 97], and the ensemble Kalman filter (EnKF) [98].

EKF relies on the linear approximation of a nonlinear system, and it has been used to estimate the traffic density [19, 99]. The computation of the Jacobin matrix in the linearization step is in general computationally heavy; hence, a simultaneous perturbation technique was proposed [100] to improve the efficiency of the linearization step.

In the traffic estimation, the nonlinearity of the traffic dynamics comes from the nonlinear relationship between the flow and density. The empirical nonlinear relationship, known as the fundamental diagram, can be approximated by a piecewise linear function. Physically, this indicates the nonlinear system (Equation 4.2) consists of several modes (i.e., free flow or congested) under which the system is linear. Based on this observation, the MKF was proposed [94, 95, 101] to model the traffic as a switched state system.

The linear approximation of the EKF can give poor performance for a nonlinear system, and the piecewise linear assumption on the fundamental diagram. Therefore, UKF [102] has been developed based on a deterministic sampling technique to estimate the propagation of the error covariance matrix, which does not require the linear approximation or assumption.

A more general approach is the Monte Carlo based PF [96, 97, 103], which can be applied to generic nonlinear systems with possibly non-Gaussian distributions. Compared with the UKF, PF gives higher estimation accuracy but at a cost of computationally expensive [104]. Assuming all probability distributions associated in the system are Gaussian, EnKF [98, 105] can achieve similar performance as PF and is more computationally efficient.

In summary, the EKF, MKF, UKF, EnKF rely on linearization of the system for closure assumptions on the state error distributions, while the PF is a fully nonlinear Bayesian estimator that can be computationally expensive for large systems. Consequently, the EnKF is implemented as representative filtering algorithm for work zone traffic state estimation. More technical detail of the EnKF algorithm and its implementation can be found in Appendix C.2.

4.4 BACK-OF-QUEUE AND TRAVEL TIME ESTIMATION

In this study, given an estimate of the velocity $\hat{v}(t, x)$ in space and time, a standard approach across algorithms was used to estimate the length of the queue and the travel time.

Algorithms specifically for queue estimation have also been previously developed. A classic approach is to estimate the queue length based on the cumulative inflow and outflow [109, 110], which is, however, sensitive to the length of the road and the measurement error of sensors. Higher queue length estimation accuracy can be achieved with more-advanced techniques, such as incorporation of the queuing dynamics [111] and the Kalman filter [112].

For fair comparison of the implemented algorithms covering three levels of sophistication, the queue length is computed based on the estimated velocity field. Specifically, the estimated length of the of the queue $\hat{l}(t)$ is determined as the maximum length of any consecutive segment in the velocity field such that $\hat{v}(t,x) < \alpha$, where α is a threshold denoting congested traffic velocities. In this study, α was selected as 40 mph.

This study uses the speed-based travel time estimation method [113] considering its simplicity. The travel time is computed using an instantaneous [114] travel time estimate:

$$\hat{\tau}(t) = \int_0^L 1/\hat{v}(t,x)dx. \tag{4.3}$$

The instantaneous travel time is valid under the assumption that the velocity field is constant over the time interval $[t, t+\tau(t)]$, which may fail in scenarios with rapid queue growth or dissipation. The primary benefit of the instantaneous travel time is that it does not require the future traffic state to be predicted. Other statistical travel time estimation and prediction models using historical data are discussed in [115, 116].

CHAPTER 5: COMPARATIVE ANALYSIS

This chapter summarizes the key findings based on the quantitative comparison across various sensor network configurations and traffic estimation algorithms. A subset of the simulation results from the I-80 work zone are visualized and discussed in this chapter to justify the findings. Similar findings were obtained from the I-57 work zone, and the complete simulation results are included in Appendix D.

5.1 TRAFFIC ESTIMATION ERROR METRICS

The error metrics used to assess the performance of the various estimators are briefly described. To calculate the errors, the true state to be estimated is first calculated from the AIMSUN trajectory data. The true velocity field (Figure 5.1a), true queue length (Figure 5.1b), and true travel time (Figure 5.1c) are constructed on a finely discretized spatio-temporal grid with $m \in \{1, \ldots, m_{max}\}$ space cells of length 50 meters and $n \in \{1, \ldots, n_{max}\}$ time steps with a duration 5 seconds. Within each grid the true velocity $v(n, m)$ is computed using Edie's definitions [117]. The true travel time $\tau\ (n)$ is taken as the average travel time of all vehicles entering the roadway during the time step n, and the true length of the queue $l(n)$ is computed as the maximum length of a space segment with a velocity of less than 40 mph.

The *mean absolute error* (MAE) is used as the error metric to quantify the estimation accuracy. Four types of MAE errors are computed, namely, (1) e_v , the MAE the estimated velocity over the entire spatio-temporal domain; (2) e_v^q , the MAE of the estimated velocity in an area near the back of the queue (i.e., the error of the velocity in an area defined by ± 0.5 mile around the true location of the back of the queue); (3) e_l, the MAE of the estimated queue length; (4) e_τ , the MAE of the estimated travel time.

Specifically, given the estimated velocity $\hat{v}(n, m)$, the MAE of the velocity estimates over the entire time-space horizon is defined as follows:

$$e_v = \frac{1}{n_{max} i_{max}} \sum_{m=1}^{m_{max}} \sum_{n=1}^{n_{max}} |\hat{v}(n, m) - v(n, m)|. \tag{5.1}$$

The metric e_v measures the average estimation accuracy of the velocity over the entire spatio-temporal domain. However, the most safety-critical area is the area around the location of the end of the queue, where accurate velocity estimates are most desirable. Therefore, the MAE of velocity estimates around the queue e_v^q is introduced:

$$e_v^q = \frac{1}{M} \sum_{n=1}^{n_{max}} \sum_{m=m_-(n)}^{m_+(n)} |\hat{v}(n, m) - v(n, m)|, \tag{5.2}$$

where $m_-(n), m_+(n)$ denotes the ± 0.5 mile location of the end of the queue at time step n. The summation of the absolute error is averaged over the number of cells M involved in the computation.

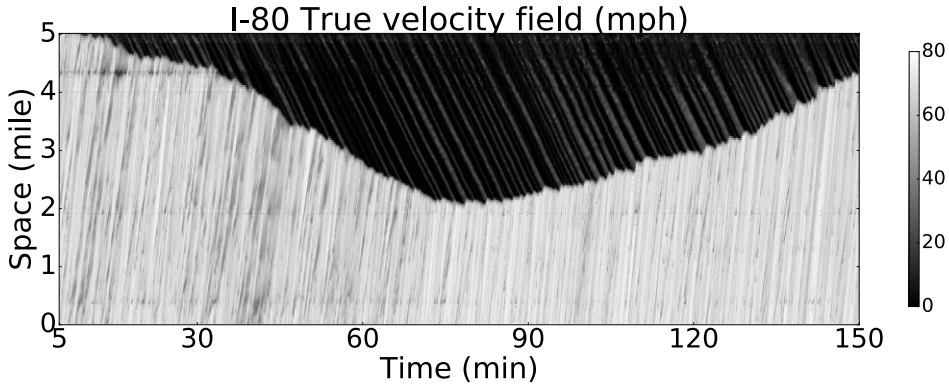

(a) True velocity field over 5 miles and 2.5 hours

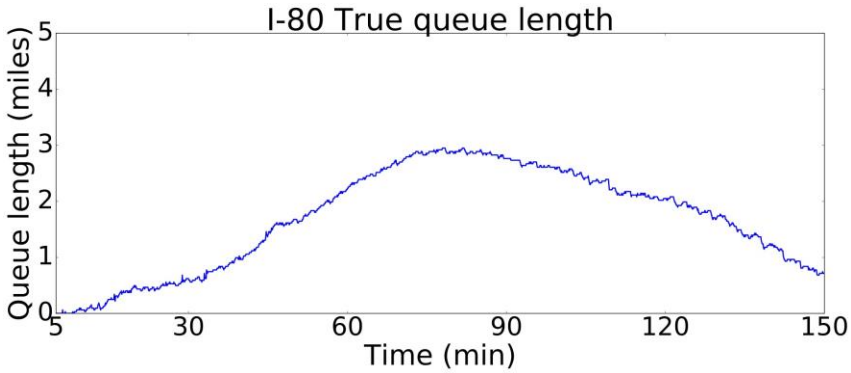

(b) True queue length over 2.5 hours.

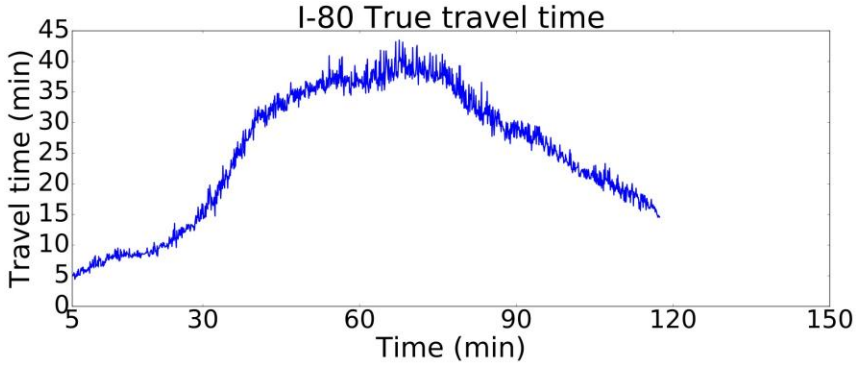

(c) True travel time over 2.5 hours. The true travel time was not obtained in the last period because vehicles that entered the road segment after approximately 2 hours did not exit before the simulation stopped.

Figure 5.1: True state of the (a) velocity field, (b) queue length, and (c) travel time obtained in simulation for I-80 over 5 miles between 1530 and 1800 hours on May 1, 2015.

Similarly, the MAEs of the queue length e_l and the travel time e_τ are defined as follows:

$$e_l = \frac{1}{n_{max}} \sum_{n=1}^{n_{max}} |\hat{l}(n) - l(n)|, \tag{5.3}$$

and

$$e_\tau = \frac{1}{n_{max}} \sum_{n=1}^{n_{max}} |\hat{\tau}(n) - \tau(n)|. \tag{5.4}$$

5.2 ALGORITHMS AND SENSOR SPACINGS

In the first set of experiments, the influence of the sensor spacing and traffic estimation algorithm on the travel time, queue length, and velocity estimation error are analyzed. For each algorithm, 11 spacings ranging from 1/8 mile to 5 miles are considered for I-80. All sensors are assumed to be RTMS in these experiments. Similar findings are made for other types of sensors and on I-57, which are attached in Appendix D.

For each experiment, the MAE on the velocity estimate is computed both as an average over the entire spatio-temporal domain, as well as in the area immediately around the true back of queue (± 0.5 mile) as identified in AIMSUN. The resulting errors as a function of the algorithm type and sensor spacing are shown in Figures 5.2 and Figure 5.3. As expected, as the density of sensors increases; all algorithms result in lower velocity errors, with the best performance (about 5 mph error overall and 6 mph around the queue) by the linear interpolation algorithm with sensors placed every 1/8 mile. Not surprisingly, all algorithms perform worse in the neighborhood of the queue compared with the MAE reported over all space and time, which is unfortunately where the errors may be most safety-critical. The spatio-temporal algorithm has the highest error around the queue, which results in higher total MAE compared with the spatial interpolation algorithm. Note that the algorithm was originally proposed as an offline algorithm [81], and the performance may change if additional measurement data is available for smoothing. At very dense sensor spacings, the EnKF performs worse than the interpolation and smoothing algorithms because the velocity is computed from the density estimate through (4.9) rather than being directly estimated, as in the better-performing algorithms. However, in the neighborhood of the queue, the EnKF localizes the queue more accurately, which generally results in higher-quality velocity estimates in the neighborhood of the queue.

The general trend of the MAE for the queue length estimation (Figure 5.4) is similar to the velocity MAE. This is a direct result of the fact that the queue length is estimated from the velocity field, and consequently improvements on the velocity field result in better queue length estimates. The true maximum true queue length during the simulation is approximately 3 miles. Traffic in the queue is characterized by speeds less than a threshold speed, set as 40 mph in the present study. The EnKF uses a traffic model and uses the flow measurements from RTMS to consistently outperform the other estimators across a wide range of sensor spacings.

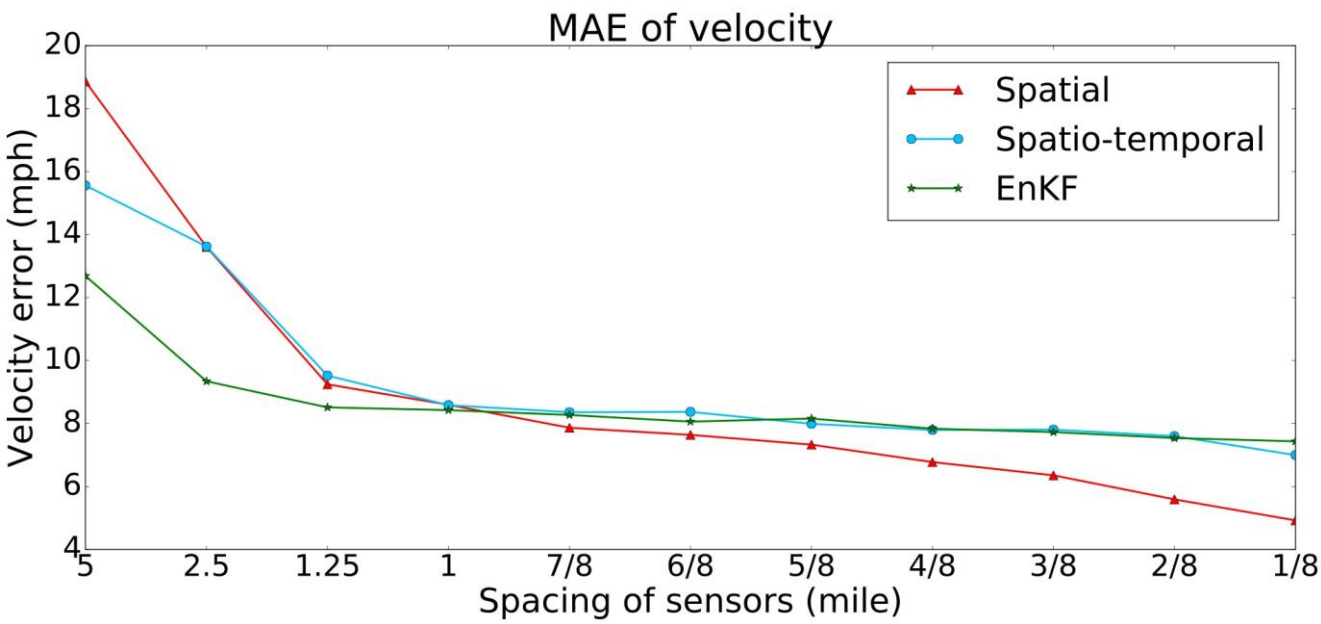

Figure 5.2: MAE of the velocity field over the entire spatio-temporal domain using RTMS across a range of spacings.

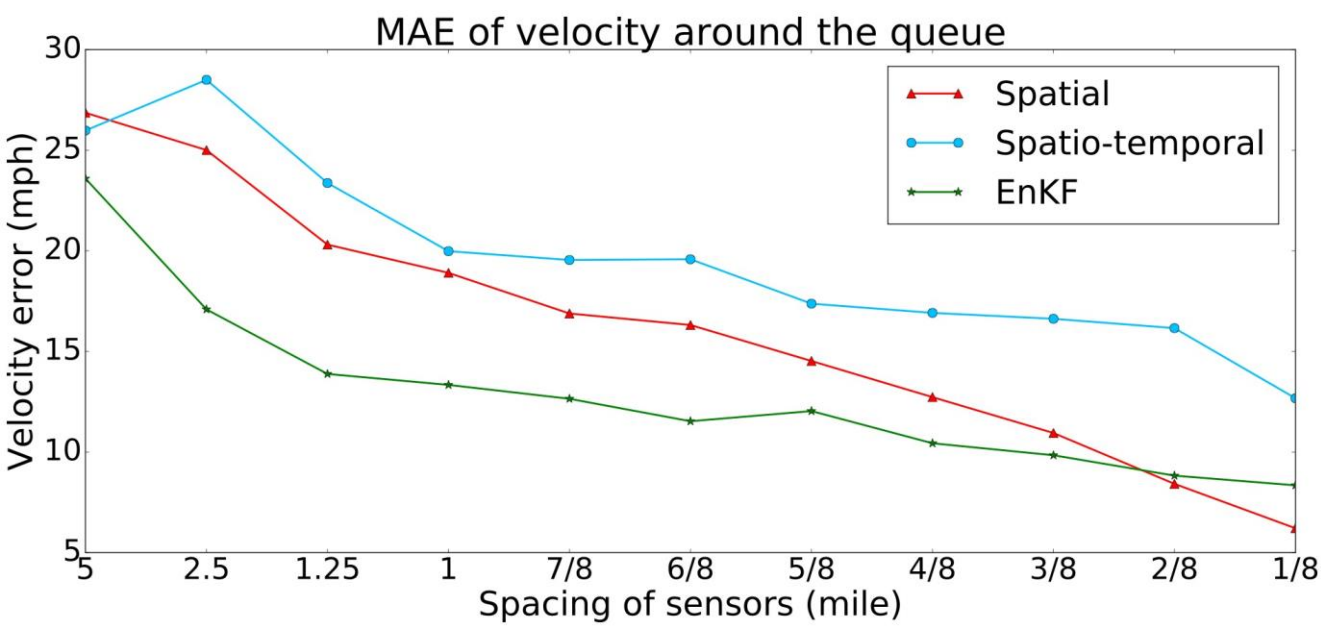

Figure 5.3: MAE of the velocity field around ± 0.5 mile of the location of the end of the queue using RTMS across a range of spacings.

Finally, the MAE of the travel time estimation over a 5-mile distance is shown in Figure 5.5. The travel time of the road section in free flow is around 5 minutes, and the longest travel time during congestion is 40 minutes. The EnKF is generally the best-performing travel time estimator, and it offers slightly improved performance over the spatio-temporal smoother. Recall that the spatio-

temporal algorithm directly estimates the pace of traffic (i.e., the inverse of traffic velocity), which results in a better estimate of the travel time than the purely spatial interpolation algorithm. The MAE for travel time is relatively large for all algorithms independent of the spacing, and the largest source of error is due to the use of the instantaneous travel time calculation (Equation 4.21), not the underlying velocity estimate. In fact, the true instantaneous travel time has an MAE of more than 6 minutes, which is comparable to the MAE observed in the travel time estimates of the best-performing algorithms. In traffic conditions with slower dynamics (e.g., in free flow or in complete congestion), the use of the instantaneous travel time may result in lower errors.

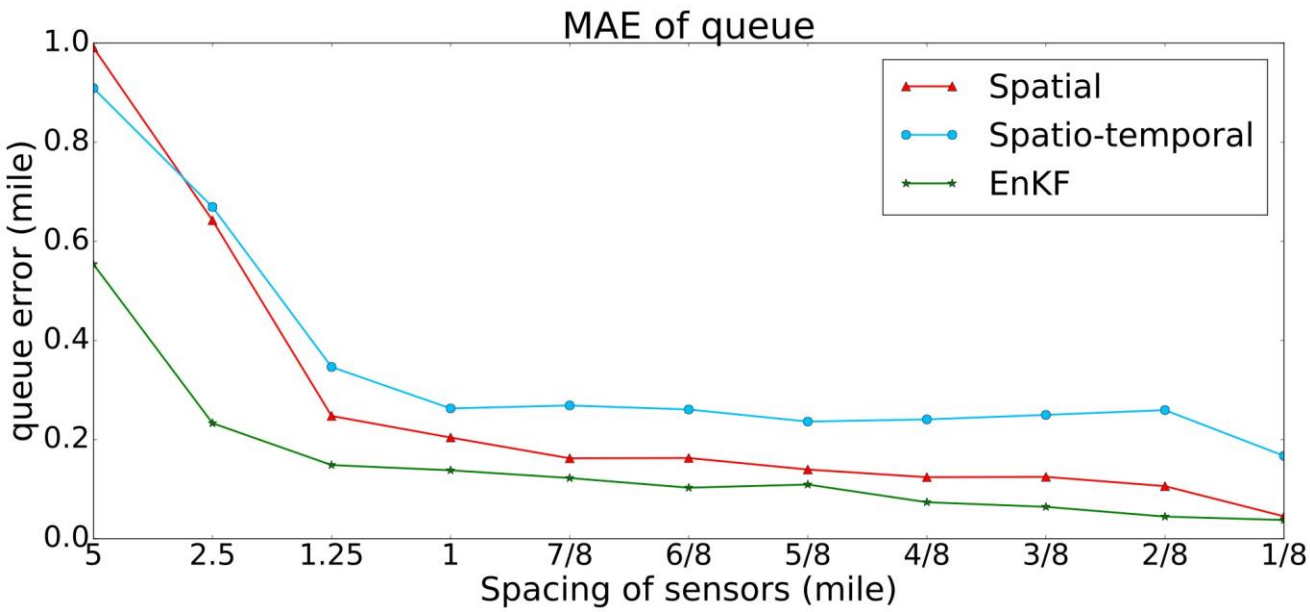

Figure 5.4: MAE of the queue length estimation using RTMS across a range of spacings.

5.3 TYPE OF SENSORS

In the next set of experiments, the influence of the sensor type (i.e., RTMS, radar, and LER) and the errors they introduce were compared across algorithms. Recall that the RTMS offers the lowest-quality velocity measurement of individual vehicles but provides more reliable count data than the radar-based sensors. The MAE for the estimated traffic velocity, the queue length, and the travel time are shown in Figure 5.6a, Figure 5.6b, Figure 5.7a, Figure 5.7b, respectively, for sensors placed at a spacing of 1 mile.

To understand the potential benefit of improved sensor technologies, traffic estimates using an ideal sensor are also generated. The ideal sensor is assumed to have zero error (i.e., it measures the velocity of every vehicle exactly and has no occlusion or dropped packets). It does have a quantization error because the count and velocity are computed within a single detection cycle. For example, if the aggregation interval is 30 seconds, the quantization error (e.g., including or excluding a single vehicle near the cycle boundary) introduces a change in the flow of 120 vehicles/hour/lane. Algorithms running with measurements from the ideal sensor have velocity, queue, and travel time

errors that are similar to those of the RTMS, which indicates that quantization error is the largest source of remaining error from the existing sensors.

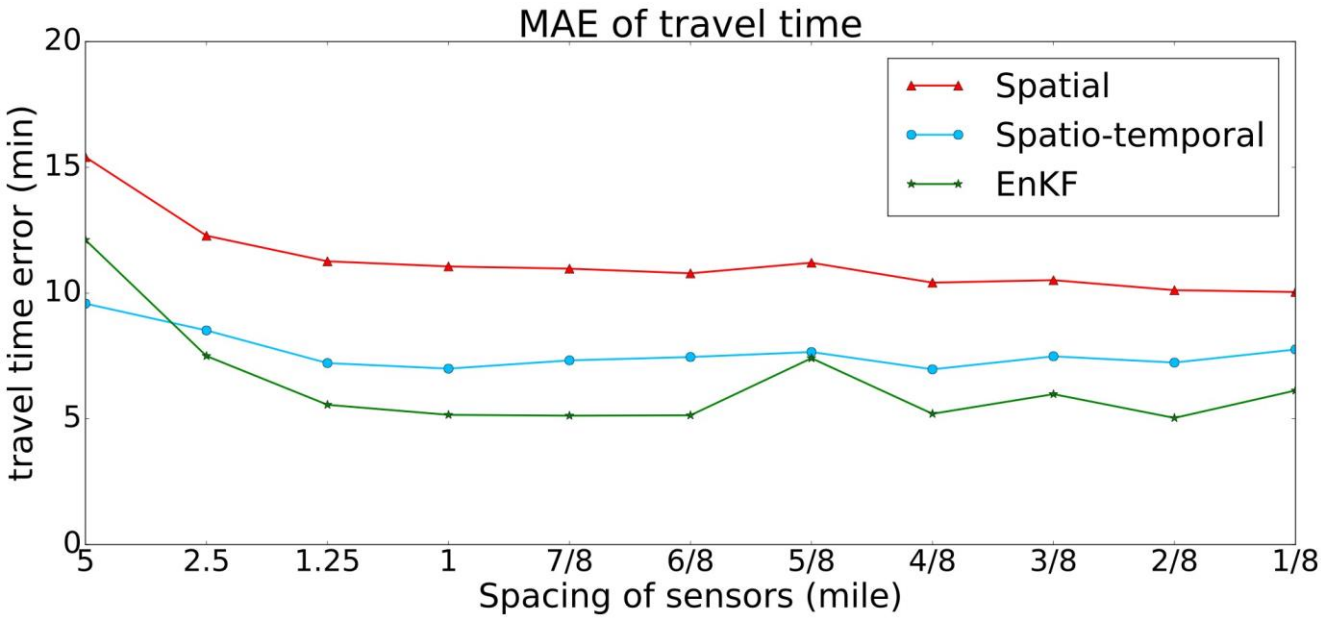

Figure 5.5: MAE of the travel time estimation using RTMS across a range of spacings.

The analysis also indicates that the EnKF algorithm is the most sensitive algorithm to the sensor type, and it provides the poorest velocity estimates when combined with LER sensors. This is due to the reliance of the EnKF algorithm on accurate flow data, which is degraded in the LER devices because vehicles are recorded for only a portion of the detection cycle (resulting in increased quantization error), and the counts are prone to larger occlusion errors. Across all traffic quantities and all algorithms, the radar and RTMS offer at least as good or better accuracy performance than the LER devices. The use of LER devices may still be warranted if the cost of the LER allows more sensors to be deployed compared to RTMS or radar systems.

5.4 ACCURACY OF SENSORS

The third set of experiments was to compare the influence of the accuracy of individual sensors with the estimation accuracy.

Synthetic sensors that may be available in the future were simulated for the RTMS, radar, and LER sensors. The synthetic sensors feature reduced the standard deviation of the measurement noise (more-accurate sensors) and the missing data rates (more reliable sensors). For example, a sensor RTMSx2 denotes a synthetic RTMS whose measurement noise and the percentage of missing data are reduced by a factor of 2 from the currently available RTMS in the market. In total, seven synthetic sensors were simulated: RTMSx2, RTMSx4, RTMSx8, RADARx2, RADARx4, RADARx8, and LERx2. In addition, an ideal type of sensor without measurement error was simulated to assess the maximum

improvement of the estimation accuracy that can be obtained by improving the accuracy of individual sensors, which was addressed in the discussion of the last experiment in Section 5.3.

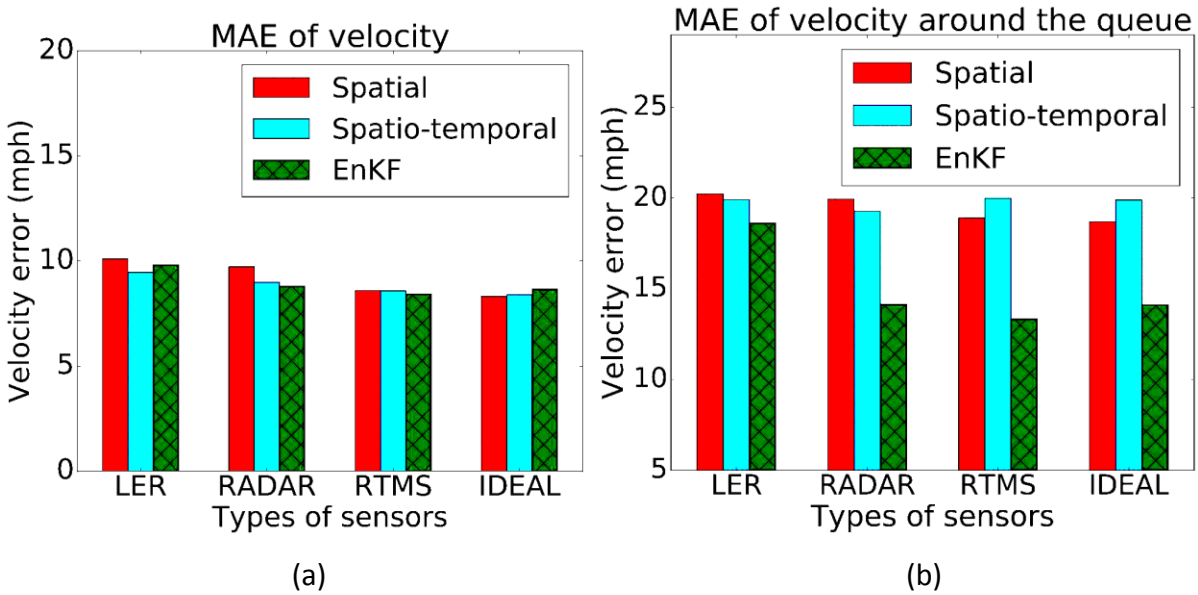

Figure 5.6: MAE of the velocity estimation: (a) over the entire spatio-temporal domain, and (b) ± 0.5 mile around the end of the queue with different types of sensors at 1 mile spacing in the I-80 work zone.

It should be noted that the occlusion error is caused by the operation principle of the radar and LER sensors. Hence, the same occlusion model as described in Section 3.5 is used for the synthetic radar and LER sensors.

The MAE estimation errors of the velocity, queue length, and travel time using multiple levels of accuracy of RTMS at 1 mile spacing are compared in Figure 5.8a, Figure 5.8b, Figure 5.9a, Figure 5.9b. As shown in the figures, further improvement of the accuracy of an individual RTMS provides negligible benefit for the estimation accuracy. Recall in the analysis of the influence of sensors types that the quantization error was around 5%. The existing commercial RTMS already achieve flow measurements to within the 5% error, which indicates that measurement accuracy will be dominated by the quantization error even if sensor accuracy is improved. Marginal benefit will be obtained if the quality of the sensing device is improved beyond the current market technologies. Similar findings were found with other types of sensors, and the general trends are similar at other sensor spacings.

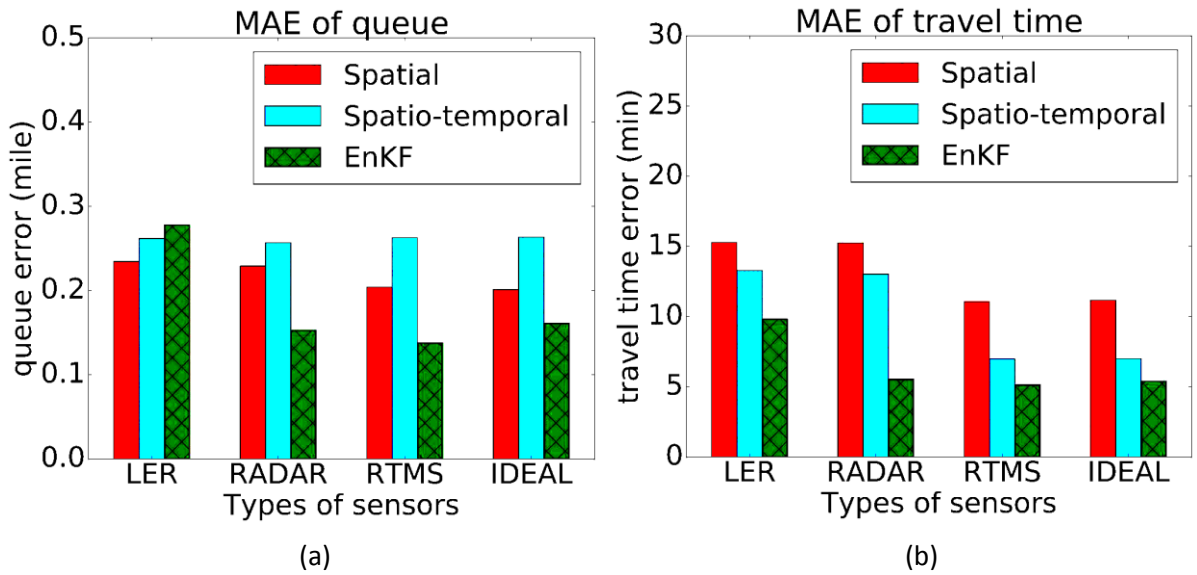

Figure 5.7: MAE of the (a) queue estimation, and (b) travel time estimation with different types of sensors at 1 mile spacing in the I-80 work zone.

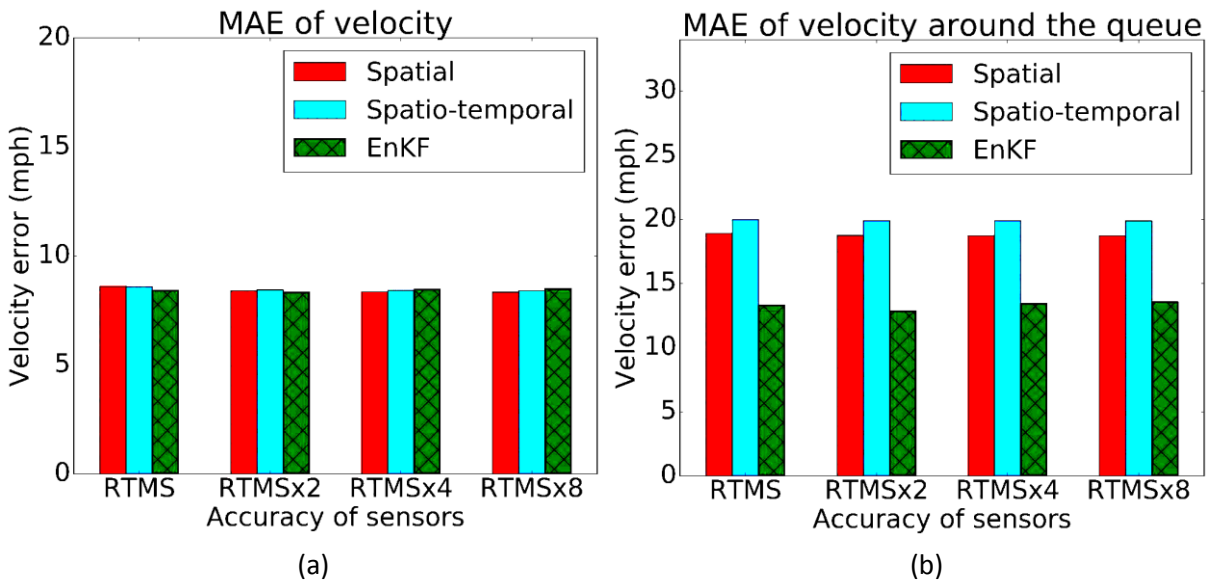

Figure 5.8: MAE of the velocity estimation: (a) over the entire spatio-temporal domain, and (b) ± 0.5 mile around the end of the queue using RTMS with multiple levels of accuracy at 1 mile spacing in the I-80 work zone.

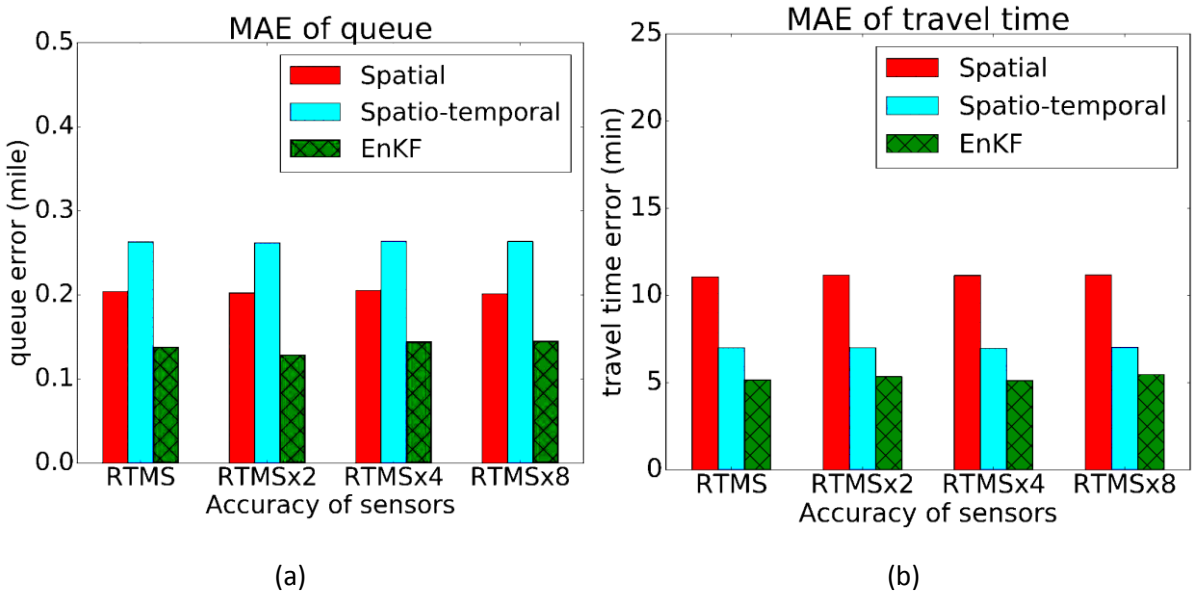

Figure 5.9: MAE of the (a) queue estimation, and (b) travel time estimation using RTMS with multiple levels of accuracy at 1 mile spacing in the I-80 work zone.

5.5 COST ACCURACY ANALYSIS

This section summarizes the cost accuracy analysis based on the estimation results across different sensor network configurations and algorithms.

The cost analysis was conducted in collaboration with IDOT, which provided several sets of cost data from deployed smart work zones. Typically, the smart work zone system is contracted to a vendor. The vendor is responsible for the deployment, maintenance, and removal of the smart work zone system. The total price of a system is provided by the vendor, which varies in the number and types of sensors used, as well as the duration of the project.

One dataset from IDOT estimated that the unit monthly cost for the radar sensor was approximately $1,500, including deployment and removal costs based on two projects of 5-month durations (Contract No. 76D20 and No. 76D21). A separate dataset provided the cost of different type of sensors in the Ver-Mac system, which likely did not include the overhead cost from the deployment and removal of the system. Based on this dataset, the unit monthly costs for the RTMS and the radar are in the ranges $600 to $1,000 and $400 to $700, respectively.

The cost analysis in this study used the monthly cost per sensor, excluding the initial deployment and final removal costs. Based on the limited cost data, the monthly cost of the RTMS is assumed to be $1,000 while the radar is $700.

The cost accuracy curves for the velocity, queue length, and travel time using sensor types and algorithms are plotted in Figure 5.10, Figure 5.11, Figure 5.12, and Figure 5.13. Two findings can be obtained from the curves.

First, the improvements of the estimation accuracy for the velocity and the queue are marginal after the monthly cost of $10,000 (approximately 10 RTMS or 14 radar units deployed in 5 miles for I-80). The travel time estimation is consistently poor regardless of the algorithms, type, or number of sensors. As discussed previously, the reason is that the dominating source of error of the travel time is the use of instantaneous travel time estimation scheme. A predictive travel time model is critical for accurate travel time estimation.

Second, the nonlinear Kalman filter algorithm is promising for achieving the same level of traffic estimation accuracy at lower cost. At the same system cost, the additional radar sensors (because of their lower price) provide higher estimation accuracy than the more-accurate but fewer RTMS. Considering the lower price for radar sensors, the combination of nonlinear Kalman filter algorithm and radar sensors appears to be the most cost effective.

The cost accuracy analysis in this study was based on very limited cost data. It did not consider the cost associated with the deployment, calibration, and removal of sensors. The actual unit price of sensors may also vary depending on the number of sensors deployed.

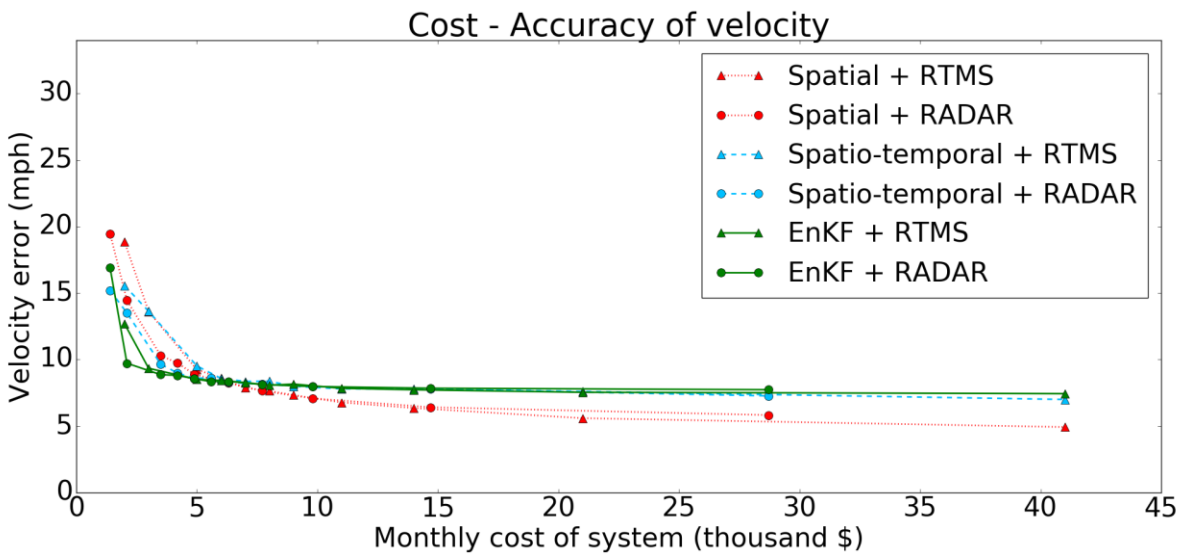

Figure 5.10: Cost accuracy for the velocity estimation over the entire spatio-temporal domain in the I-80 work zone.

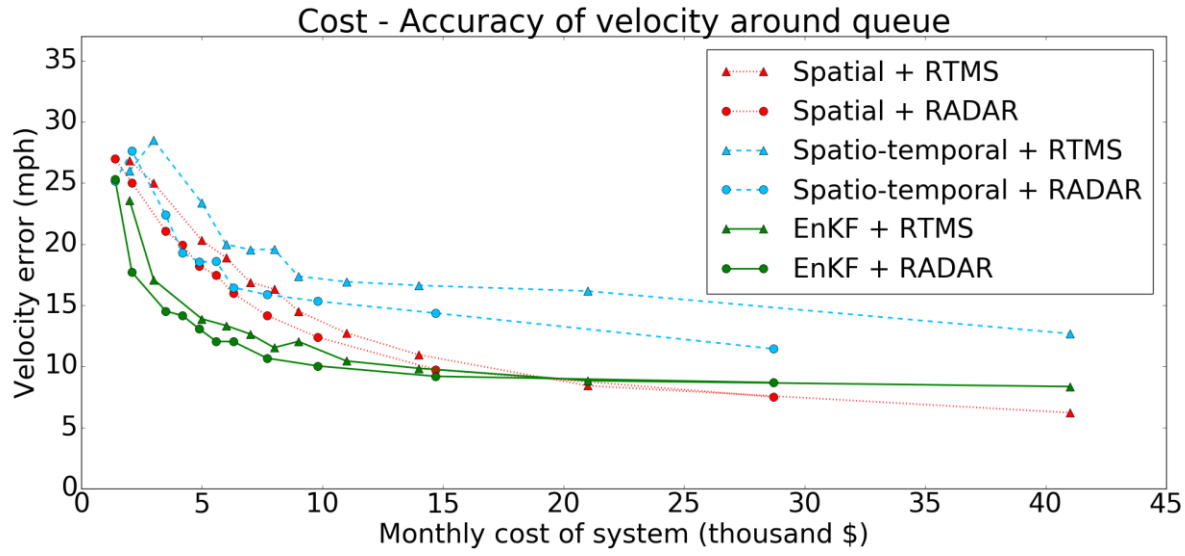

Figure 5.11: Cost accuracy for the velocity estimation at ± 0.5 mile around the queue in the I-80 work zone.

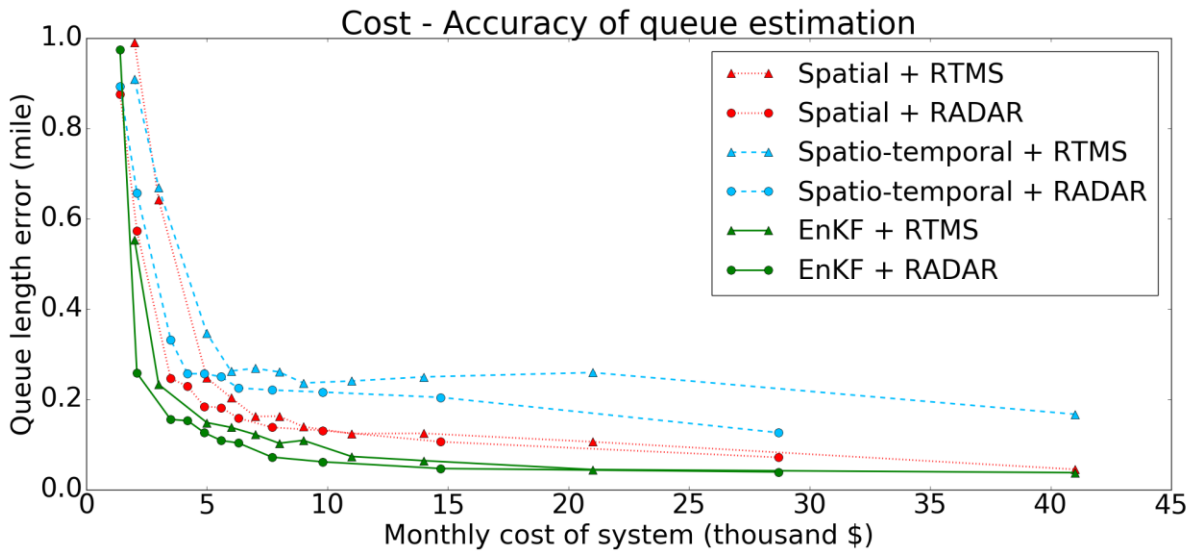

Figure 5.12: Cost accuracy for the queue length estimation in the I-80 work zone.

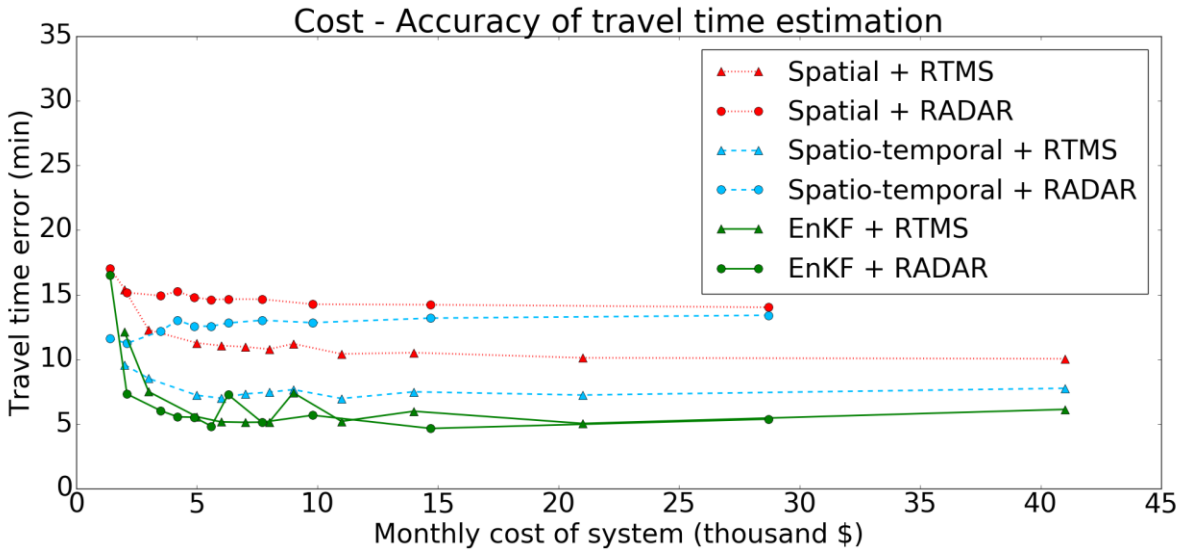

Figure 5.13: Cost accuracy for the travel time estimation in the I-80 work zone.

CHAPTER 6: SUMMARY AND CONCLUSIONS

This study evaluated a variety of sensor network configurations and algorithms with different levels of sophistication to estimate the traffic velocity, from which back-of-queue and travel time were estimated. The main outcomes from this report and potential suggestions for future work zone deployments are provided next. Due to the limited nature of the present study (e.g., experiments on two work zones in microsimulation), the suggestions should not be viewed as a formal guideline. They suggestions are based on the conclusions supported by this study, which should be verified with field deployments before a guideline can be constructed. The main findings and outcomes are as follows.

- The spacing of sensors is an important factor for improving the accuracy of traffic estimation, especially at greater than 0.5 mile sensor spacings. When the sensor spacing is smaller than 0.5 mile, the benefit of additional sensors or the choice of algorithm is marginal (i.e., less than 5% per sensor). It should also be noted that the spacing or locations of sensors also subject to the geometric constraints of the work zone and the work zone system requirements. For example, this study did not consider the proper locations for PCMS to disseminate the traffic condition information, and it is noted that there may be benefit to locating a sensor at the same location as a PCMS. Sensor spacings above a mile have potential to significantly increase errors especially in the neighborhood of queues, and should be considered only on a case by case basis.

  Outcome: It is suggested that sensor spacings of less than 0.5 mile are unlikely to provide significant benefit in the accuracy of estimating traffic conditions. Denser sensor spacings could still be warranted based other considerations (e.g., to co-locate with a PCMS).

- The advanced nonlinear Kalman filtering algorithm is promising for achieving the same level of estimation accuracy with fewer sensors, and consequently at a lower sensor deployment cost. Implementing advanced algorithms (such Kalman filtering) requires significant amount of additional implementation effort compared to the simpler interpolation algorithms, which in turn can increase the cost of the smart work zone system. To reduce the deployment effort, all the source code developed in this study is publically available. It may require significant training to use the algorithm in practice.

  Outcome: The advanced algorithms are used as a proof-of-concept that sophisticated algorithms may reduce the error, especially when sensor spacings are high. Due to the implementation complexity of the algorithm, it is not expected that many commercial vendors will be able to implement the algorithms without significant training from the research community, which remains an important challenge to its implementation.

- The analysis indicates, when using simple algorithms (spatial interpolation and spatio-temporal filtering), the types of sensors have insignificant influence on estimation accuracy of the traffic conditions. Meanwhile, the advanced EnKF algorithm is sensitive to the sensor type due to its reliance on accurate flow data. Considering the fact that advanced algorithms are not yet commercially available, it is concluded that the sensor type is not a determining factor

in the current smart work zone system. The types of sensors should be determined based on other practical requirements and limitations in the field beyond estimation accuracy, which were not comprehensively investigated in this study. For example, one smart work zone vendor confirmed that the RTMS requires significantly more effort for installation and calibration, and hence should not be installed in a location that will require moving the sensor as the project progresses through the construction phases. In other applications, deployment of several RTMS in the work zone is desired since the more-accurate flow data from RTMS can be used to obtain performance measures of the smart work zone system, such as the total delay.

> ***Outcome***: The analysis indicates the types of sensors do not have significant influence of the performance of existing smart work zone systems. It is suggested the choice of sensor types should depend on the specific requirements and constraints in each work zone.

- Improving the accuracy of existing sensors provides marginal benefit. The main reason is that the dominating sources of the measurement error are the quantization error and the occlusion error. Based on the data quality analysis, the findings in this study suggest that it is more important to increase the reliability of sensors. For example, there are many causes for the data quality issues ranging from sensor failures to communication failures (e.g., caused by the cellular network provider). Some of the causes may be difficult for the work zone vendor to resolve directly, such as the prioritization of voice communications over data communication by the cellular providers.

  > ***Outcome***: It is suggested that the current smart work zone systems are not constrained by the accuracy of the individual sensors. It is also suggested that the smart work zone systems have varying degrees of data quality problems such as missing data that could be monitored and potentially reduced to improve the work zone performance.

- The travel time estimation is consistently poor for all algorithms and sensor networks investigated in this study. The main reason is that the instantaneous travel time calculation is a poor estimator of the true travel time in a dynamic traffic environment. In addition, the use of Bluetooth sensors can only provide the travel time of vehicles that just exited the work zone. Consequently, the travel time estimation even using Bluetooth sensors is not likely to improve the accuracy of the travel time estimates when the traffic conditions (and consequently the travel time) are quickly changing. Further predictive analytics are needed to reduce the travel time error.

  > ***Outcome***: It is suggested that the future development of travel time prediction algorithms may lead to improvements in travel time estimates in work zones when the traffic conditions are quickly changing. No travel time prediction algorithms were investigated/evaluated in the present study.

- A cost performance analysis was conducted to identify the most cost effective configuration of sensor networks and algorithms for estimating three quantities: the traffic velocity, the queue length, and the travel time. The recommended sensor network and algorithm are summarized in a table for each estimated quantity. Considering the fact that the advanced

algorithm (EnKF) is unlikely to be implemented in practice in the near future, a separate set of suggestions of the sensor network and algorithm is summarized for each estimated quantity excluding the use of advanced algorithms. The suggestions are presented from two perspectives: (i) given the budget (standardized as thousand dollars per month per mile of monitored roadway), the best-performing smart work zone system is identified; (ii) given the performance requirement, the lowest-cost smart work zone system is identified. It should be noted that these findings are made based on limited cost data. Specifically, the LER cost information was not available from a comparable data source, hence was not included in the cost performance analysis.

Outcome. Table 6.1 summarizes the best work zone configurations and algorithms for the velocity estimation around the queue. The EnKF and radar sensors dominate the lowest-error and lowest-cost smart work zone configurations. This outcome is consistent with the finding that the spacing of sensors plays a more important role than the type of sensors. When excluding the EnKF, the best alternative algorithm identified in the microsimulation is the spatial interpolation algorithm.

Table 6.1: Best Smart Work Zone Deployments for Velocity Estimation

	Best SWZ within specified budget						
	Budget ($k/month /mile)	Best SWZ			Best SWZ excluding EnKF		
		Algorithm	Sensor spacing (miles)	Error (mph)	Algorithm	Sensor spacing (miles)	Error (mph)
Velocity estimation around the queue	1	EnKF	Radar (7/8)	13	Spatial	Radar (7/8)	18
	2	EnKF	Radar (3/8)	10	Spatial	Radar (3/8)	12
	Lowest cost SWZ within specified error target						
	Error target (mph)	Lowest cost SWZ			Lowest cost SWZ excluding EnKF		
		Algorithm	Sensor spacing (miles)	Cost ($k/month /mile)	Algorithm	Sensor spacing (miles)	Cost ($k/month /mile)
	10	EnKF	Radar (3/8)	2	Spatial	Radar (1/4)	2.9
	15	EnKF	Radar (1.25)	0.7	Spatial	Radar (1/2)	1.5
	20	EnKF	Radar (2.5)	0.4	Spatial	Radar (1.0)	0.8

Table 6.2 summarizes the recommended smart work zone configurations and algorithms for queue length estimation. Due to the lower cost of radar sensors, the best-performing or lowest-cost smart work zone systems are dominated by radar sensors. This also suggests lower-cost sensors are preferable.

Table 6.2: Best Smart Work Zone Deployments for Queue Length Estimation

	Best SWZ within specified budget						
	Budget ($k/month /mile)	Best SWZ			Best SWZ excluding EnKF		
		Algorithm	Sensor spacing (miles)	Error (mile)	Algorithm	Sensor spacing (miles)	Error (mile)
Queue length estimation	0.5	EnKF	Radar (2.5)	0.26	Spatial	Radar (2.5)	0.57
	1	EnKF	Radar (7/8)	0.13	Spatial	Radar (7/8)	0.18
	1.5	EnKF	Radar (1/2)	0.1	Spatial	Radar (1/2)	0.16
	2	EnKF	Radar (3/8)	0.06	Spatial	Radar (3/8)	0.13
	Lowest cost SWZ within specified error target						
	Error target (miles)	Lowest cost SWZ			Lowest cost SWZ excluding EnKF		
		Algorithm	Sensor spacing (miles)	Cost ($k/month /mile)	Algorithm	Sensor spacing (miles)	Cost ($k/month /mile)
	0.1	EnKF	Radar (1/2)	1.5	Spatial	Radar (1/8)	5.7
	0.2	EnKF	Radar (1.25)	0.7	Spatial	Radar (7/8)	1
	0.3	EnKF	Radar (2.5)	0.4	Spatial	Radar (1.25)	0.5

Table 6.3 summarizes the recommended smart work zone deployments for travel time estimation based on microsimulation. The combination of radar sensors and EnKF generally provides the best performance. When excluding EnKF, the spatio-temporal filtering algorithm performs best combined with RTMS. The reason that RTMS is more favorable is because the travel time estimation is very sensitive to the traffic speed estimation in congested traffic, and radar sensors have difficulty in reliably measuring slow traffic.

Table 6.3: Best Smart Work Zone Deployments for Travel Time Estimation

	Best SWZ within specified budget						
	Budget ($k/month /mile)	Best SWZ			Best SWZ excluding EnKF		
		Algorithm	Sensor spacing (miles)	Error (min)	Algorithm	Sensor spacing (miles)	Error (min)
Travel time estimation	0.5	EnKF	Radar (2.5)	7.3	Spatio-temporal	RTMS (5.0)	9.6
	1	EnKF	Radar (7/8)	5.5	Spatio-temporal	RTMS (1.25)	7.2
	1.5	EnKF	Radar (3/4)	4.8	Spatio-temporal	RTMS (1.0)	7
	2	EnKF	Radar (3/4)	4.8	Spatio-temporal	RTMS (1.0)	7
	Lowest cost SWZ within specified error target						
	Error target (min)	Lowest cost SWZ			Lowest cost SWZ excluding EnKF		
		Algorithm	Sensor spacing (miles)	Cost ($k/month /mile)	Algorithm	Sensor spacing (miles)	Cost ($k/month /mile)
	5	EnKF	Radar (3/4)	1.1	N/A	N/A	N/A
	7.5	EnKF	Radar (2.5)	0.42	Spatio-temporal	RTMS (1.25)	1
	10	Spatio-temporal	RTMS (5.0)	0.4	Spatio-temporal	RTMS (5.0)	0.4

The main limitation of the study is that the analysis was conducted in a microsimulation environment. Further field testing is needed to validate the findings. Furthermore, the present analysis was restricted to the accuracy of the traffic state estimate only, and it did not consider other practical factors such as maintenance and redeployment costs, which may also play a critical role in the development of practical sensor network configuration guidelines.

REFERENCES

[1] G. Ullman, J. Schroeder, and D. Gopalakrishna. Work zone intelligent transportation systems implementation guide: Use of technology and data for effective work zone management. Technical Report FHWA-HOP-14-008, Federal Highway Administration, 2014.

[2] FHWA. Intelligent transportation systems in work zones: A cross-cutting study. Technical Report FHWA-OP-02-025, Federal Highway Administration, 2002.

[3] L. Tudor, A. Meadors, and R. Plant. Deployment of smart work zone technology in Arkansas. *Transportation Research Record: Journal of the Transportation Research Board*, 1824:3–14, 2003.

[4] FHWA. Real-time work zone traffic control system, using an automated traffic information system to reduce congestion and improve safety during reconstruction of the I-55 Lake Springfield Bridge in Illinois. Technical Report FHWA-HOP-04-018, Federal Highway Administration, 2004.

[5] T. Roelofs and C. Brookes. Synthesis of intelligent work zone practices. Technical Report ENT-2014-1, Michigan Department of Transportation, 2014.

[6] G. Ullman and J. Schroeder. Mitigating work zone safety and mobility challenges through Intelligent Transportation Systems: Case Studies. Technical Report FHWA-HOP-14-007, Federal Highway Administration, 2014.

[7] FHWA. Dynamic lane merge system: Reducing aggressive driving and optimizing throughput at work zone merges in Michigan. Technical Report FHWA-HOP-04-033, Federal Highway Administration, 2004.

[8] E. Radwan, R. Harb, and S. Ramasamy. Evaluation of safety and operational effectiveness of dynamic lane merge system in Florida. Technical Report BD 584-24, Florida Department of Transportation, 2009.

[9] FHWA. Reducing congestion with the use of a traffic management contract incentive during the reconstruction of Arizona State Route 68. Technical Report FHWA-HOP-04-032, Federal Highway Administration, 2004.

[10] T. Luttrell, M. Robinson, J. A. Rephlo, R. Haas, J. Srour, R. F. Benekohal, J. Oh, and T. Scriba. Benefits of using intelligent transportation systems in work zones: A summary report. Technical Report FHWA-HOP-08-021, Federal Highway Administration, 2008.

[11] R. P. Maccubbin, B. L. Staples, F. Kabir, C. F. Lowrance, M. R. Mercer, B. H. Philips, and R. Gordon. Intelligent transportation systems benefits, costs, deployment, and lessons learned. Technical Report FHWA-JPO-08-032, Federal Highway Administration, 2008.

[12] L. Grillo, T. Datta, and C. Hartner. Dynamic late lane merge system at freeway construction work zones. *Transportation Research Record: Journal of the Transportation Research Board,* 2055:3–10, 2008.

[13] P. J. Carlson, M. D. Fontaine, and H. G. Hawkins. Evaluation of traffic control devices for rural high-speed maintenance work zones. Technical Report FHWA/TX-00/1879-1, Texas Transportation Institute, 2000.

[14] E. Lee and C. Kim. Automated work zone information system on urban freeway rehabilitation: California implementation. *Transportation Research Record: Journal of the Transportation Research Board*, 2006:77–85, 2006.

[15] R. Bushman and C. Berthelot. Estimating the benefits of deploying intelligent transportation systems in work zones. In *Proceedings of Transportation Research Board 83rd Annual Meeting Compendium of Papers*, 2004.

[16] C. Dankocsik, M. Zarean, D. Register, and K. Timpone. Best practices of rural and statewide ITS strategic planning. Technical Report FHWA-OP-02-037, Federal Highway Administration, 2002.

[17] T. Luttrell, M. Robinson, J. A. Rephlo, R. Haas, J. Srour, R. Benekohal, J. Oh, and Scriba. Comparative analysis report: The benefits of using intelligent transportation systems in work zones. Technical Report FHWA-HOP-09-002, Federal Highway Administration, 2008.

[18] A. Haghani, M. Hamedi, R. Fish, and A. Nouruzi. Evaluation of dynamic message signs and their potential impact on traffic flow. Technical Report MD-13-SP109B4C, Maryland Department of Transportation, 2013.

[19] Y. Wang and M. Papageorgiou. Real-time freeway traffic state estimation on extended Kalman filter: A general approach. *Transportation Research Part B: Methodological,* 39(2):141–167, 2005.

[20] S. Blandin, A. Couque, A. Bayen, and D. Work. On sequential data assimilation for scalar macroscopic traffic flow models. *Physica D: Nonlinear Phenomena*, 241(17):1421–1440, 2012.

[21] G. Ullman, J. Schroeder, and D. Gopalakrishna. Use of technology and data for effective work zone management: Work zone ITS implementation guide. Technical Report FHWA- HOP-14-008, Federal Highway Administration, 2014.

[22] A. Horowitz and V. Lachhwani. Criteria for portable ATIS in work zones: Lane merge, travel time and speed advisory systems. Technical Report, Smart Work Zone Deployment Initiative, 2005.

[23] R. Browne and A. Byrne. Highway 402 queue warning system. In *Proceedings of the 2008 Annual Conference of the Transportation Association of Canada*, 2008.

[24] T. Morris, J. Schwach, and P. Michalopoulos. Low-cost portable video-based queue detection for work-zone safety. Technical Report CTS 11-02, Center for Transportation Studies, University of Minnesota, 2011.

[25] Inc. SRF Consulting Group. Ramp queue detection. Technical Report SRF No. 0086298, Minnesota Department of Transportation, 2009.

[26] G. Pesti, R. Brydia, and C. Poe. Evaluating the operational impacts of the I-35 reconstruction. 2014 ITS Texas Annual Meeting, 2014.

[27] A. Petter and C. Poe. I-35 queue detection warning system. Texas Department of Transportation Short Course Slides, 2013.

[28] Texas Department of Transportation. Facilitating deployment decisions of highly portable end-of-queue warning systems. Online article, 2013.

[29] J. Habermann. I-35 smart work zone update. Texas Department of Transportation Short Course Slides, 2015.

[30] T. Datta, K. Schattler, P. Kar, and A. Guha. Development and evaluation of an advanced dynamic lane merge traffic control system for 3 to 2 lane transition areas in work zones. Technical Report RC-1451, Michigan Department of Transportation, 2004.

[31] FHWA. Keeping traffic moving during reconstruction of the big I, a major interstate-interstate interchange in Albuquerque. Technical Report FHWA-OP-04-072, Federal Highway Administration, 2004.

[32] E. Kwon, D. Brannan, K. Shouman, C. Isackson, and B. Arseneau. Development and field evaluation of variable advisory speed limit system for work zones. Transportation Research Record: Journal of the Transportation Research Board, 2015:12–18, 2007.

[33] R. Lyles, W. Taylor, D. Lavansiri, and J. Grossklaus. A field test and evaluation of variable speed limits in work zones. In *Proceedings of the 83rd Transportation Research Board Annual Meeting*, 2004.

[34] T. McMurtry, M. Saito, Riffkin M., and S. Heath. Variable speed limit signs: Effects on speed and speed variation in work zones. In *Proceedings of the 88th Transportation Research Board Annual Meeting*, 2009.

[35] N. J. Fudala and M. D. Fontaine. Work zone variable speed limit systems: Effectiveness and system design issues. Technical Report VTRC 10-R20, Virginia Transportation Research Council, 2010.

[36] M. Mirshahi, J. Obenberger, C. Fuhs, C. Howard, R. Krammes, B. Kuhn, R. Mayhew, M. Moore, K. Sahebjam, and C. Stone. Active traffic management: The next step in congestion management. Technical Report FHWA-PL-07-012, Federal Highway Administration, 2007.

[37] M. D. Robinson. Examples of variable speed limit applications. In *Workshop of the 79th Transportation Research Board Annual Meeting*, 2000.

[38] J. Sparmann. Freeway operation in Germany: Experiences in Hessen. In *Presentation to 1st International Symposium on Freeway & Tollway Operations, Athens, Greece*, 2006.

[39] M. Saito and A. Wilson. Evaluation of the effectiveness of a variable advisory speed system on queue mitigation in work zones. In *Proceedings of the 8th International Conference on Traffic and Transportation Studies*, 2012.

[40] R. Benekohal, A. Hajbabaie, J. Medina, M. Wang, and M. Chitturi. Speed photo-radar enforcement evaluation in Illinois work zones. Technical Report ICT-10-064, Illinois Center for Transportation, 2010.

[41] C. Wang, K. Dixon, and D. Jared. Evaluating speed reduction strategies for highway work zones. *Transportation Research Record: Journal of the Transportation Research Board*, 1824:44–53, 2003.

[42] M. Brewer, G. Pesti, and W. Schneider IV. Improving compliance with work zone speed limits effectiveness of selected devices. *Transportation Research Record: Journal of the Transportation Research Board,* 1948:67–76, 2006.

[43] D. W. Soole, B. C. Watson, and J. J. Fleiter. Effects of average speed enforcement on speed compliance and crashes: A review of the literature. *Accident Analysis & Prevention,* 54:46–56, 2013.

[44] B. Ravani, C. Wang, D. Ma, W. White, and P. Fyhrie. Evaluation of methods to reduce speeds in work zones. Technical Report CA-13-2247, California Department of Transportation, 2012.

[45] M. Joerger. Photo radar speed enforcement in a state highway work zone: Yeon Avenue demonstration project. Technical Report SR 500-390, Oregon Department of Transportation, 2010.

[46] G. Ullman, T. Lomax, and T. Scriba. A primer on work zone safety and mobility performance measurement. Technical Report FHWA-HOP-11-033, Federal Highway Administration, 2011.

[47] G. Ullman, T. Lomax, F. Ye, and T. Scriba. Work zone performance measures pilot test. Technical Report FHWA-HOP-11-022, Federal Highway Administration, 2011.

[48] S. Hallmark, J. Turner, and C. Albrecht. Synthesis of work-zone performance measures. Technical Report InTrans Project 12-436, Smart Work Zone Deployment Initiative, 2013.

[49] M. Fontaine. Using private sector probe data to examine work zone performance: The Virginia DOT experience. Short Slides, Virginia Center for Transportation Innovation & Research, 2013.

[50] R. Mudge, H. Mahmassani, R. Haas, A. Talebpour, and L. Carroll. Work zone performance measurement using probe data. Technical Report FHWA-HOP-13-043, Federal Highway Administration, 2013.

[51] M. Saito, G. G. Schultz, and E. J. Chau. Evaluating the feasibility of incorporating mobility-based work zone traffic control performance measures in highway construction project specifications: Volume 1, Feasibility of continuous monitoring of performance measures. Technical Report UT-13.13a, Utah Department of Transportation, 2013.

[52] J. Bunch, C. Burnier, E. Greer, G. Hatcher, A. Jacobi, F. Kabir, C. Lowrance, M. Mercer, and K. Wochinger. Intelligent transportation systems benefits, costs, deployment, and lessons learned desk reference: 2011 update. Technical Report FHWA-JPO-11-140, Federal Highway Administration, 2011.

[53] G. Hatcher, C. Burnier, E. Greer, D. Hardesty, D. Hicks, A. Jacobi, C. Lowrance, and M. Mercer. Intelligent transportation systems benefits, costs, deployment, and lessons learned: 2014 update. Technical Report FHWA-JPO-14-159, Federal Highway Administration, 2014.

[54] P. Wiles, S. Cooner, C. Walters, and E. Pultorak. Advance warning of stopped traffic on freeways: Current practices and field studies of queue propagation speeds. Technical Report FHWA-TX-03-4413-1, Texas Department of Transportation, 2003.

[55] SRF Consulting Group. Monitoring traffic in work zones: The iCone® system. Technical Report for Project No. 0106845, Minnesota Department of Transportation, 2010.

[56] Minnesota Department of Transportation. Minnesota intelligent work zone toolbox: Guideline for intelligent work zone system selection, Minnesota Department of Transportation, 2008.

[57] P.G. Gipps. A behavioral car-following model for computer simulation. *Transportation Research Part B: Methodological,* 15(2):105 – 111, 1981.

[58] B. Park and J. Won. Microscopic simulation model calibration and validation handbook. Technical Report FHWA/VTRC 07-CR6, Virginia Transportation Research Council, 2006.

[59] M. Figueiredo, A. Seco, and A. Silva. Calibration of microsimulation models the effect of calibration parameters errors in the models performance. *Transportation Research Procedia,* 3:962–971, 2014.

[60] Q. Ge and M. Menendez. An efficient sensitivity analysis approach for computationally expensive microscopic traffic simulation models. *International Journal of Transportation*, 2(2):49–69, 2014.

[61] K. Kwong, R. Kavaler, R. Rajagopal, and P. Varaiya. A practical scheme for arterial travel time estimation based on vehicle re-identification using wireless sensors. In *Proceedings of the 89th TRB Annual Meeting*. Transportation Research Board of the National Academies, 2009.

[62] J. Hourdakis, P. Michalopoulos, and J. Kottommannil. Practical procedure for calibrating microscopic traffic simulation models. *Transportation Research Record: Journal of the Transportation Research Board,* 1852:130–139, 2003.

[63] K. Kim and R. Simplex-based calibration of traffic microsimulation models with intelligent transportation systems data. *Transportation Research Record: Journal of the Transportation Research Board,* 1855:80–89, 2003.

[64] J. Ma, H. Dong, and H. Zhang. Calibration of microsimulation with heuristic optimization methods. *Transportation Research Record: Journal of the Transportation Research Board,* 1999:208–217, 2007.

[65] J. Maryak and D. Chin. Global random optimization by simultaneous perturbation stochastic approximation. *IEEE Transactions on Automatic Control*, 53(3):756–762, 2008.

[66] B. Ciuffo, V. Punzo, and M. Montanino. The calibration of traffic simulation models: Report on the assessment of different goodness of fit measures and optimization algorithms. Technical Report JRC68403, European Commission Joint Research Centre, 2012.

[67] S. Le Digabel. NOMAD: Nonlinear optimization with the MADS algorithm. *ACM Transactions on Mathematical Software,* 37(4):44:1–44:15, 2001.

[68] L. Gauthier, N. Saunie, S. Le Digabel, and G. Cao. Calibration of driving behavior models using derivative-free optimization and video data for Montreal highways. In *Proceedings of the 94th Transportation Research Board Annual Meeting,* 2016.

[69] R. Dowling, A. Skabardonis, J. Halkias, G. McHale, and G. Zammit. Guidelines for calibration of microsimulation models: framework and applications. *Transportation Research Record: Journal of the Transportation Research Board,* 1876:1–9, 2004.

[70] V. Punzo and B. Ciuffo. Sensitivity analysis of car-following models: methodology and application. In *Proceedings of the 90th Transportation Research Board Annual Meeting,* 11-2805, 2011.

[71] B. Ciuffo, V. Punzo, and V. Torrieri. Comparison of simulation-based and model-based calibrations of traffic-flow microsimulation models. *Transportation Research Record: Journal of the Transportation Research Board,* 2088:36–44, 2008.

[72] B. Park and H. Qi. Development and evaluation of a procedure for the calibration of simulation models. *Transportation Research Record: Journal of the Transportation Research Board,* 1934:208–217, 2005.

[73] V. Punzo and B. Ciuffo. How parameters of microscopic traffic flow models relate to traffic dynamics in simulation: Implications for model calibration. *Transportation Research Record: Journal of the Transportation Research Board,* 2124:249–256, 2009.

[74] L. Klein, M. Mills, and D. Gibson. Traffic detector handbook: Volume I. Technical Report FHWA-HRT-06-108, Federal Highway Administration, 2006.

[75] L. Klein, M. Mills, and D. Gibson. Traffic detector handbook: Volume II. Technical Report FHWA-HRT-06-139, Federal Highway Administration, 2006.

[76] Houston Radar LLC. Installation and user manual for K-band Doppler radar DR500, 2011.

[77] RTMS G4 User Guide. Inc. Image Sensing Systems, 2012.

[78] J. Oh, R. Jayakrishnan, and W. Recker. Section travel time estimation from point detection data. In *Proceedings of the 82nd Transportation Research Board Annual Meeting*, 2002.

[79] B. Fariello. ITS America RFI travel time projects in North America. *Report of San Antonio TransGuide Program,* 2002.

[80] C. Cortes, R. Lavanya, J.-S. Oh, and R. Jayakrishnan. General-purpose methodology for estimating link travel time with multiple-point detection of traffic. *Transportation Research Record: Journal of the Transportation Research Board,* 1802:181–189, 2002.

[81] J. Van Lint. Empirical evaluation of new robust travel time estimation algorithms. *Transportation Research Record: Journal of the Transportation Research Board,* 2160:50–59, 2010.

[82] E. Kwon. Development of operational strategies for travel time estimation and emergency evacuation on a freeway network. Technical Report MN/RC-2004-49, Minnesota Department of Transportation, 2004.

[83] J. Van Lint and N. Van der Zijpp. Improving a travel-time estimation algorithm by using dual loop detectors. *Transportation Research Record: Journal of the Transportation Research Board,* 1855:41–48, 2003.

[84] L. Sun, J. Yang, and H. Mahmassani. Travel time estimation based on piecewise truncated quadratic speed trajectory. *Transportation Research Part A: Policy and Practice,* 42(1):173–186, 2008.

[85] D. Ni and H. Wang. Trajectory reconstruction for travel time estimation. *Journal of Intelligent Transportation Systems,* 12(3):113–125, 2008.

[86] B. Coifman. Estimating travel times and vehicle trajectories on freeways using dual loop detectors. *Transportation Research Part A: Policy and Practice*, 36(4):351–364, 2002.

[87] M. Treiber and D. Helbing. Reconstructing the spatio-temporal traffic dynamics from stationary detector data. *Cooper@tive Tr@nsport@tion Dyn@mics,* 1:3.1–3.24, 2002.

[88] J. Van Lint and S. Hoogendoorn. A robust and efficient method for fusing heterogeneous data from traffic sensors on freeways. *Computer-Aided Civil and Infrastructure Engineering,* 24(1):1–17, 2009.

[89] M. Treiber, A. Kesting, and R. Wilson. Reconstructing the traffic state by fusion of heterogeneous data. *Computer-Aided Civil and Infrastructure Engineering,* 26(6):408–419, 2011.

[90] M. Lighthill and G. Whitham. On kinematic waves. II. A theory of traffic flow on long crowded roads*. Proceedings of the Royal Society of London. Series A. Mathematical and Physical Sciences,* 229:317–345, 1955.

[91] P. Richards. Shock waves on the highway. *Operations Research,* 4(1):42–51, 1956.

[92] R. E. Kalman. A new approach to linear filtering and prediction problems. *Journal of Basic Engineering,* 82(1):35–45, 1960.

[93] A. Hegyi, D. Girimonte, R. Babuska, and B. De Schutter. A comparison of filter configurations for freeway traffic state estimation. In *Proceedings of the International Conference on Intelligent Transportation Systems,* pages 1029–1034, 2006.

[94] X. Sun, L. Munoz, and R. Horowitz. Highway traffic state estimation using improved mixture Kalman filters for effective ramp metering control. In *Proceedings of the 42nd IEEE Conference on Decision and Control,* volume 6, pages 6333–6338, 2003.

[95] Y. Sun and D. B. Work. A distributed local Kalman consensus filter for traffic estimation. In *Proceedings of the 53rd IEEE Conference on Decision and Control*, pages 6484–6491, 2014.

[96] L. Mihaylova, R. Boel, and A. Hegyi. Freeway traffic estimation within particle filtering framework. *Automatica,* 43(2):290–300, 2007.

[97] R. Wang, D. B. Work, and R. Sowers. Multiple model particle filter for traffic estimation and incident detection. *IEEE Transactions on Intelligent Transportation Systems,* pages 1–10, 2016.

[98] D. Work, S. Blandin, O. Tossavainen, B. Piccoli, and A. M. Bayen. A traffic model for velocity data assimilation. *Applied Mathematics Research eXpress,* 2010(1):1–35, 2010.

[99] Y. Wang, M. Papageorgiou, A. Messmer, P. Coppola, A. Tzimitsi, and A. Nuzzolo. An adaptive freeway traffic state estimator. *Automatica,* 45(1):10–24, 2009.

[100] C. Antoniou, H. N. Koutsopoulos and G. Yannis. An efficient non-linear Kalman filtering algorithm using simultaneous perturbation and applications in traffic estimation and prediction. In *Proceedings of the 2007 IEEE Intelligent Transportation Systems Conference*, pages 217–222, 2007.

[101] L. Munoz, X. Sun, R. Horowitz, and L. Alvarez. Traffic density estimation with the cell transmission model. In *Proceedings of the 2003 American Control Conference,* volume 5, pages 3750–3755, 2003.

[102] S. J. Julier and J. K. Uhlmann. Unscented filtering and nonlinear estimation. In *Proceedings of the IEEE,* 92(3):401–422, 2004.

[103] L. Mihaylova and R. Boel. A particle filter for freeway traffic estimation. In *Proceedings of the 43rd IEEE Conference on Decision and Control,* volume 2, pages 2106–2111. IEEE, 2004.

[104] L. Mihaylova, R. Boel, and A. Hegiy. An unscented Kalman filter for freeway traffic estimation. In *Proceedings of the 11th IFAC Symposium on Control in Transportation Systems,* 2006.

[105] G. Evensen. The ensemble Kalman filter: Theoretical formulation and practical implementation. *Ocean Dynamics,* 53(4):343–367, 2003.

[106] S. K. Godunov. A difference method for numerical calculation of discontinuous solutions of the equations of hydrodynamics. *Matematicheskii Sbornik,* 89(3):271–306, 1959.

[107] C. F. Daganzo. The cell transmission model: A dynamic representation of highway traffic consistent with the hydrodynamic theory. *Transportation Research Part B: Methodological,* 28(4):269–287, 1994.

[108] R. Lorentzen and G. Nævdal. An iterative ensemble Kalman filter. *IEEE Transactions on Automatic Control,* 56(8):1990–1995, 2011.

[109] F. V. Webster. Traffic signal settings. London H.M. Stationery Off., No. 29, 1958.

[110] A. Sharma, D. Bullock, and J. Bonneson. Input-output and hybrid techniques for real-time prediction of delay and maximum queue length at signalized intersections. *Transportation Research Record: Journal of the Transportation Research Board,* 2035:69–80, 2007.

[111] G. Qian, J. Lee, and E. Chung. Algorithm for queue estimation with loop detector of time occupancy in off-ramps on signalized motorways. *Transportation Research Record: Journal of the Transportation Research Board,* 2278:50–56, 2012.

[112] G. Vigos and M. Papageorgiou. A simplified estimation scheme for the number of vehicles in signalized links. *IEEE Transactions on Intelligent Transportation Systems,* 11(2):312–321, 2010.

[113] R. Li, G. Rose, and M. Sarvi. Evaluation of speed-based travel time estimation models. *Journal of Transportation Engineering,* 132(7):540–547, 2006.

[114] P. E. Mazare, O. P. Tossavainen, and D. B. Work. Computing travel times from filtered traffic states. *Discrete & Continuous Dynamical Systems-Series S,* 7(3), 2014.

[115] B. L. Smith, B. M. Williams, and R. K. Oswald. Comparison of parametric and non-parametric models for traffic flow forecasting. *Transportation Research Part C: Emerging Technologies,* 10(4):303–321, 2002.

[116] R. Chrobok, O. Kaumann, J. Wahle, and M. Schreckenberg. Different methods of traffic forecast based on real data. *European Journal of Operational Research,* 155(3):558–568, 2004.

[117] L.C. Edie. Discussion of traffic stream measurements and definitions. In *Proceedings of the 2nd International Symposium on the Theory of Road Traffic Flow,* pages 139–154, 1965.

[118] M. J. Anderson. A new method for non-parametric multivariate analysis of variance. *Austral ecology,* 26(1):32–46, 2001.

[119] G. Dervisoglu, G. Gomes, J. Kwon, R. Horowitz, and P. Varaiya. Automatic calibration of the fundamental diagram and empirical observations on capacity. In *Proceedings of the 88th Transportation Research Board Annual Meeting,* volume 15, 2009.

APPENDIX A: CALIBRATION PROCEDURE

A.1 SENSITIVITY ANALYSIS

Sensitivity analysis is a method for determining the influence of each factor to the system response. Ideally, an analysis of variance (ANOVA) [118] should be performed to obtain statistical significance of each factor and the interaction between factors. However, a full factorial ANOVA requires a large number of simulations. For example, the ANOVA of 12 factors with four levels of values each would require 4^{12} = 16,777,216 simulations, which takes 5.3 years to complete assuming each simulation takes 10 seconds.

An alternative approach is to infer the sensitivity by investigating one factor at a time while keeping other factors fixed at the default value using X-Y plots [58]. The underlying assumption is that factors are independent in terms of influencing the response. Though this assumption is not well justified, it provides a faster way to infer the sensitivity of factors.

A comprehensive parameter sensitivity analysis in AIMSUN has been previously conducted [73]. Initially, 32 parameters were selected and then reduced to eight parameters based on engineering and empirical knowledge. The sensitivity analysis showed four out of the eight parameters explained more than 95% of the output variance, including the reaction time, speed acceptance, maximum acceleration, and the coefficient of variance.

This study followed the previously cited selection [73] and an initial set of six parameters were selected for each type of vehicle for the sensitivity analysis:

- *reactionTime*. This is the time for a driver to react to speed changes of the preceding vehicle. In AIMSUN, the reaction time is required to be multiplications of the simulation step. In the analysis of this parameter, to obtain a finer resolution, the simulation step was modified to 0.2 seconds.
- *speedAcceptance*. The speed acceptance determines the speed of the vehicle. In AIMSUN simulation, the speed acceptance of vehicle is a stochastic parameter determined by four values *[mean, std, min, max]*. The *speedAcceptance* parameter analyzed refers to the mean value. In AIMSUN, the vehicle speed is also determined by another parameter *maxDesiredSpeed*. To allow maximum flexibility for adjusting *speedAcceptance*, the parameter *maxdesiredSpeed* should be set at a high value as suggested in [73].
- *maxAccel*. This parameter influences the maximum acceleration rate of vehicles. In AIMSUN, the maximum acceleration rate of vehicles is a stochastic parameter determined by four values defining a random distribution *[mean, std, min, max].* The parameter *maxAccel* refers to the mean value.
- *minDist*. This parameter influences the minimum stopping distance of vehicle. In AIMSUN, the minimum distance is a stochastic parameter determined by *[mean, std, min, max].* The parameter *minDist* refers to the mean value. This parameter was neglected in [73] where the minimum distance was directly measured in field. However, the minimum distance is not available in the data for this study. Therefore, the *minDist* is included in the set of parameters for a sensitivity analysis.
- *cov*. This parameter represents the coefficient of variance (the standard deviation divided by the mean) for the stochastic parameters (i.e., *speedAcceptanc, maxAcce, minDist)*. Assuming

that the distributions of parameters of each type of vehicle are approximately the same [73], the standard deviation for the stochastic parameters can be determined the multiplication of *cov* with the corresponding mean values.

- *sensitivityFactor*. In the deceleration component of the car-following model, the follower makes an estimation of the deceleration of the leader using the sensitivity factor. If the parameter *sensitivityFactor* is lower or higher than 1, then the vehicle underestimates or overestimates the deceleration rate of the leading vehicle, hence driving more or less aggressively. This parameter was found to be very influential in terms of changing the traffic behavior, hence included in the initial parameter set. This parameter is assumed to be deterministic.

In this study, the sensitivity analysis was performed on a synthetic highway (approximately one mile). Four detectors were evenly spaced on the road measuring the speeds, and the traffic demand was specified such that a queue propagates upstream. The total simulated time horizon is 40 minutes.

Table A.1: Initial Parameters for Sensitivity Analysis

Parameters	Default value	Range
car *speedAcceptance*	1.1	[0.85, 1.3]
truck *speedAcceptance*	1.05	[0.85, 1.1]
car *maxAccel* (m/s^2)	3	[2.6, 3.4]
truck *maxAccel* (m/s^2)	1	[0.6, 1.8]
car *minDist* (m)	1	[0.5, 1.5]
truck *minDist* (m)	1.5	[1.0, 2.5]
car *sensitivityFactor*	1	[0.5, 1.5]
truck *sensitivityFactor*	1	[0.5, 1.5]
car *reactionTime* (s)	0.8	$\{0.4, 0.6, \ldots, 2.0\}$
truck *reactionTime* (s)	0.8	$\{0.4, 0.6, \ldots, 2.0\}$
car *cov*	0.3	[0.1, 0.5]
truck *cov*	0.33	[0.1, 0.5]

Prior to the sensitivity analysis for the parameters specified in Table A.1, the following configurations were conducted in AIMSUN.

- All other parameters in the AIMSUN were left as default, except that the desired speeds for the cars and trucks are set at a high value [105, 6.2, 100, 112] mph to allow maximum flexibility of adjusting *speedAcceptance*.
- The detection interval for all detectors was configured as 5 minutes.
- The simulation step was configured as 0.2 seconds.
- The generation of vehicles was set as *const*; hence, vehicles were generated exactly as specified in the traffic demand.

The procedure of the sensitivity analysis is briefly summarized as follows:

- With all other parameters fixed, change the value of the parameter under analysis, and simulate the new set of parameters in AIMSUN.
- For each set of parameters, run ten simulations and obtain the corresponding responses. Using ten simulations allows us to see the influence level of each parameter compared to stochastic errors. In addition, within each simulation, ten replications with random seeds were simulated to compute the average response.
- Use the simulated speed data to compute the root mean square error (RMSE) against the speed data generated using default parameter values.
- Visualize the response (RMSE of speed) versus the levels of values for each parameter, and identify the parameters that are sensitive.

The sensitivity analysis results are visualized in Figure A.1, Figure A.2, and Figure A.3.

In Figure A.1, clearly, the car *speedAcceptance* and the truck *maxAccel* are both very sensitive, while the car *maxAccel* is not sensitive at all. The truck *speedAcceptance* is mildly sensitive. However, the stochastic error is relatively large and this parameter is not included the final calibration parameters.

In Figure A.2, the car *sensitivityFactor* and the truck *sensitivityFactor* both exhibit high sensitivity. In comparison, the car *minDist* and the truck *minDist* both show mild sensitivity, and are not included in the final calibration parameters.

In Figure A.3, the *reactionTime* parameters for both types of vehicles are sensitive when the value is below 1.6. Therefore, the car *reactionTime* and truck *reactionTime* are included in the final calibration parameters, with levels of value $\{0.4, 0.6, 0.8, 1.0, 1.2, 1.4, 1.6\}$ seconds.

In summary, based on the sensitivity analysis of 12 initial parameters, six parameters were identified as sensitive which were included in the final set of parameters to be calibrated in Table A.2. In addition, it was later identified during this study that the minimum headway was also an influential parameter. Therefore, the minimum headways of cars and trucks were included in the actual calibration of two work zones.

Table A.2: Parameters for Calibration

Parameter	Default value	Range
car *speedAcceptance*	1.1	[0.85, 1.3]
truck *maxAccel* (m/s^2)	1	[0.6, 1.8]
car *sensitivityFactor*	1	[0.5, 1.5]
truck *sensitivityFactor*	1	[0.5, 1.5]
car *reactionTime* (s)	0.8	$\{0.4, 0.6, \ldots, 1.6\}$
truck *reactionTime* (s)	0.8	$\{0.4, 0.6, \ldots, 1.6\}$
car *minHeadway* (s)	0	$\{1.0, 1.5, 2.0, 2.5\}$
truck *minHeadway* (s)	0	$\{1.0, 1.5, 2.0, 2.5\}$

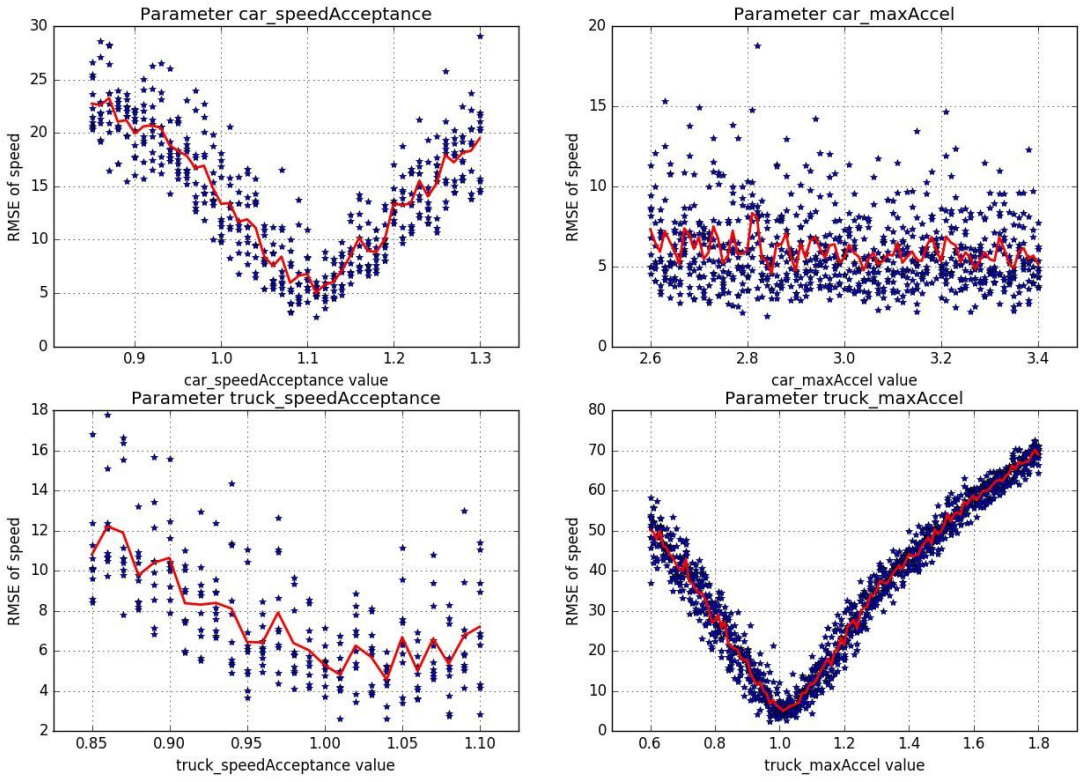

Figure A.1: Sensitivity analysis of speedAcceptance and maxAccel.

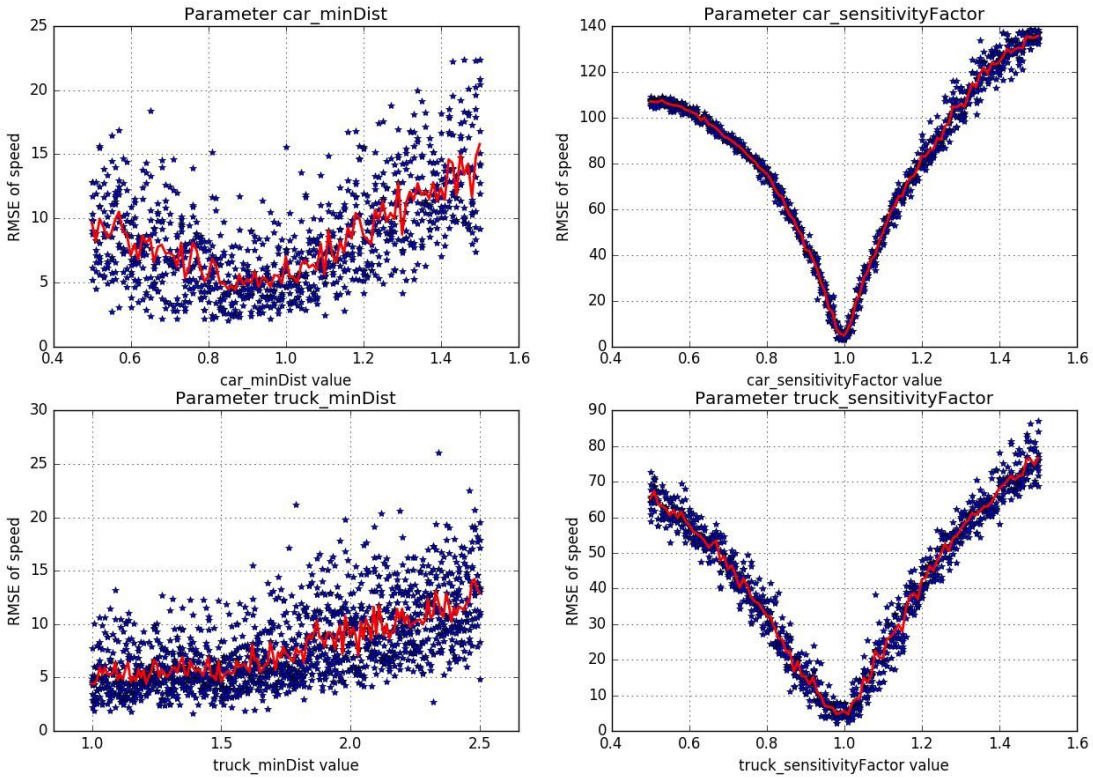

Figure A.2: Sensitivity analysis of minDist and sensitivityFactor.

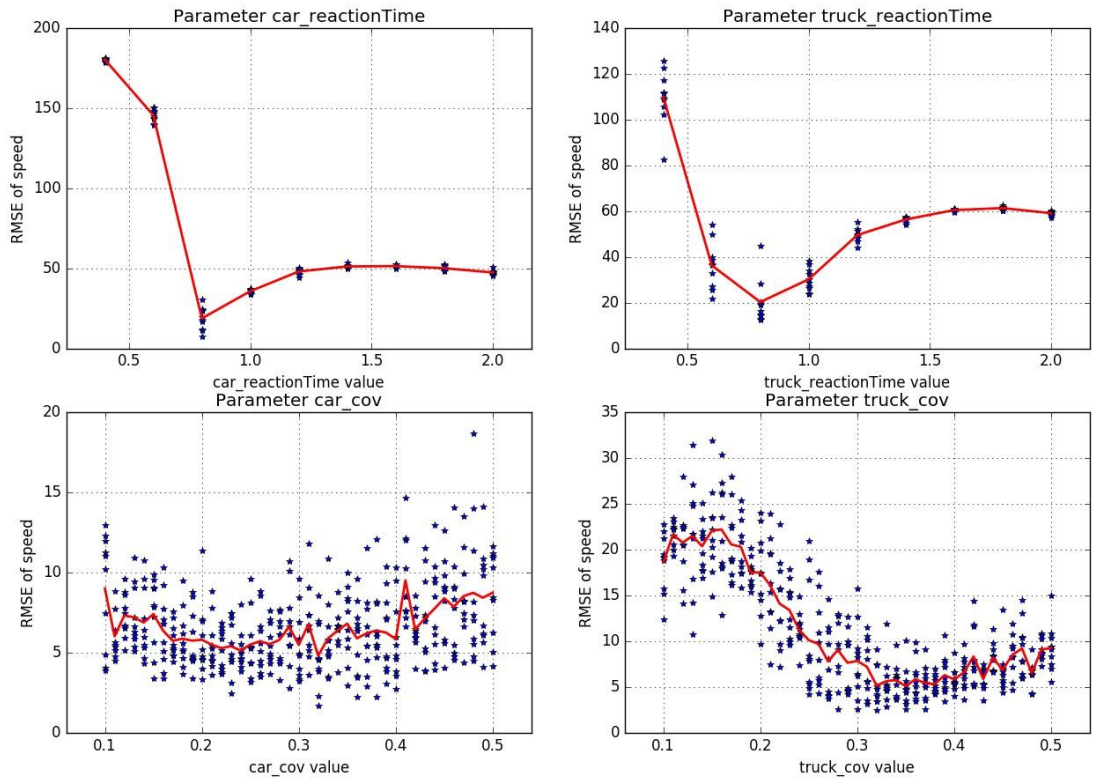

Figure A.3: Sensitivity analysis of reactionTime and cov.

A.2 VERIFICATION OF AUTO CALIBRATION FRAMEWORK

This study proposed to calibrate the micro simulation model parameters (Table A.2) using an automated calibration framework. To validate the feasibility of the proposed approach, a verification of the framework was conducted.

A synthetic highway section (approximately 1 mile) was modeled with four detectors evenly spaced on the road. A set of true values were configured for the parameters for generating the true traffic data. The true traffic data mimics the field data collected in the field and is required in the computation of the measure of fit. The auto calibration framework proposed in Section 3.4.2 was applied to the synthetic highway section to recover the true values.

Considering the complexity and nonlinearity of the calibration problem, the optimization program NOMAD was configured with the following features activated:

- Latin hypercube sampling. This feature allows maximum coverage of the search space.
- The variable neighborhood search parameter is activated and configured at its maximum value 0.99. This feature enables searching in the neighborhood to avoid being trapped in a local minimum.

- Integer programming. All parameters to be calibrated were assumed to have a granularity 0.1 or higher. Hence the integer programming feature was activated to avoid unnecessary evaluation of parameters with finer resolution.

After in total 1536 iterations, the optimal values of parameters were summarized in Table A.3 and the visualized in Figure A.4. Though the optimal parameters did not recover the true parameters, the speed RMSE is improved from the simulation using the default parameters by 89.7%. Moreover, the speed RMSE using optimal values was 5.15 which was on the same level of error introduced by the stochasticity in the simulation.

Table A.3: Calibration Results for the Synthetic Model

Parameter	True value	Default value	Optimal value	Error
car *speedAcceptance*	1.08	1.1	1.29	19%
truck *maxAccel* (m/s^2)	0.9	1.0	1.18	31%
car *sensitivityFactor*	0.95	1.0	0.88	7.3%
truck *sensitivityFactor*	1.03	1.0	1.1	6.8%
car *reactionTime* (s)	0.8	0.8	1.0	25%
truck *reactionTime* (s)	1.2	0.8	1.0	16.7%
speed RMSE	0	49.77	5.15	89.7%*

*: Improvement over default values

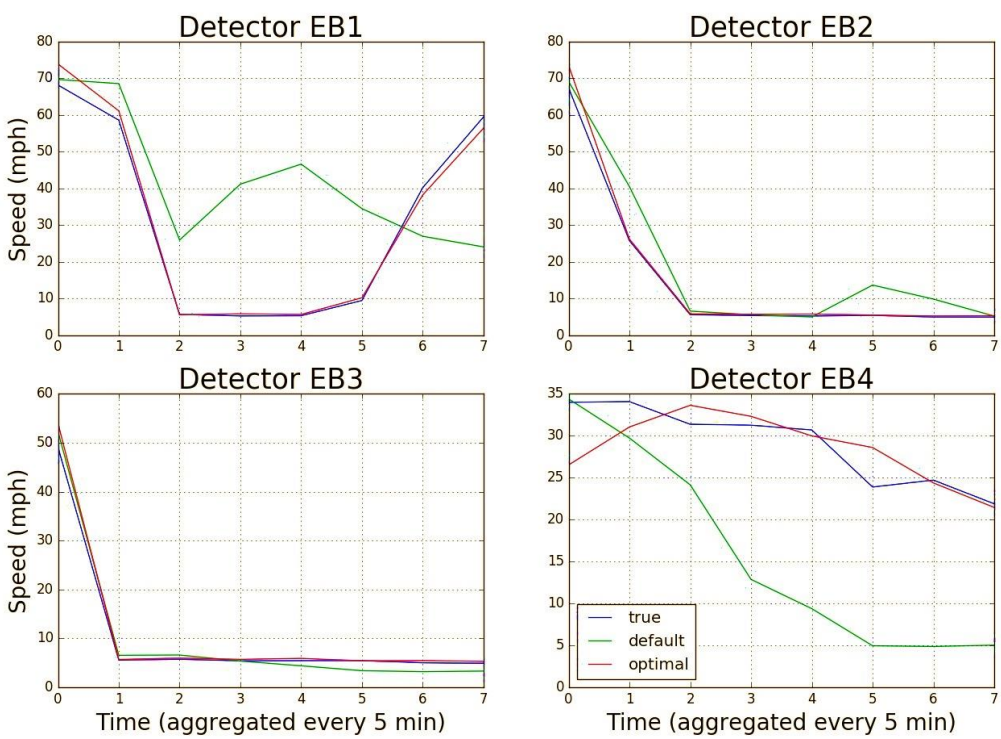

Figure A.4: Calibration result for the synthetic model.

Considering the high nonlinearity of the optimization problem, the parameters are correlated and the combined effect of different values can be comparable. For example, the autocalibration program overestimates truck *maxAccel* and underestimates truck *reactionTime* which combined can produce similar acceleration and deceleration characteristics in congested traffic. Therefore, the auto calibration framework was concluded as a valid solution for calibrating the parameters in this study.

APPENDIX B: DATA QUALITY ANALYSIS

B.1 METHODOLOGY

This section presents the procedures and data quality metric used for analyzing the dataset.

B.1.1 Metric for Data Incompleteness

The percentage of missing speed data for sensor i denoted m_{v_i} is calculated over n consecutive measurement intervals as follows:

$$m_{v_i} = \frac{1}{n}\sum_{t=0}^{n} \chi\big(v_i\,(t)\big),$$

where

$$\chi\big(v_i(t)\big) = \begin{cases} 0 & \text{if the measurement } v_i(t) \text{ is missing} \\ 1 & \text{otherwise,} \end{cases}$$

is an indicator function that returns one (1) when the speed data $v_i(t)$ of sensor i during time interval t, is recorded, and zero (0) when the data is missing. The percentage of missing count data is computed similarly.

For each work zone, the missing data is computed over four time intervals as defined above (i.e., the entire month, the peak hours over the entire month, the estimated congested hours and a typical free-flow period). These intervals are selected to understand when the missing data occurs and how it is distributed throughout the day and month. It emphasizes that missing data during peak or congested traffic may be more important from a safety perspective than missing data spread intermittently throughout the month.

B.1.2 Metric for Data Inconsistency

The mean absolute percent change between the count readings of sensors i and $i+1$, denoted Δm_c, is calculated over n consecutive measurement intervals as follows:

$$\Delta m_c = \frac{100}{n}\sum_{t=0}^{n} \frac{|c_{i+1}(t) - c_i(t)|}{c_i(t)},$$

where $c_{i+1}(t)$ and $c_i(t)$ are the count measurements of sensor $i+1$ and i respectively, during time interval t. The mean absolute percent change between the speed readings is computed similarly. If the count measurements of either sensor i or $i+1$ are missing at time t, the timestamp is not included in the calculation of the mean absolute percent change. The value n is taken as the number of intervals where the measurements are not missing.

This procedure is applied on pairs of sensors that are close in distance (e.g., less than 1 mile spacing) with no significant geometric changes (e.g., lane drops, entrance or exit ramps). In free-flow traffic, the average speed and count measurements should be approximately the same from these sensor pairs. The inconsistency analysis is performed over (1) the entire month of interest and (2) a typical free-flow interval. Large discrepancies between sensor pairs are likely due to sensor measurement

errors and not due to traffic dynamics such as a congestion wave, which occur on faster timescales than the data aggregation.

B.2 SMART WORK ZONE DATA QUALITY REPORT

This section presents the report titled Smart Work Zone Data Quality Report (ICT R27-155), which was submitted to IDOT and forwarded to the vendor Ver-Mac. Additional information was provided by Ver-Mac after the submission of the report. Please refer to the main body of the report for the updated analysis and findings.

Smart Work Zone Data Quality Report (ICT R27-155)

Juan Carlos Martinez Mori, Yanning Li, and Prof. Daniel Work[1]
Department of Civil and Environmental Engineering
University of Illinois at Urbana Champaign

December 26, 2015

1. Introduction

This report documents the data analysis for ICT project R27-155, "Improving the Effectiveness of Smart Work Zone Technologies." The project goal is to evaluate the effectiveness of smart work zone technologies by assessing the performance of different sensor network configurations in a microscopic traffic simulation software. The micro simulation software was used to model and calibrate two work zones on I-57/I-64 and I-80 using field data obtained from the Ver-Mac traffic management system deployed on each site.

This brief report summarizes a set of preliminary findings on the data quality of the two Illinois work zones studied in the R27-155 project. It reports on two data quality measures, namely missing data percentages and sensor measurement inconsistencies for the data examined in the project. The main finding is that data streams examined from both work zones contain significant missing and inconsistent data which increased the difficulty of the micro simulation calibration in project R27-155. We would like to share the preliminary findings with IDOT & Ver-Mac to allow further investigation into their potential causes. We welcome questions and feedback on the contents of this report.

2. Data Description

The following work zones were investigated in this study:

1. I-57/I-64: IDOT Contract No. 78276, in Jefferson County, IL. In total, 25 sensors were deployed on the work zone site, including 22 radar sensors and three remote traffic microwave sensors (RTMS).
2. I-80: IDOT Contract No. 60Y64, in Will County, IL. In total, 30 sensors were deployed on the work zone site, including 18 radar sensors and 12 RTMS.

The data quality analysis performed on the data is limited to the time and sensors of interest for simulation in the R27-155 project. Specifically, we limited the analysis to the following:

- *Southbound/eastbound direction of the I-57/I-64 work zone between November 1, 2014 and November 30, 2014.* This dataset is of interest for modeling due to the occurrence of severe congestion, and the simplicity of the work zone geometry during this stage of construction. For the data quality assessment, we considered the data from:

[1] Corresponding author. email: dbwork@illinois.edu

i. The entire month of November 2014.
ii. An estimated peak hour between 1630 and 1730 hours (4:30-5:30 p.m.) for the entire month of November 2014, based on visual inspection of the speed data patterns from the RTMS.
iii. Three time intervals with apparent congestion (i.e., November 26 from 1600 to 1800 hours, November 26 from 2100 to 2300 hours, and November 16 from 1700 to 1830 hours), based on visual inspection of the speed data patterns.
iv. A typical free-flow time interval (November 18, 2014 from 0600 to 1100 hours).

- *Eastbound direction of the I-80 work zone between May 1, 2015 and May 31, 2015.* This dataset was selected for modeling due to the availability of the data (micro simulation modeling of this work zone began in June 2015) and the relative simplicity of the network geometry. For the data quality assessment, we considered the data from:
  i. The entire month of May 2015.
  ii. An estimated peak hour between 0700 and 0800 hours. for the entire month of May 2015, based on visual inspection of the speed data patterns.
  iii. Three time intervals with apparent congestion (May 1 from 1530 to 1800 hours, May 3 from 1100 to 1630 hours, and May 7 from 0700 to 1630 hours), based on visual inspection of the speed data patterns.
  iv. A typical free-flow time interval (May 1, 2015 from 1300 to 1530 hours).

The data from each work zone was accessed through JamLogic, developed by Ver-Mac. It includes the speed and count data aggregated in five-minute intervals.

3. Methodology

This section presents the procedures and data quality metric used for analyzing the dataset.

3.1 Metric for Data Incompleteness

The percentage of missing speed data for sensor i denoted m_{v_i} is calculated over n consecutive measurement intervals as follows:

$$m_{v_i} = \frac{1}{n}\sum_{t=0}^{n} \chi\big(v_i\,(t)\big),$$

where

$$\chi\big(v_i(t)\big) = \begin{cases} 0 & \text{if the measurement } v_i(t) \text{ is missing} \\ 1 & \text{otherwise,} \end{cases}$$

is an indicator function that returns one (1) when the speed data $v_i(t)$ of sensor i during time interval t, is recorded, and zero (0) when the data is missing. The percentage of missing count data is computed similarly.

For each work zone, the missing data is computed over four time intervals as defined above (i.e., the entire month, the peak hours over the entire month, the estimated congested hours and a typical free-flow period). These intervals are selected to understand when the missing data occurs and how it is distributed throughout the day and month. It emphasizes that missing data during peak or congested traffic may be more important from a safety perspective than missing data spread intermittently throughout the month.

3.2 Metric for Data Inconsistency

The mean absolute percent change between the count readings of sensors i and $i+1$, denoted Δm_c, is calculated over n consecutive measurement intervals as follows:

$$\Delta m_c = \frac{100}{n} \sum_{t=0}^{n} \frac{|c_{i+1}(t) - c_i(t)|}{c_i(t)},$$

where $c_{i+1}(t)$ and $c_i(t)$ are the count measurements of sensor $i+1$ and i, respectively, during time interval t. The mean absolute percent change between the speed readings is computed similarly. If the count measurements of either sensor i or $i+1$ are missing at time t, the timestamp is not included in the calculation of the mean absolute percent change. The value n is taken as the number of intervals where the measurements are not missing.

This procedure is applied on pairs of sensors that are close in distance (e.g., less than 1 mile spacing) with no significant geometric changes (e.g., a lane drop, entrance or exit ramps). In free-flow traffic, the average speed and count measurements should be approximately the same from these sensor pairs. The inconsistency analysis is performed over (1) the entire month of interest and (2) a typical free-flow interval. Large discrepancies between sensor pairs are likely due to sensor measurement errors and not due to traffic dynamics such as a congestion wave, which occur on faster timescales than the data aggregation.

4. Findings

This section presents the numerical results of the data quality assessment procedures performed on the datasets in each of the work zones. The findings are organized by work zone. RTMS are denoted with the symbol '*' after the sensor ID.

4.1 I-57/I-64

The data completeness findings for all of the sensors in the direction and the time intervals presented in the Data Description (Section 2) are presented in Table 1.

Table 1: November 2014 Southbound/Eastbound Percent Missing Data

Sensor	Entire Period		Peak Hour		Congested Intervals		Free-Flow Interval	
	Speed	Count	Speed	Count	Speed	Count	Speed	Count
SB1	1.33%	1.20%	1.54%	0.77%	10.67%	0.00%	1.64%	1.64%
SB2	1.15%	0.75%	3.59%	0.26%	44.00%	0.00%	0.00%	0.00%
SB3	0.83%	0.44%	3.59%	0.26%	33.00%	0.00%	0.00%	0.00%
SB4	0.54%	0.38%	1.79%	0.26%	16.00%	0.00%	0.00%	0.00%
SB5	7.14%	6.91%	10.51%	8.72%	21.33%	0.00%	0.00%	0.00%
SB6	3.68%	3.02%	7.18%	3.85%	58.67%	0.00%	0.00%	0.00%
SB7*	5.19%	5.00%	7.18%	7.18%	0.00%	0.00%	0.00%	0.00%
SB8	1.52%	1.01%	4.36%	1.03%	49.33%	0.00%	0.00%	0.00%
SB9	0.31%	0.08%	2.82%	0.00%	25.33%	0.00%	0.00%	0.00%
Average	2.41%	2.09%	4.73%	2.48%	28.74%	0.00%	0.18%	0.18%

Note: The symbol '*' denotes an RTMS.

Note the following observations:

- The low percentages of data missing during the typical free-flow interval suggest that the dataset is largely complete when the traffic is in free-flow.
- On average, the radar sensors have a 10-fold increase in the missing speed data percentages during congested periods compared to the monthly average.
- The percentage of missing speed data during congestion is significantly higher than the percentage of missing count data during the same time interval. This may be explained by the way the sensors work; if a speed is not recorded, the vehicle count is set to zero (0), which is regarded as not missing.
- The RTMS does not have any missing speed or count records during the congested intervals but has higher than average missing data percentages over the entire month compared to the radar sensors. As reported on JamLogic, SB7* had low battery and communication timeout issues between November 1 and November 4, which resulted in missing 34.98% of the speed data and 34.38% of the count data.

Given the high percentage of missing radar data during the congested time intervals, the speed and count data from sensors SB1, SB7*, and SB9 are plotted for November 26, 2014, from 1200 to 1900 hours in Figure 1.

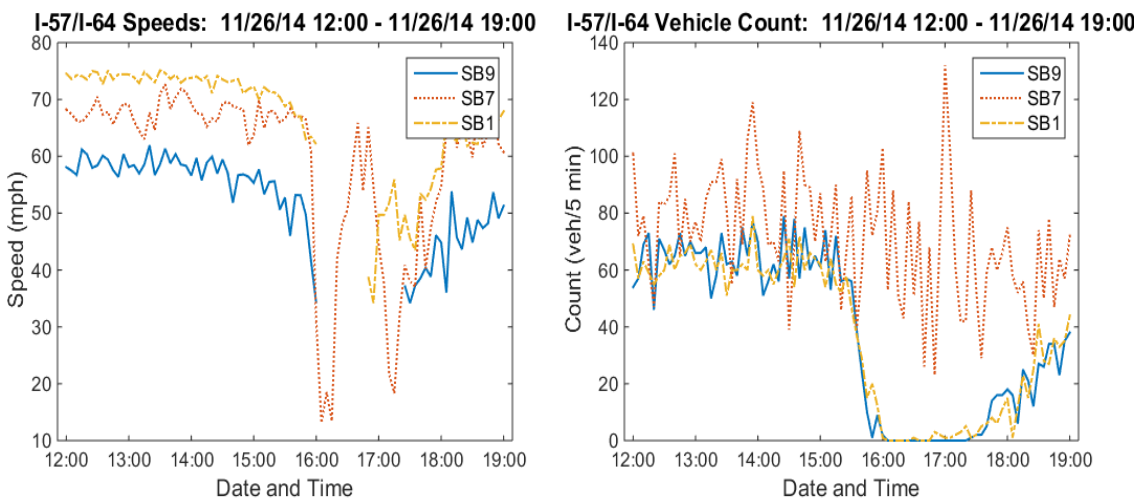

a) Vehicle speeds are missing from radar

b) Vehicle count (veh/ 5 min) drops near zero in radar sensors.

Figure 1: Radar sensors (SB1, SB9) present abnormal readings as traffic congestion starts

It was observed that the radar speed information drops out around 1600 hours, while the vehicle counts drop to zero (0). The speed data is recorded again around 1700 hours, and the vehicle counts become nonzero.

The results of the inconsistency assessment between samples of neighboring sensors for the direction and time intervals shown in the Data Description section are presented in Tables 2 and 3. The notation $i \rightarrow i+1$ refers to the data percent change from sensor i to $i+1$.

Table 2: November 2014 Data Percent Change

Sensor Pair	Percent Change	
	Speed	Count
SB5→SB6	1.64%	23.49%
SB6→SB7*	12.45%	39.64%
SB7*→SB8	10.06%	39.37%
SB8→SB9	6.06%	46.15%

Note: The symbol '*' denotes an RTMS.

Table 3: November 18, 2014 (0600-1100 hr) Data Percent Change

Sensor Pair	Percent Change	
	Speed	Count
SB5→SB6	1.19%	28.39%
SB6→SB7*	10.38%	27.94%
SB7*→SB8	5.26%	24.24%
SB8→SB9	6.93%	19.85%

Note the following observations:

- The count inconsistencies between sensor pairs are large regardless of the sensor type, both averaged over the entire month and averaged over a typical free-flow time interval.
- The inconsistency of speed readings between radar and RTMS pairs is relatively large compared to that of radar – radar sensor pairs.

4.2 I-80

The data completeness findings for the I-80 sensors in the direction and time intervals presented in the Data Description section are summarized in Table 4.

Table 4: May 2015 Eastbound Percent Missing Data

Sensor	Entire Period		Peak Hours		Congested Intervals		Free-Flow Interval	
	Speed	Count	Speed	Count	Speed	Count	Speed	Count
EB3	0.41%	0.41%	0.99%	0.99%	1.99%	1.99%	0.00%	0.00%
EB4	0.44%	0.44%	1.49%	1.49%	3.28%	3.28%	0.00%	0.00%
EB5*	0.27%	0.27%	1.24%	1.24%	2.99%	2.99%	0.00%	0.00%
EB6	0.53%	0.53%	1.49%	1.49%	2.99%	2.99%	0.00%	0.00%
EB7*	0.24%	0.24%	0.74%	0.74%	2.99%	2.99%	0.00%	0.00%
EB8	0.46%	0.46%	2.23%	2.23%	6.47%	6.47%	0.00%	0.00%
EB9*	27.40%	27.40%	30.27%	30.27%	34.83%	34.83%	0.00%	0.00%
EB10	0.52%	0.52%	1.74%	1.74%	10.45%	10.45%	0.00%	0.00%
EB11	0.84%	100.00%	3.23%	100.00%	0.00%	100.00%	0.00%	100.00%
EB12*	4.84%	4.84%	7.69%	7.69%	2.99%	2.99%	0.00%	0.00%
EB14	0.85%	0.85%	1.99%	1.99%	15.92%	15.92%	0.00%	0.00%
EB15	0.74%	0.74%	1.24%	1.24%	16.92%	16.92%	0.00%	0.00%
EB16	0.75%	0.75%	1.24%	1.24%	19.90%	19.90%	0.00%	0.00%
Average	2.95%	10.57%	4.28%	11.72%	9.36%	17.05%	0.00%	7.69%
Average Excluding EB9* & EB11	0.91%	0.91%	2.01%	2.01%	7.90%	7.90%	0.00%	0.00%

Note: The symbol '*' denotes an RTMS.

Note the following observations:

- EB9* has a large number of missing speed and count records, while EB11 did not report any count data over the time period investigated A possible explanation for the issues with EB9* is the multiple communication timeouts during May 2015, as reported by JamLogic.

- During the congested intervals, EB10, EB14, EB15, and EB16 each have data incompleteness percentages above 10%, but lower data incompleteness percentages when averaged over the entire month.
- RTMS EB12* appears to have an intermittent data completeness problem, since the percentages of missing data are highest averaged over the entire month, but lower for any other interval investigated.
- Sensors EB16 through EB8 experienced significant issues during the congestion intervals. Sensors EB7 through EB3 produced more complete datasets, possibly because the queue did not extend to their location.
- Overall, the sensors performed better during the free-flow intervals compared to the congested periods.

The quantitative data inconsistency results between sample pairs of sensors on I-80 for all of May 2015 and a typical free-flow interval are shown in Table 5 and Table 6, respectively.

Table 5: May 2015 Data Percent Change

Sensor Pair	Percent Change	
	Speed	Count
EB4→EB5*	17.08%	73.79%
EB4→EB6	3.12%	22.58%
EB8→EB9*	14.23%	84.49%
EB8→EB10	8.29%	26.35%

Note: The symbol '*' denotes an RTMS.

Table 6: May 1, 2015 (1300-1530 hr) Data Percent Change

Sensor Pair	Percent Change	
	Speed	Count
EB4→EB5*	16.31%	79.85%
EB4→EB6	1.73%	10.35%
EB8→EB9*	10.81%	93.73%
EB8→EB10	6.93%	13.68%

This information can be better understood by observing Figure 2, which plots the data of the typical free-flow interval selected for the quantitative analysis.

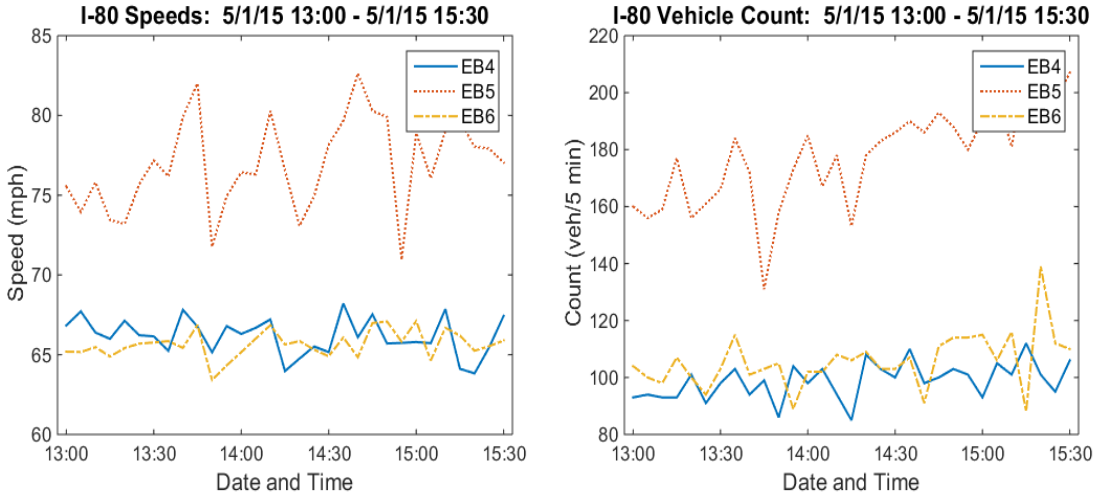

a) Inconsistent average vehicle speed. b) Inconsistent average vehicle count (veh/5

Figure 2: Inconsistency between sensors EB4 and EB6 (radar) and EB5* (RTMS) during free flow.

Note the following observations:

- As seen in Table 5, Table 6 and Figure 2, the RTMS report higher speeds and count measurements than the radar sensors.
- The largest inconsistencies for speeds (10-17%) and counts (73-93%) occur between RTMS and radar sensors. Lower discrepancies are observed between radar sensors.

5. Conclusions

This report documents the data analysis procedures and findings for the Ver-Mac data collected in two work zones. The conclusions include:

1. Data incompleteness and inconsistency issues are common in field data, especially if collected in complex environments such as work zones. Data quality issues were found in both work zones.
2. The I-57/I-64 work zone had severe data incompleteness issues (28% missing) during the congested intervals investigated due to the relatively poor performance of the radar sensors compared to the single RTMS. The I-80 work zone had a lower missing data percentages during congestion, although high missing data percentages were observed on two sensors (EB9* and EB11).
3. Both work zones exhibit data consistency issues, with the I-80 work zone having the largest disagreement between neighboring sensors. Inconsistencies were largest between RTMS and radar sensor pairs, where speed and count errors exceeded 10% and 70%, respectively, on the I-80 work zone.
4. These results/conclusions are limited in scope. A more complete analysis of all of the sensors in each work zone throughout the entire duration of each sensor deployment may provide additional insights. To aid additional analysis, the Python code used to generate the results shown in this report is available at https://github.com/Lab-Work/sensor_quality.

APPENDIX C: IMPLEMENTATION OF ALGORITHMS

C.1 IMPLEMENTATION OF THE SPATIO-TEMPORAL FILTERING ALGORITHM

It has been shown that that estimating the pace of traffic (i.e., the inverse speed), $p(t,x) = 1/v(t,x)$, rather than the velocity, is necessary to avoid the structural bias in the travel times constructed from the velocity field estimated by the spatio-temporal method [81]. The pace estimate $\hat{p}(t,x)$ at time t and space x is as follows:

$$\hat{p}(t,x) = \gamma(t,x)p_{\text{cong}}(t,x) + (1-\gamma(t,x))p_{\text{free}}(t,x), \tag{1}$$

which is a convex combination of two pace estimates p_{free} and p_{cong} weighted by $\gamma(t,x)$. The free-flow and congested pace estimates are computed by averaging a set of measurements $M(t,x)$ in the neighborhood of (t,x) along the free-flow and congested wave speeds of traffic flow, respectively, given by kinematic wave theory [90, 91]. To generate real-time estimates required in work zone applications, the measurement set $M\ (t,x)$ includes only measurements obtained up to time t.

Let $\tilde{p}_m = 1/\tilde{v}_m$ denote the corresponding pace of a velocity measurement obtained at (t_m, x_m). The congested pace p_{cong} is a weighted average of the measurements $M(t,x)$:

$$p_{\text{cong}}(t,x) = \frac{1}{\sum\limits_{m\in M(t,x)} \phi_{\text{cong}}\left(t_m - t, x_m - x\right)} \sum_{m\in M(t,x)} \tilde{p}_m \phi_{\text{cong}}\left(t_m - t, x_m - x\right). \tag{2}$$

The weight of each measurement is computed with a decaying exponential aligned with maximum congested wave speed w:

$$\phi_{\text{cong}}(t,x) = \exp\left(-\frac{|t - x/w|}{\zeta} - \frac{|x|}{\kappa}\right), \tag{3}$$

where κ and ζ are parameters to control the decay rates. The free-flow pace estimate p_{free} traffic is obtained similarly, with the modification that traffic is smoothed along the free-flow wave speed v_{max} instead of the congested wave speed w.

The weighting coefficient $\gamma\ (t,x)$ is defined as follows:

$$\gamma(t,x) = \frac{1}{2}\left[1 + \tanh\left(\frac{v_c - u^*(t,x)}{\Delta V}\right)\right]. \tag{4}$$

In (4), v_c is the critical velocity (i.e., where traffic transitions from free flowing to congested), ΔV is a smoothing width for the traffic state transition, and $u(t,x)$ is given as follows:

$$u^*(t,x) = \min\left\{\frac{1}{p_{\text{cong}}(t,x)}, \frac{1}{p_{\text{free}}(t,x)}\right\}. \tag{5}$$

The purpose of $u\ (t,x)$ is to determine whether p_{cong} or p_{free} indicates that traffic conditions are congested. As a result, Equation 4 produces coefficients that favor the congested estimate when

either p_{cong} or p_{free} indicate congestion (i.e., $\gamma(t,x) \rightarrow 1$), and favors the free-flow estimate otherwise.

A final step to recover the velocity estimate is to invert the resulting pace estimate $\hat{v}(t,x) = 1/\hat{p}(t,x)$.

For the I-80 work zone, the parameters of the spatio-temporal algorithm w, v_{max} and v_c were set according to the calibrated fundamental diagram C.1, respectively $w = -9.29$ mph, $v_{max} = 60.82$ mph, and $v_c = 56.52$ mph.

For the I-57 work zone, the parameters of the spatio-temporal algorithm w, v_{max} and v_c were set according to the calibrated fundamental diagram C.2, respectively $w = -10.92$ mph, $v_{max} = 52.71$ mph, and $v_c = 47.84$ mph.

The additional parameter ΔV is set to 12.43 mph as in [87, 89]. The decay rate controllers κ and ζ are fixed at 0.75 times the sensor spacing and sensor aggregation, respectively, based on an optimization procedure that evaluated the performance of multiple combinations of values that fell in the ranges recommended in [89]. To avoid using excessively old measurements and unnecessarily long computation times, the measurements older than 2.5 minutes are ignored.

C.2 IMPLEMENTATION OF THE ENSEMBLE KALMAN FILTER ALGORITHM

Evolution Equation

The traffic dynamics on a road segment is governed by the Lighthill-Whitham-Richards (LWR) partial differential equation (PDE) [90, 91], which expresses conservation of vehicles on the roadway:

$$\frac{\partial \rho(t,x)}{\partial t} + \frac{\partial \psi\left(\rho(t,x)\right)}{\partial x} = 0, \tag{6}$$

where $\psi(\rho) = \rho V(\rho)$ is the fundamental diagram describing the relationship between the density and flow on a highway. The model is closed by assuming an empirical relationship between the velocity and density of traffic, defined by the velocity function $\mathcal{V}$. In this work, the following velocity function is used:

$$\mathcal{V}(\rho) = \begin{cases} v_{\max}\left(1 - \frac{1}{\beta}\right) & \text{if } \rho \leq \rho_c, \\ w(\rho - \rho_{max})/\rho & \text{if } \rho > \rho_c, \end{cases} \tag{7}$$

where the parameter v_{max} is the maximum free-flow velocity, β controls the slope of the velocity function in free flow, ρ_c and ρ_{max} are the critical and jam density, and w is the maximum backward wave speed.

The LWR PDE is discretized using the Godunov scheme [106], resulting in the cell transmission model [107]. Suppose the time and space domain $[0,T] \times [0,L]$ is evenly discretized into time steps of size ΔT indexed by $n \in \{0,\ldots,n_{max}\}$, and spatial cells indexed by $i \in \{0,\ldots,i_{max}\}$ with cell length Δx. By the conservation of vehicles, at time step n, the traffic density ρ^n in cell i evolves according to the following equation:

$$\rho_i^n = \rho_i^{n-1} + \frac{\Delta T}{\Delta x}\left(q_{i-1/2}^{n-1} - q_{i+1/2}^{n-1}\right), \tag{8}$$

where $q_{i-1/2}^n$ represents the flow between cell $i-1$ and cell i during time step n. The flow over the cell boundary is computed as the minimum flow that can be sent from the upstream cell $i-1$, and the flow that can be received by the downstream cell i:

$$q_{i-1/2}^n = \min\left\{S(\rho_{i-1}^n), R(\rho_i^n)\right\}, \tag{9}$$

where S and R are known as the sending and receiving functions. The functions are constructed from the fundamental diagram as:

$$S(\rho) = \begin{cases} \psi(\rho) & \text{if } \rho \leq \rho_c, \\ q_{max} & \text{otherwise,} \end{cases} \qquad R(\rho) = \begin{cases} q_{max} & \text{if } \rho \leq \rho_c, \\ \psi(\rho) & \text{otherwise.} \end{cases} \tag{10}$$

In the present application, the system state at time n consists of the density in each cell. The upstream inflow to the road $q_{-1/2}^n$ and the downstream outflow $q_{i_{max}+1/2}^n$ are also modeled as state variables, and they are assumed to have stationary dynamics. The concatenated state vector is given as $x^n := [\rho_0^n, \rho_1^n, \dots, \rho_{i_{max}}^n, q_{-1/2}^n, q_{i_{max}+1/2}^n\ ] \in\ \mathbb{R}^{N\times 1}$. The forward model $\mathcal{F}$ is constructed from Equations 4.10 and 4.11, and the stationary dynamic is assumed for the inflow and outflow states.

The model noise variance selected for the density states in cells with an on-ramp or off-ramp, and the noise variance associated with the inflow and outflow $q_{-1/2}^n$, $q_{i_{max}+1/2}^n$, are elevated to account for the larger uncertainty in the state evolution.

Observation Equation

The flow measurements $\tilde{q}_m^n$ and velocity measurements $\tilde{v}_m^n$ at time n and indexed by m are related to the traffic state variables as follows. The flow measurements at the boundaries are direct observations of the flow state variables. For example, the inflow measurement is related to the inflow state variable by $\tilde{q}_m^n = q_{-1/2}^n$ for the appropriate flow measurement m. Consider a flow measurement m on the interior of the road segment located at the boundary between cells $i-1$ and i. The measurement is related to the density state variable in cell $i-1$ or cell i depending on whether traffic is free flowing or congested:

$$\tilde{q}_m^n = \min\left\{S(\rho_{i-1}^n), R(\rho^n i)\right\} + \epsilon_m^n, \tag{11}$$

where ϵ_m^n is the noise associated with the flow measurement.

Velocity measurements are related to the state variables as follows. Let $\tilde{v}_m^n$ denote the velocity measurement at time n at the boundary between cells $i-1$ and i. The velocity is linked to the density state variable in either the upstream or downstream cell depending on the traffic conditions as follows:

$$\tilde{v}_m^n = \begin{cases} \mathcal{V}(\rho_{i-1}^n) + \epsilon_m^n & \text{if } S(\rho_{i-1}^n) < R(\rho_i^n), \\ \mathcal{V}(\rho_i^n) + \epsilon_m^n & \text{if } R(\rho_i^n) < S(\rho_{i-1}^n), \\ \mathcal{V}(\rho_c) + \epsilon_m^n & \text{if } R(\rho_i^n) = S(\rho_{i-1}^n), \end{cases} \tag{12}$$

where ϵ_m^n is represents the noise on the velocity measurement.

The complete set of measurements at time n is written as a vector:

$$\tilde{y}^n := [\tilde{q}_1^n, \cdots, \tilde{q}_{M_q}^n, \tilde{v}_1^n, \cdots, \tilde{v}_{M_v}^n]^T \in \mathbb{R}^{M_v+M_q}, \tag{13}$$

where M_q and M_v denote the number of flow and velocity measurements, respectively. The nonlinear observation equations (11) and (12) and the appropriate measurement error models are used to construct the observation equation in (4.2) in Chapter 4.

Ensemble Kalman Filter

The general algorithmic steps of the ensemble Kalman filtering algorithm are briefly summarized following [108]. The interested reader is referred to [105] for the theoretical foundation and detailed interpretation of the technique. Consider the discrete-time nonlinear system (Equation 4.2 in Chapter 4). Because the observation equation is nonlinear, an augmented state approach [108] is adopted to linearize the observation equation. In the augmented system, the state is denoted by $s^n = \left[(x^n)^T \ \left(\mathcal{H}(x^n)\right)^T\right]^T$, which has the following observation equation:

$$\tilde{y}^n = \mathbf{H}s^n + \epsilon^n = \left[\mathbf{0}_{(M_v+M_q)\times N} \quad \mathbf{I}_{(M_v+M_q)\times(M_v+M_q)}\right] s^n + \epsilon^n. \tag{14}$$

Given the augmented state s with a linear observation equation (14), the EnKF algorithm consists of the following steps: initialization, prediction, and correction. After the algorithm is initialized, it predicts the best estimate at time n with measurements through time $n-1$, denoted $\hat{s}^{n|n-1}$, using the traffic evolution equation and the best estimate $\hat{s}^{n-1|n-1}$. After measurements are received at time n, the predicted state $\hat{s}^{n|n-1}$ is updated to $\hat{s}^{n|n}$ by incorporating the new information contained in the measurements. The algorithm is as follows:

- Initialize a set of state ensembles $\hat{s}^{0|0}(k), \forall k \in \{1, \dots, k_{max}\}$ from the initial state distribution with covariance $\mathbf{P}^{0|0}$.
- Predict the traffic states $\hat{s}^{n|n-1}(k)$ for all ensembles using $\mathcal{F}$ and $\mathcal{H}$ where the model noise $\eta^n(k)$ is independently sampled for each ensemble k from a distribution with model noise covariance $\mathbf{Q}$.

Then the predicted state error covariance can be computed:

$$\mathbf{P}^{n|n-1} = \frac{1}{k_{max}-1}\mathbf{E}^{n|n-1}\left(\mathbf{E}^{n|n-1}\right)^T. \tag{15}$$

In Equation 15, $\mathbf{E}^{0|0}$ is the state error matrix, which is computed by subtracting the estimated state $\hat{s}^{n|n-1}(k)$ for each ensemble k by the mean of estimated states $\bar{s}^{n|n-1}$:

$$\mathbf{E}^{n|n-1} = \left[\hat{s}^{n|n-1}(1) - \bar{s}^{n|n-1}, \dots, \hat{s}^{n|n-1}(k_{max}) - \bar{s}^{n|n-1}\right], \tag{16}$$

where $\bar{s}^{n|n-1} = \frac{1}{k_{max}}\sum_{k=1}^{k_{max}} \hat{s}^{n|n-1}(k)$.

- Given the measurement data $\tilde{y}^n$, the predicted state $\hat{s}^{n|n-1}(k)$ for each ensemble is corrected by the prediction error on the output multiplied by a Kalman gain $\mathbf{K}^n$:

$$\hat{s}^{n|n}(k) = \hat{s}^{n|n-1}(k) + \mathbf{K}^n(\tilde{y}^n - \mathbf{H}\hat{s}^{n|n-1}(k)), \tag{17}$$

where the Kalman gain is computed using the predicted state error covariance (Equation 15):

$$\mathbf{K}^n = \mathbf{P}^{n|n-1}\left(\mathbf{H}^n\right)^T\left(\mathbf{H}\mathbf{P}^{n|n-1}\mathbf{H}^T + \mathbf{R}\right)^{-1}. \tag{18}$$

The second and third steps are repeated sequentially for each time step n until the estimated state over the entire time horizon is obtained. The final velocity estimate is directly computed from the density estimate by applying the velocity function $\mathcal{V}$ to the estimated density field.

Implementation of EnKF

The implementation of the nonlinear Kalman filter first requires a calibration of the fundamental diagram (Equation 7), which captures the macroscopic traffic characteristics.

To calibrate the fundamental diagram, a variety of traffic conditions, consist of one 2-hour free-flow period and three 2-hour congestion periods, were simulated in AIMSUN, where two RTMS were modeled to extract the velocity and flow measurements. During the calibration process, several lessons were learned, and the calibration of a fundamental diagram for the field implementation of the nonlinear Kalman filter may encounter the following difficulties:

- The calibration requires traffic data collected in a variety of traffic conditions, particularly in traffic congestion. This may raise difficulty for field implementation (e.g., traffic congestion may occur rarely).
- In total, 8 hours of data was collected from the micro simulation model for each work zone, resulting in 960 data points for the calibration of the fundamental diagram. The small quantity of data points resulted in inaccurate calibration of the fundamental diagram. For better performance of the nonlinear Kalman filtering, more data points covering all traffic densities are highly recommended.
- The flow and velocity data from RTMS were used to compute the traffic density, which then was used to calibrate the flow density fundamental diagram. However, in traffic with a high percentage of trucks, the same traffic condition can generate significantly different traffic flows due to the different lengths of trucks and cars, causing large spread in the computed density. For instance, the maximum density can range from 340 veh/mile (if all vehicles passed were trucks) to 580 veh/mile (if all vehicles passed were cars). It is recommended to use the directly measured density to calibrate the flow density fundamental diagram, or use a longer detection cycle to mitigate such error.
- Outliers, caused by quantization, erroneous sensor measurements, and numerical errors, in the dataset should be removed before the calibration of the fundamental diagram.

Given the collected data, the parameters of the fundamental diagram were determined following the calibration procedure [119] except the maximum density was computed directly from the minimum stopping distance of vehicles.

The calibrated fundamental diagram for the I-80 work zone is shown in Figure C.1. The fundamental diagram parameters in (7) calibrated for the I-80 work zone are $v_{max} = 60.82$ mph, $\beta = 1000$ veh/mile, $w = -9.29$ mph, and $\rho_{max} = 500$ veh/mile.

The calibrated fundamental diagram for the I-57 work zone is shown in Figure C.2. The fundamental diagram parameters in (7) calibrated for the I-57 work zone are $v_{max} = 52.71$ mph, $\beta = 1000$ veh/mile, $w = -10.92$ mph, and $\rho_{max} = 500$ veh/mile.

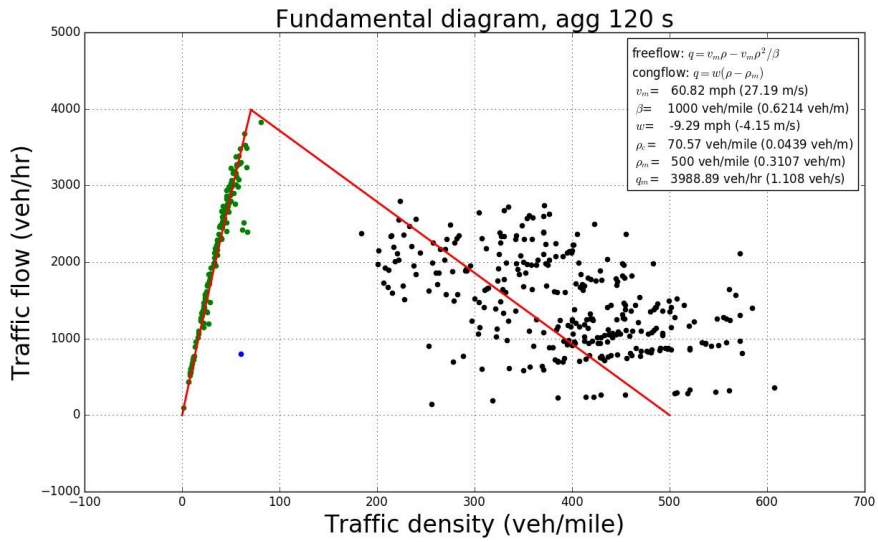

Figure C.1: The calibrated fundamental diagram for the I-80 work zone. The free-flow traffic and congested traffic data points were plotted in green and black, respectively. Blue data points were considered outliers.

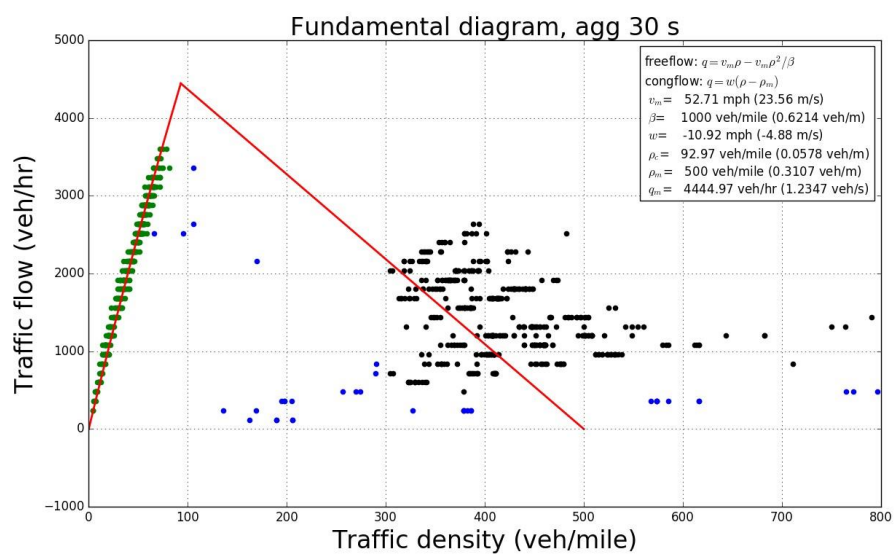

Figure C.2: The calibrated fundamental diagram for the I-57 work zone. The free-flow traffic and congested traffic data points were plotted in green and black, respectively. Blue data points were considered outliers. All data points were aggregated in 30 seconds.

APPENDIX D: COMPLETE EVALUATION RESULTS

Two work zones, one each on I-80 and I-57, were modeled, calibrated, and simulated in a micro simulation environment. This chapter presents the compete evaluation results of over 700 smart work zone configurations.

D.1 I-80 WORK ZONE

In the I-80 work zone, the evaluation results from five simulation replications were averaged to minimize the stochasticity in the micro simulation. For illustration, the true state of one of the simulation is plotted in Figure D.1. The true states of the other four replications were similar.

An example of the velocity estimation using three algorithms with RTMS sensors deployed at 0.5 mile spacing is depicted in Figure D.2. The spatial interpolation simply interpolated the speed measurements to the entire spatial domain, hence the congestion propagated at an infinite speed (i.e., the congestion propagated to the adjacent sensor within a single time step). The spatio-temporal filtering algorithm considered limited free flow and backward propagation speed of traffic, hence produced a smoother propagation of the congestion during the queue formation phase. The main reason for the less favorable transition during the queue dissipation phase was because of the online use of the spatio-temporal filtering algorithm which was initially designed for offline estimation. The nonlinear Kalman filtering algorithm integrated a traffic dynamic model with the sensor measurements, hence produced the smoothest velocity field estimation. The small variance of the velocity estimation in the free-flow area was due to the inverse computation of the velocity based on a fundamental diagram.

The corresponding queue length estimation is plotted in Figure D.3. An online smoother was used to smooth the instantaneous increase of the queue length for the spatial interpolation algorithm. Consequently, the spatial interpolation produced satisfactory queue length estimation. The spatio-temporal filtering algorithm consistently overestimated the queue length due to the assumption of the influence domain of each measurement. The nonlinear Kalman filter generally produced the most accurate estimation of the queue length.

The typical travel time estimation example using RTMS at 0.5 mile spacing is plotted in Figure D.4. The spatial interpolation only considered the spatial measurements at each time step, hence produced the largest variance in the estimation of the travel time. The spatio-temporal produced smoother and better travel time estimation due to the consideration of measurements in the temporal dimension. The nonlinear Kalman filter in general outperformed other algorithms. It should be noted that, the travel time estimation for all algorithms were not satisfactory due to the use of instantaneous travel time computation scheme. For more accurate travel time estimation in fast changing traffic dynamics, a predictive model is recommended.

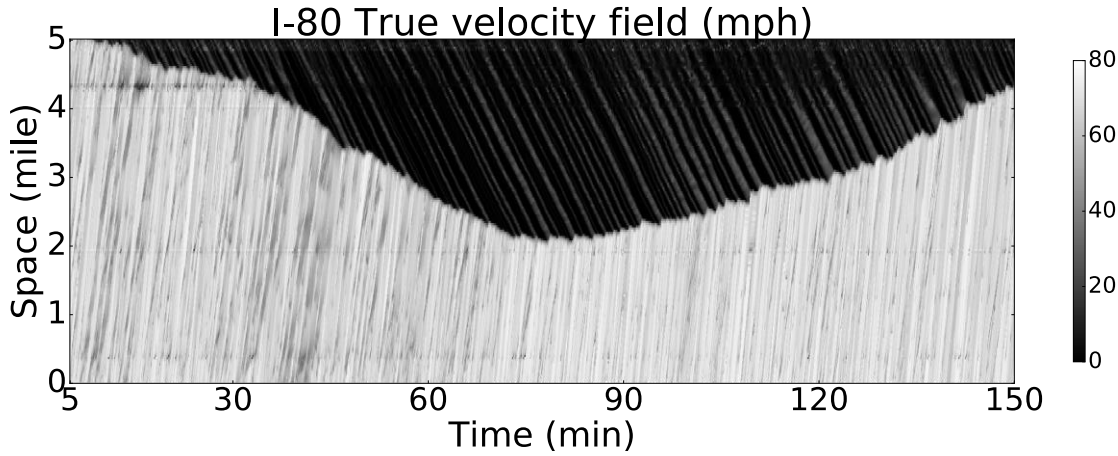

(a) True velocity field over 5 miles and 2.5 hours

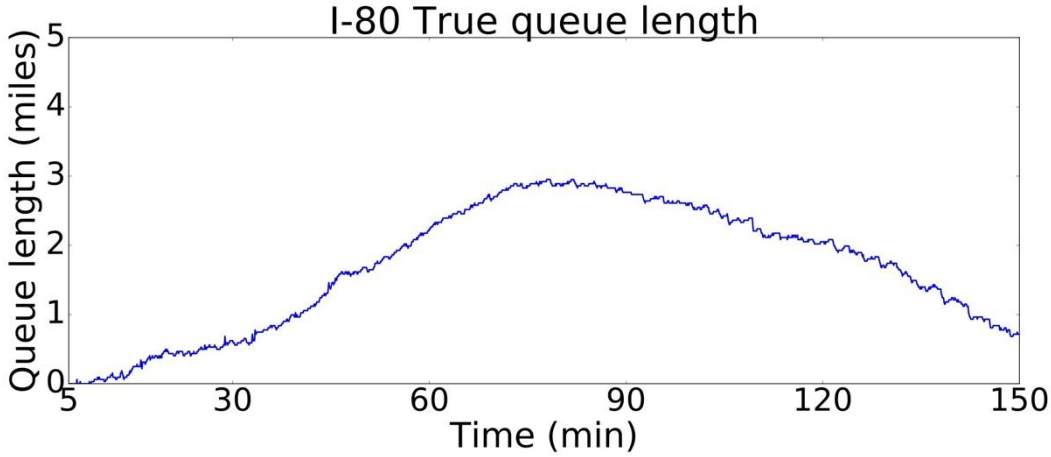

(b) True queue length over 2.5 hours

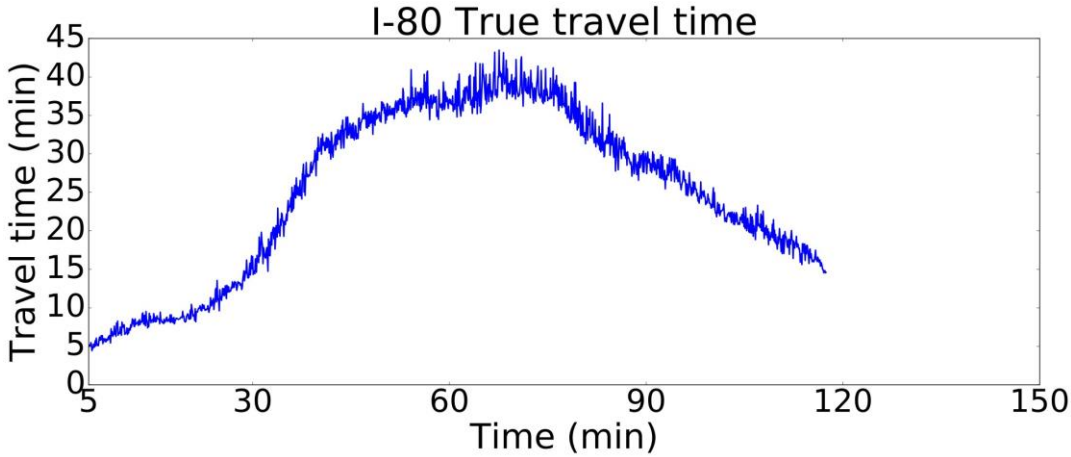

(c) True travel time over 2.5 hours. The true travel time was not obtained in the last period because vehicles that entered the road after approximately 2 hours did not exit before the simulation stopped.

Figure D.1: True state of the (a) velocity field, (b) queue length, and (c) travel time obtained in simulation for I-80 over 5 miles during 1530 to 1800 hours on May 1, 2015.

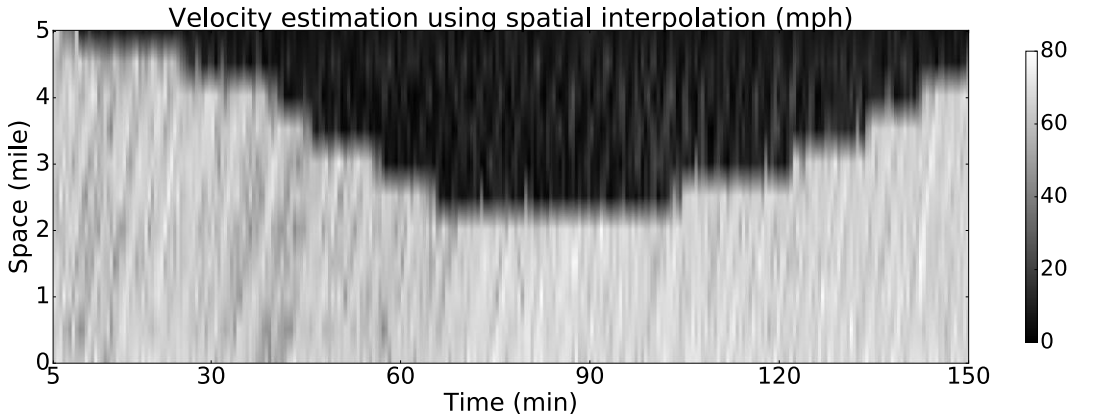

(a)

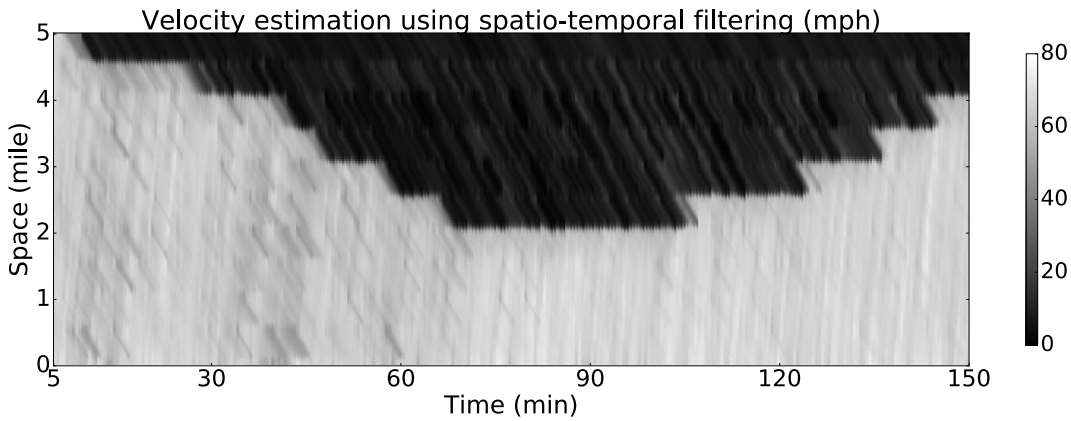

(b)

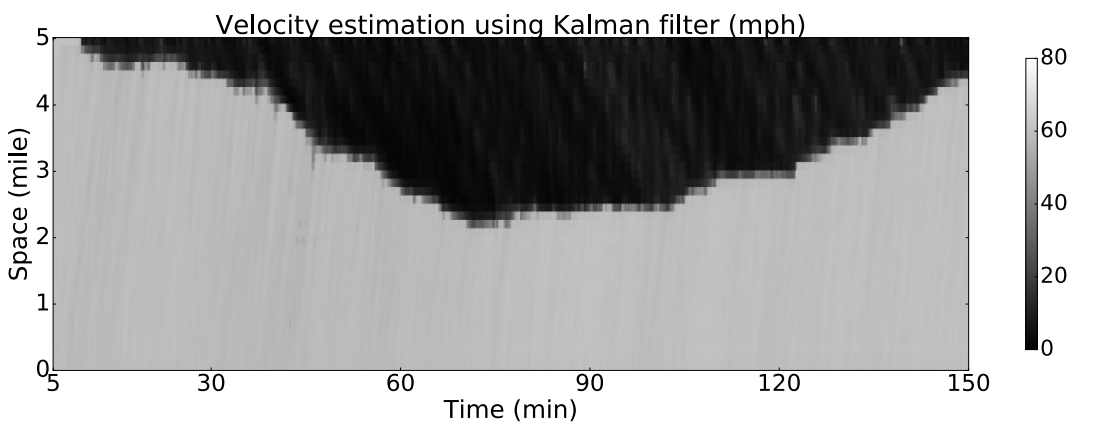

(c)

Figure D.2: An example of estimated velocity field in I-80 work zone using (a) spatial interpolation, (b) spatio- temporal filtering, and (c) nonlinear Kalman filter, with RTMS at 0.5 mile spacing.

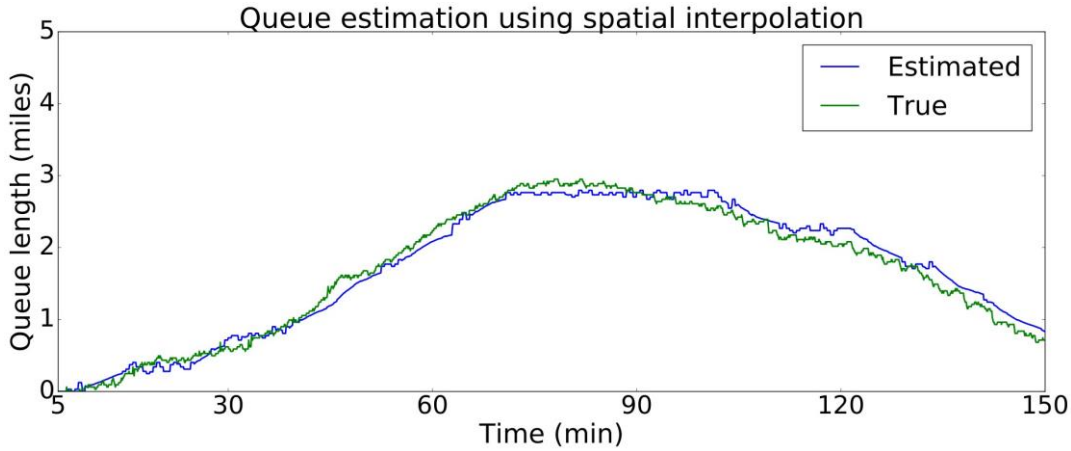

(a)

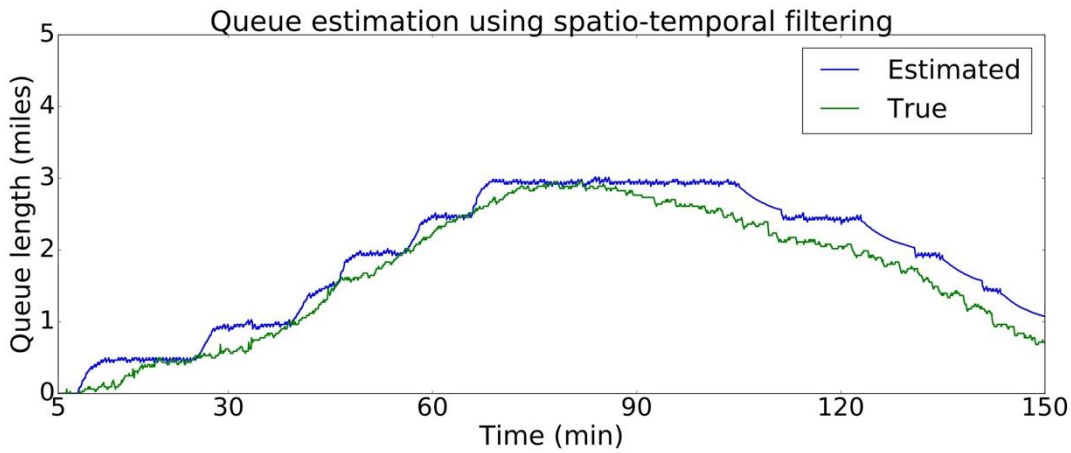

(b)

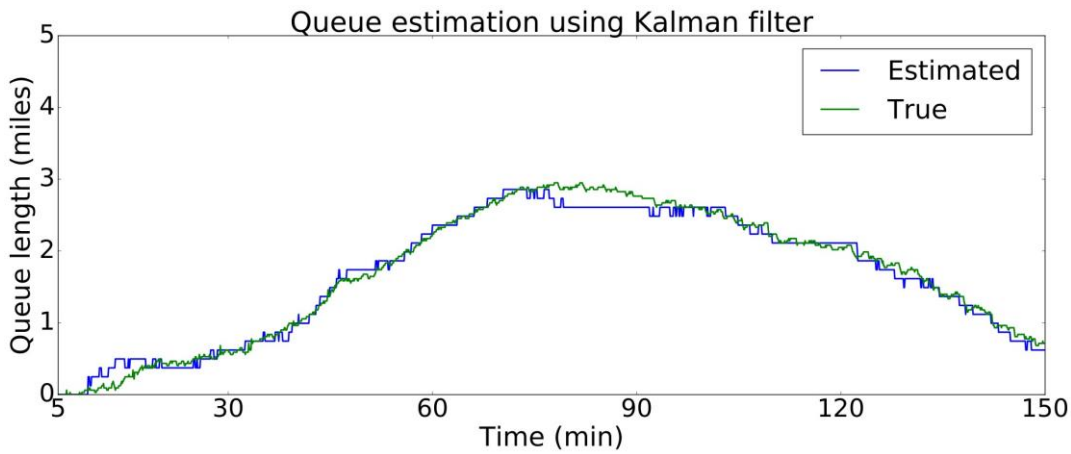

(c)

Figure D.3: An example of estimated queue length in I-80 work zone using (a) spatial interpolation, (b) spatio-temporal filtering, and (c) nonlinear Kalman filter, with RTMS at 0.5 mile spacing. The estimated and true queue length are plotted respectively in blue and green lines.

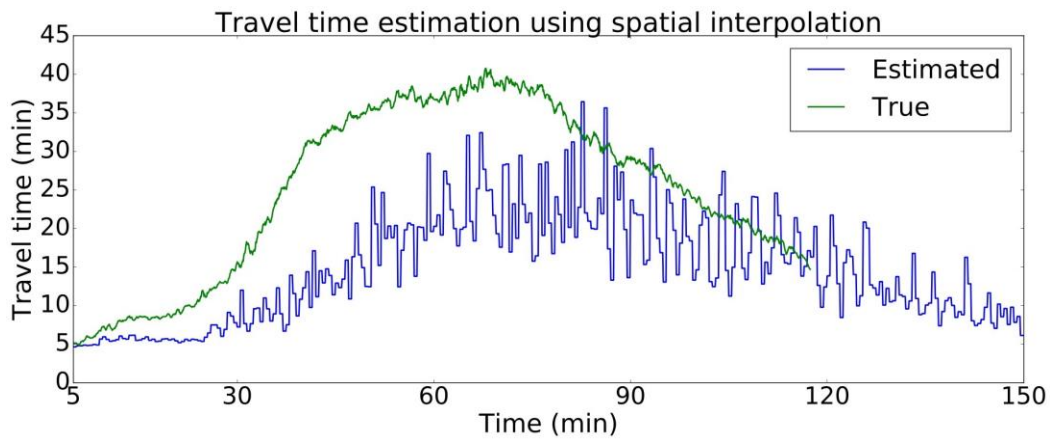

(a)

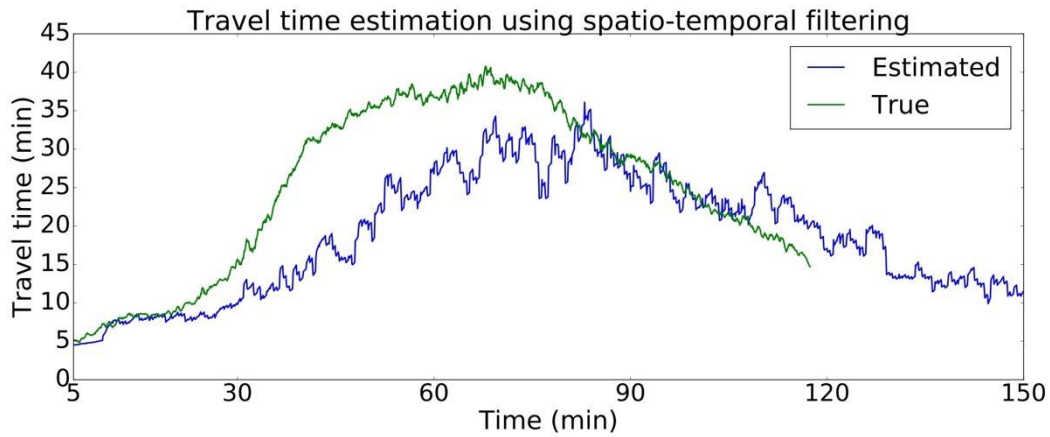

(b)

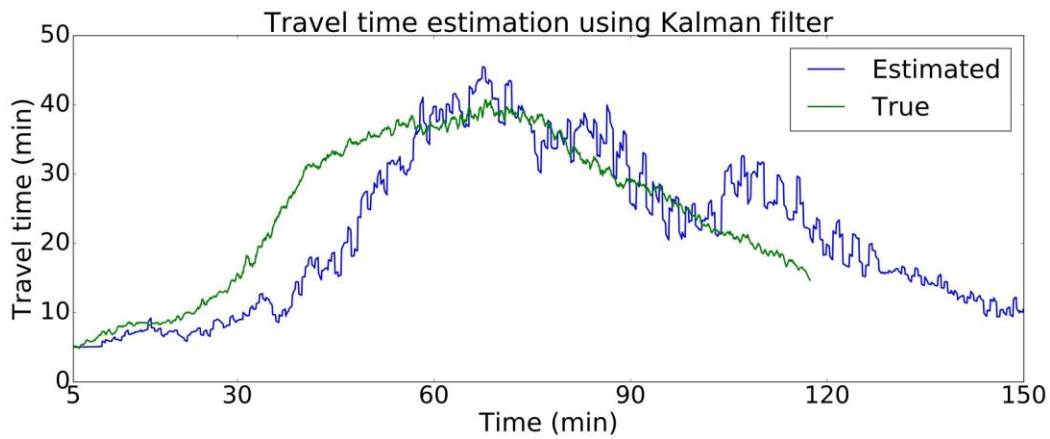

(c)

Figure D.4: An example of estimated travel time in I-80 work zone using (a) spatial interpolation, (b) spatio-temporal filtering, and (c) nonlinear Kalman filter, with RTMS at 0.5 mile spacing. The estimated and true travel times are plotted respectively in blue and green lines.

D.1.1 Algorithms and Sensor Spacing

This subsection summarizes how the algorithms and sensor spacing influence the estimation accuracy for the velocity, the queue length, and the travel time.

The algorithms and spacing were evaluated in three scenarios, respectively using RTMS, radar, and LER. It was identified that, regardless of the types of sensors, (1) the nonlinear Kalman filter generally outperformed other algorithms in the estimation accuracy for the velocity around the queue, the queue length, and the travel time at sparse spacing; and (2) marginal benefits can be obtained at dense spacing (generally less than 10% improvement of the estimation accuracy per sensor at 1 mile spacing and less than 5% per sensor at 0.5 mile spacing).

RTMS

The estimation results when using RTMS at different combinations of algorithms and spacings are summarized in Figure D.5, Figure D.6, Figure D.7, and Figure D.8. The general trend clearly showed the performance for all algorithms improved at denser spacings. The nonlinear Kalman filtering algorithm consistently outperformed other algorithms in the estimation of the velocity, queue length, and travel time. However, the difference across different algorithms became less prominent at denser spacing.

To assess the benefit of additional sensors at each spacing, the percent improvements of the estimation accuracy are plotted in Figure D.9, Figure D.10, Figure D.11, and Figure D.12. Overall, approximately, the percent improvement of the estimation accuracy per RTMS was found to be less than 10% after 1 mile spacing, and less than 5% after 0.5 mile spacing.

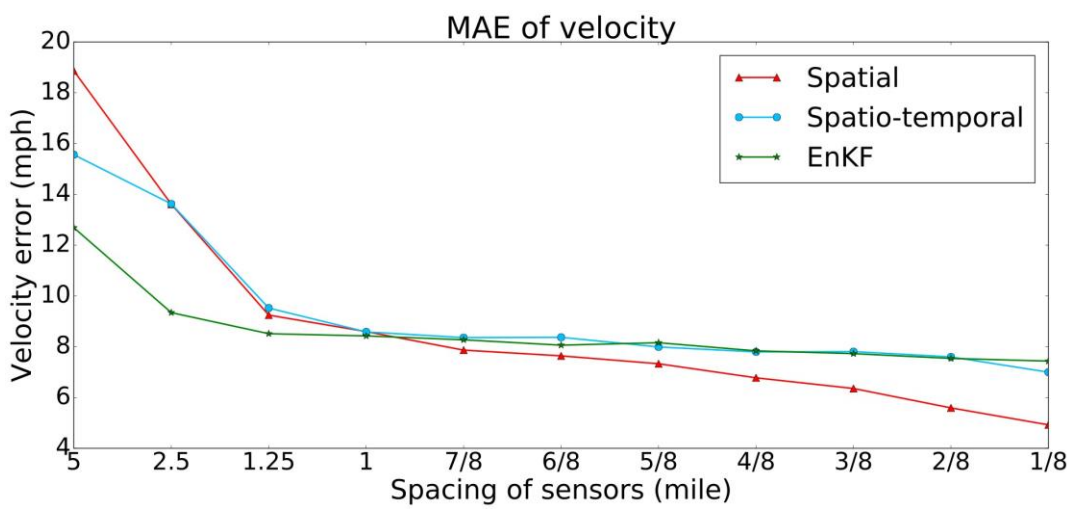

Figure D.5: MAE of the velocity field over the entire spatio-temporal domain using RTMS across a range of spacings in I-80 work zone.

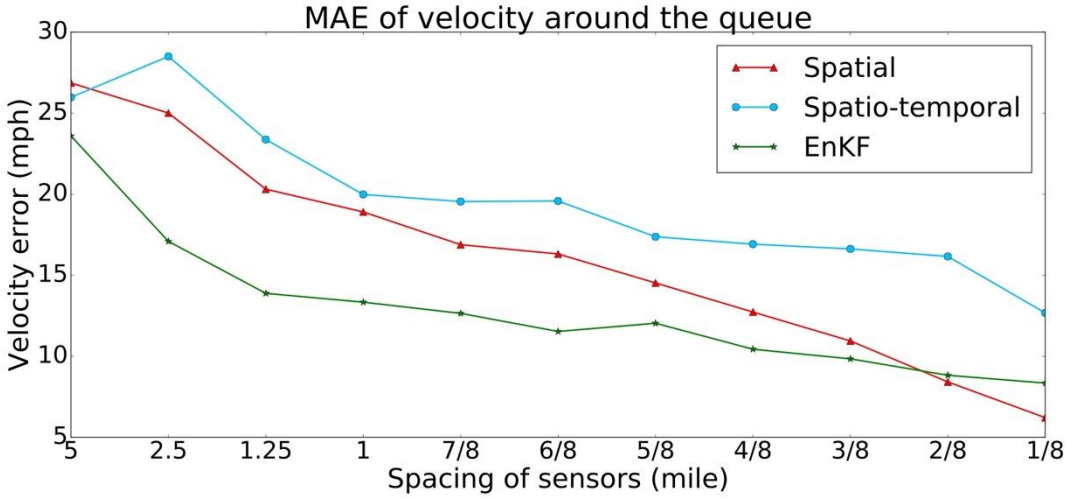

Figure D.6: MAE of the velocity field ± 0.5 mile around the queue using RTMS across a range of spacings in I-80 work zone.

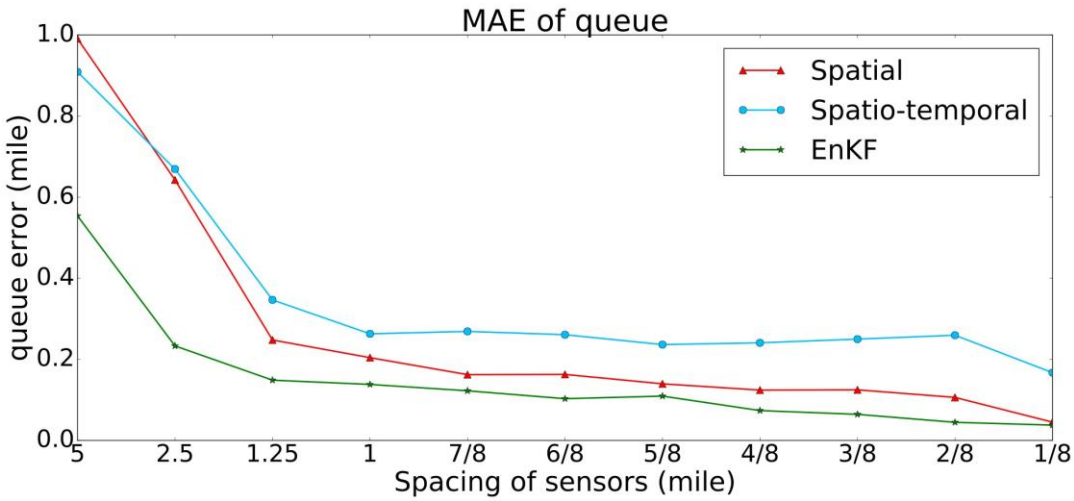

Figure D.7: MAE of the queue length using RTMS sensors across a range of spacings in I-80 work zone.

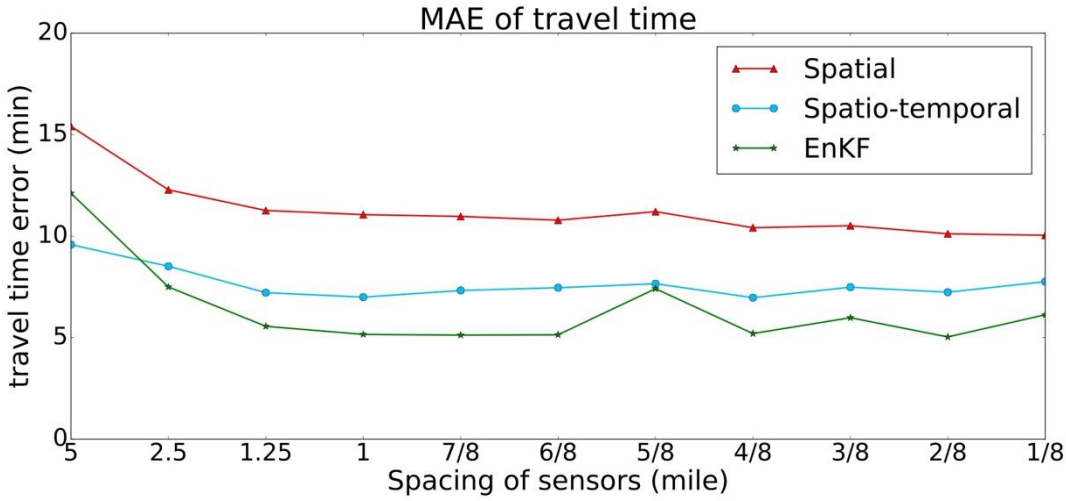

Figure D.8: MAE of the travel time using RTMS across a range of spacings in I-80 work zone.

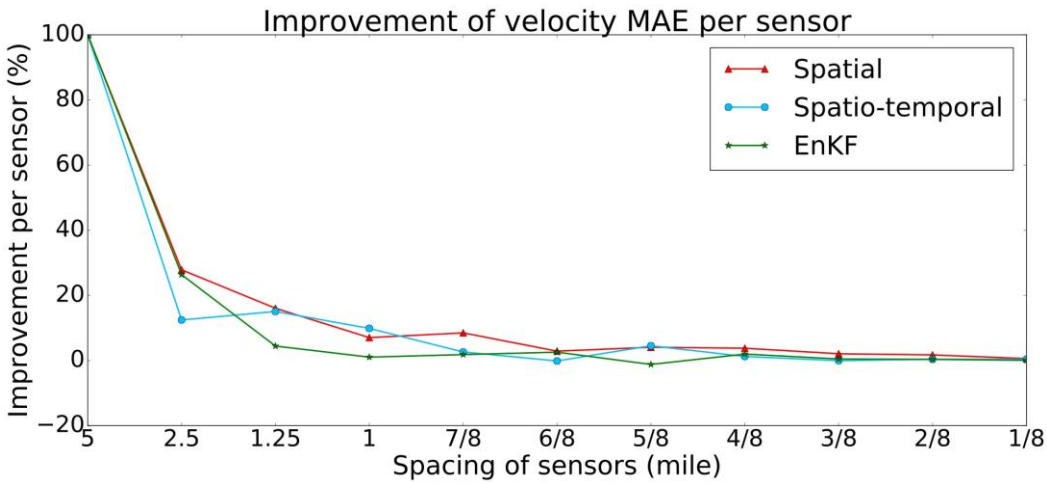

Figure D.9: The percent improvement of the estimation accuracy of the velocity field over the entire spatio-temporal domain per RTMS at each spacing in I-80 work zone.

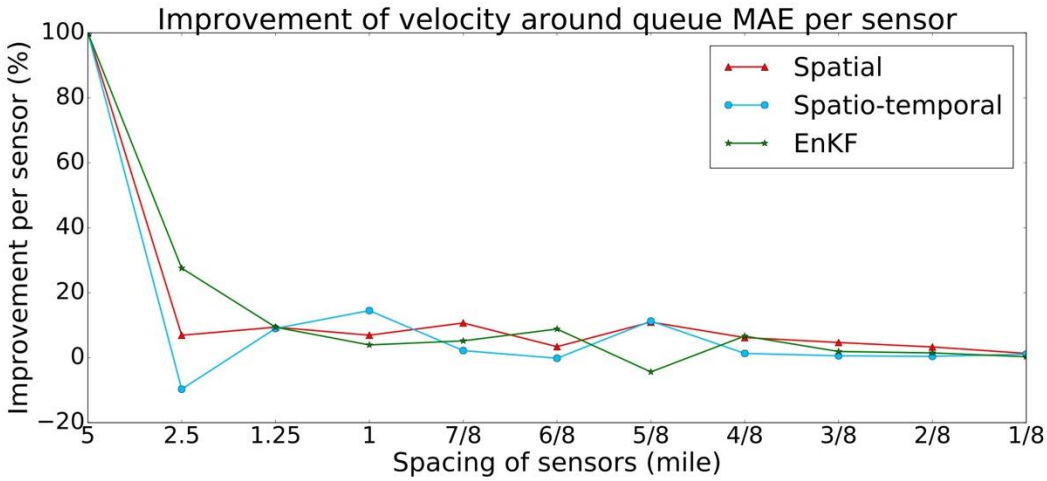

Figure D.10: The percent improvement of the estimation accuracy of the velocity field at ± 0.5 mile around the queue per RTMS at each spacing in I-80 work zone.

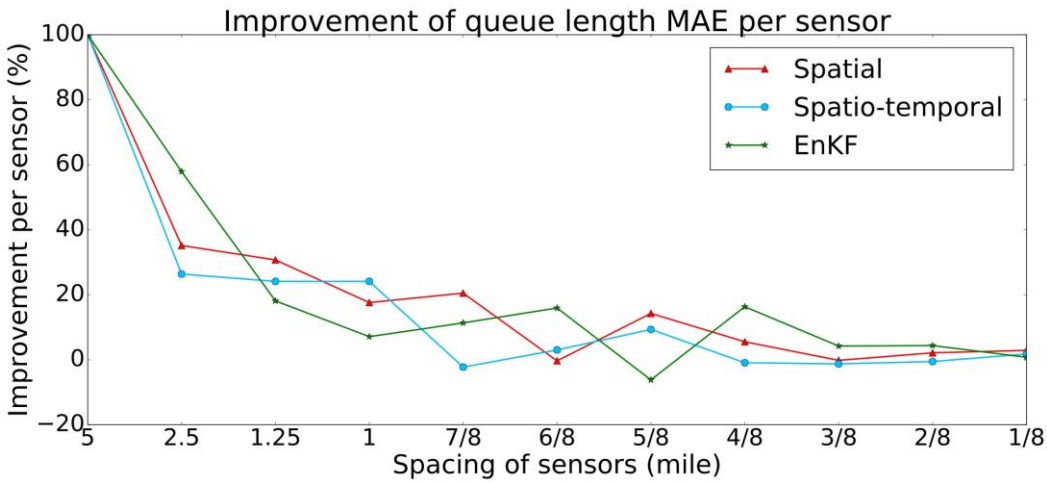

Figure D.11: The percent improvement of the estimation accuracy of the queue length per RTMS at each spacing in I-80 work zone.

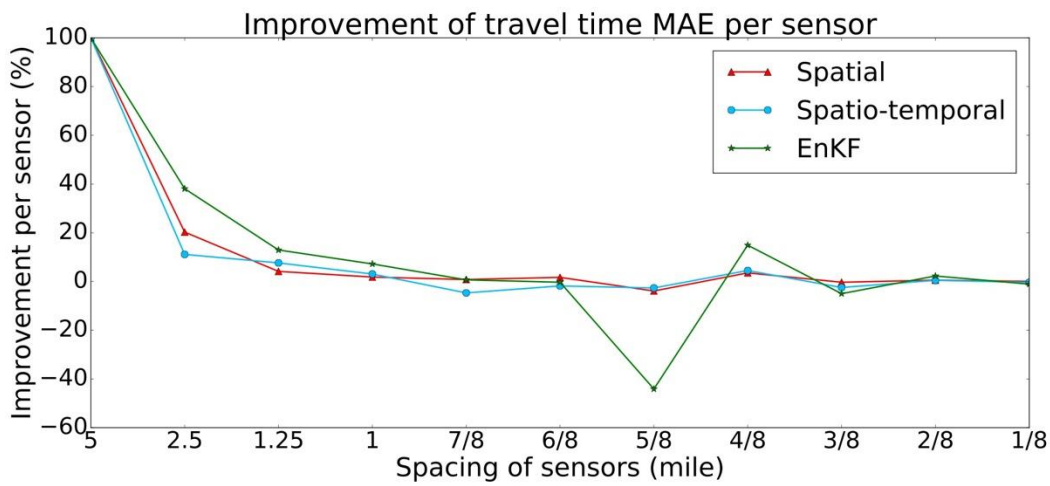

Figure D.12: The percent improvement of the estimation accuracy of the travel time per RTMS at each spacing in I-80 work zone.

Radar

The estimation errors for the velocity, the velocity around the queue, the queue length, and the travel time when using radar sensors at different combinations of algorithms and spacings are visualized in Figure D.13, Figure D.14, Figure D.15, and Figure D.16. The findings were similar to the RTMS scenarios.

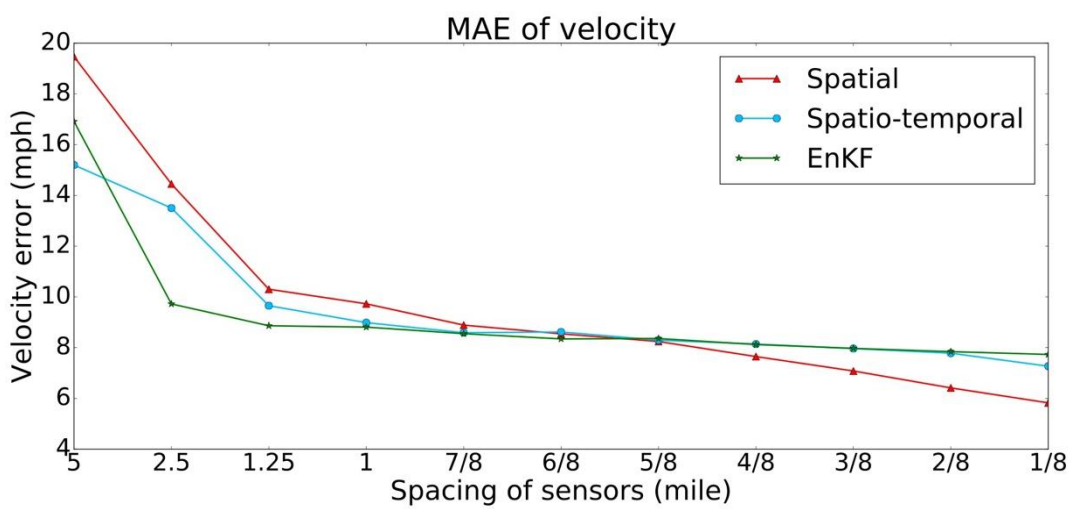

Figure D.13: MAE of the velocity field over the entire spatio-temporal domain using radar sensors across a range of spacings in I-80 work zone.

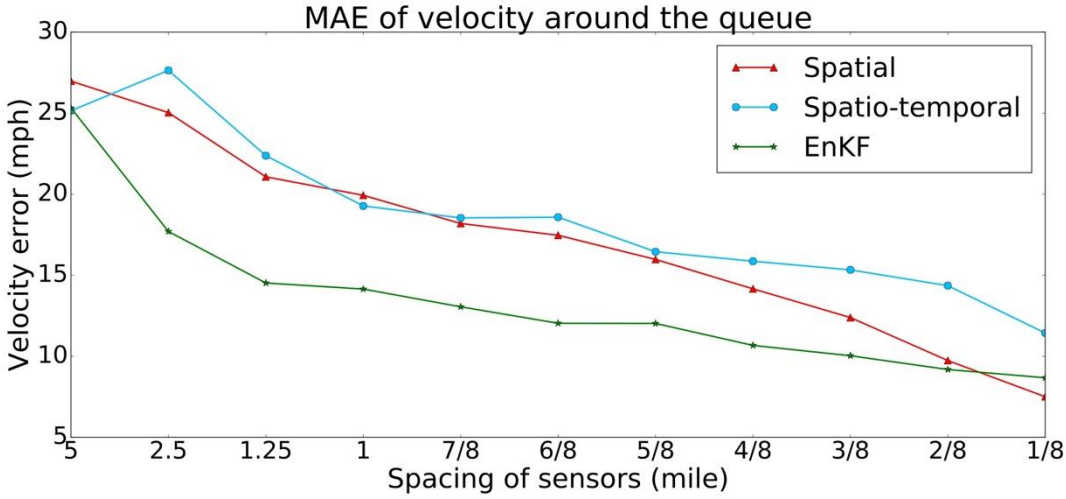

Figure D.14: MAE of the velocity field at ± 0.5 mile around the queue using radar sensors across a range of spacings in I-80 work zone.

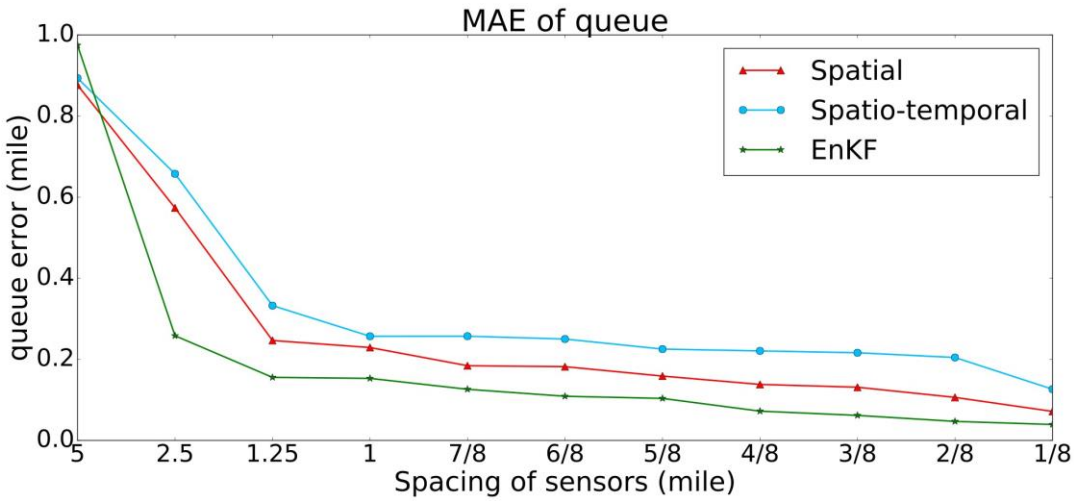

Figure D.15: MAE of the queue length using radar sensors across a range of spacings in I-80 work zone.

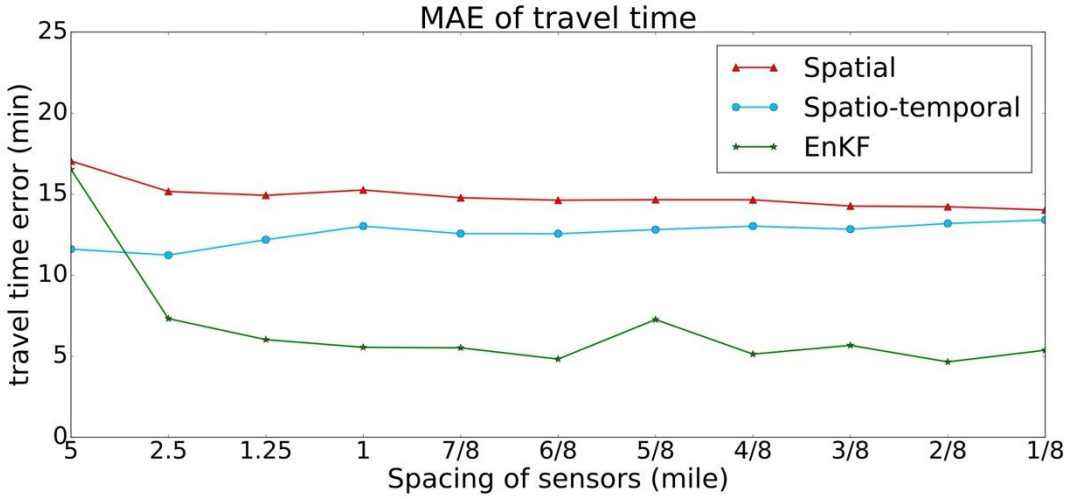

Figure D.16: MAE of the travel time using radar sensors across a range of spacings in I-80 work zone.

LER

The estimation errors for the velocity, the velocity around the queue, the queue length, and the travel time when using LER sensors at different combinations of algorithms and spacings are visualized in Figure D.17, Figure D.18, Figure D.19, and Figure D.20. The findings were similar to the RTMS and radar scenarios with one exception. The advantage of using the nonlinear Kalman filter was found to be much less prominent compared to scenarios using RTMS and radar sensors. The main reason was due to the inaccurate flow measurement from LER sensors, which were critical for good performance of the nonlinear Kalman filter.

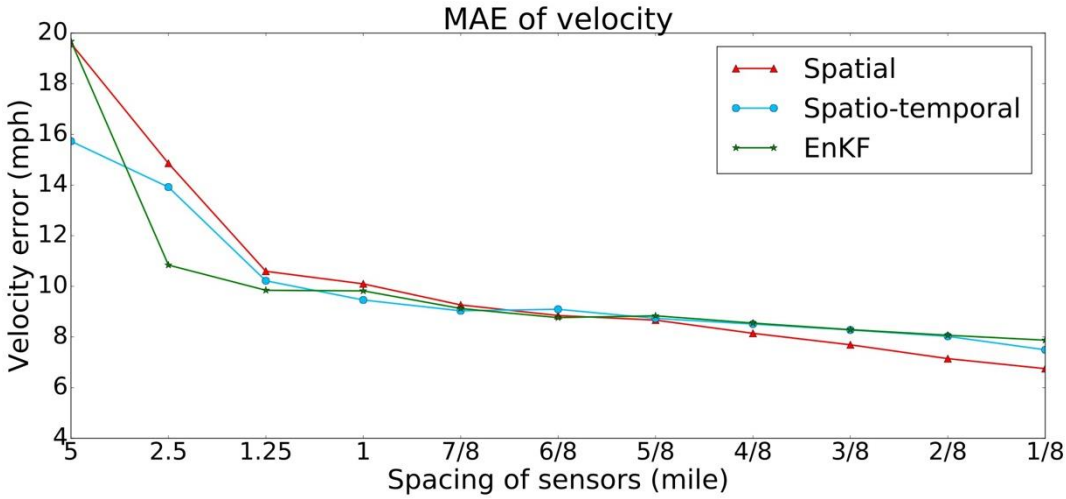

Figure D.17: MAE of the velocity field over the entire spatio-temporal domain using LER sensors across a range of spacings.

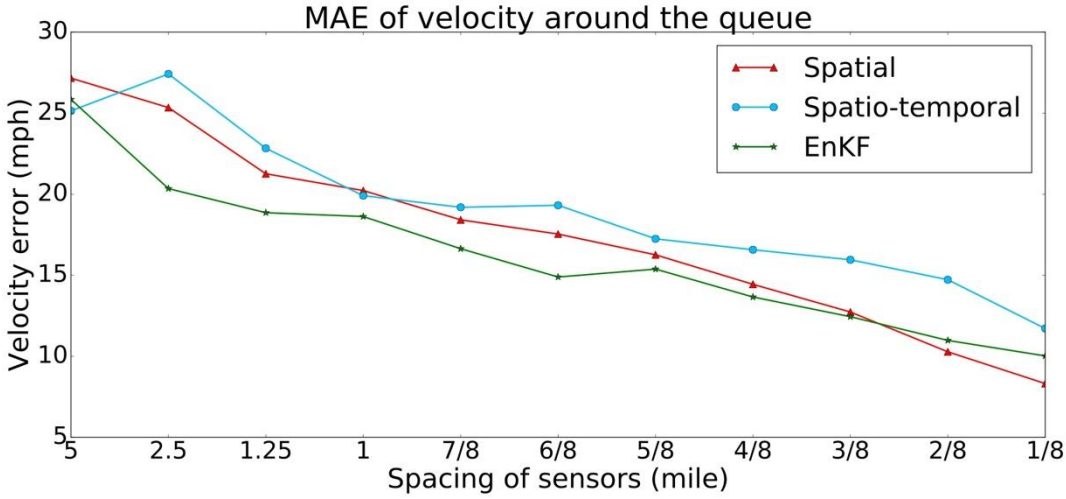

Figure D.18: MAE of the velocity field at ± 0.5 mile around the queue using LER sensors across a range of spacings in I-80 work zone.

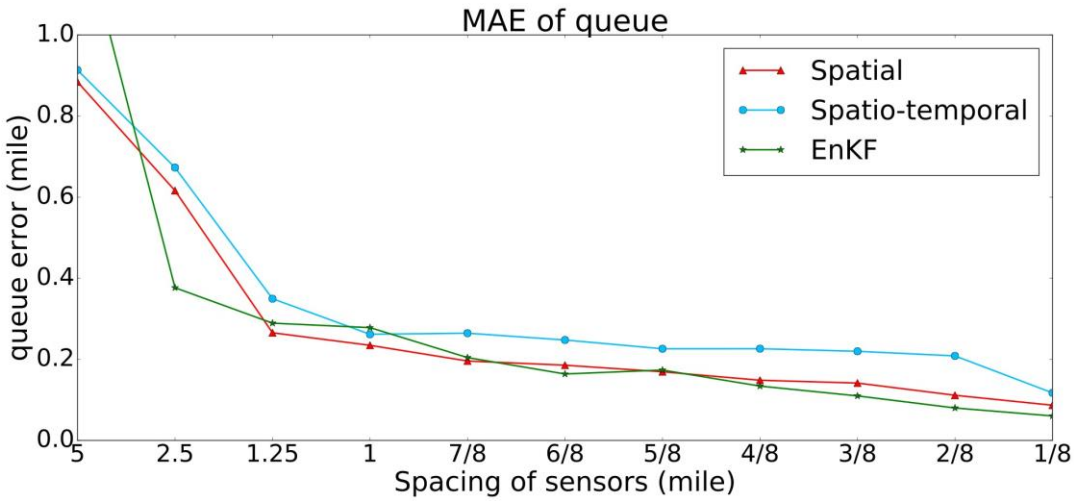

Figure D.19: MAE of the queue length using LER sensors across a range of spacings in I-80 work zone.

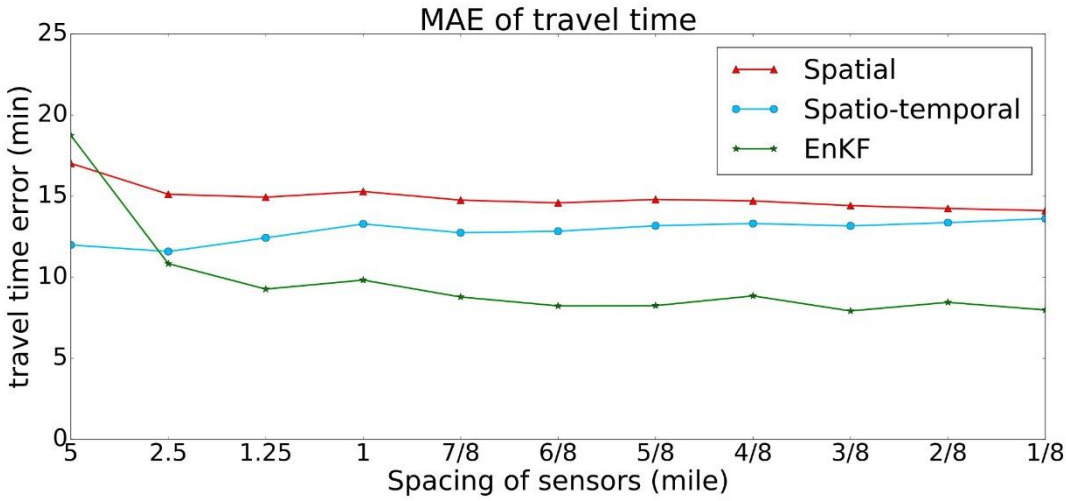

Figure D.20: MAE of the travel time using LER sensors across a range of spacings in I-80 work zone.

D.1.2 Type of Sensors

This subsection presents two scenarios where the influence of the type of sensors is evaluated, respectively at 0.5 mile spacing (Figure D.21) and at 1 mile spacing (Figure D.22).

At 0.5 Mile Spacing

The evaluation result is shown in Figure D.21. The performance of the spatial interpolation and the nonlinear Kalman filter increased from LER to the IDEAL sensors due to the increasing data quality from sensors. In addition, the estimation accuracy when using LER, radar, and RTMS was found to be similar as using ideal sensors, which confirmed the one of the largest sensor measurement error sources was the quantization error. In addition, the nonlinear Kalman filter performed significantly worse when using LER compared to other three types of sensors. The main reason was the increased flow measurement error of LER due to its operation strategy (operates only during half of each detection cycle) and the occlusion issue. It should be noted that good performance of the nonlinear Kalman filtering using radar was based on manual adjustment of the biased flow measurement from radar, which could not be guaranteed in a general field deployment. Finally, the spatio-temporal filtering performed worst when estimating the velocity around the queue and the queue length due to its assumption on the influence domain of each sensor measurement.

At 1 Mile Spacing

The evaluation result is shown in Figure D.22. The magnitudes of the estimation error all increased compared to the scenario at 0.5 mile spacing. Nevertheless, the findings were similar. The good performance of the nonlinear Kalman filter requires accurate flow measurement data (e.g., from RTMS). The biased flow measurement data from radar can be adjusted based on the estimated percentage of occluded vehicles to achieve similar performance, which however could not be guaranteed in a field deployment where the percentage of occluded vehicles may vary dramatically.

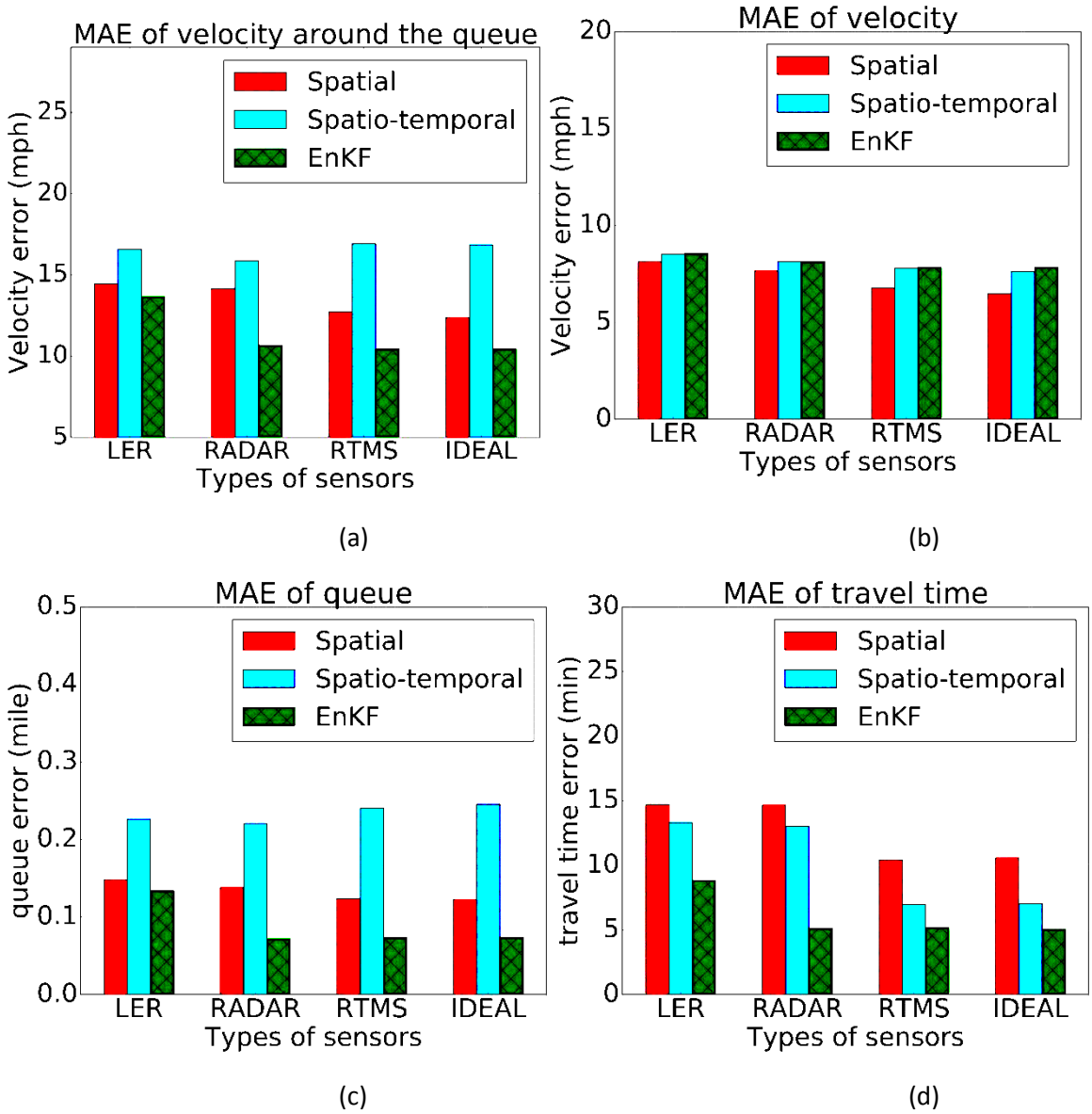

Figure D.21: MAE of the (a) velocity estimation over the entire spatio-temporal domain, (b) velocity estimation at ± 0.5 mile around the queue, (c) queue length estimation, and (d) travel time estimation using different types of sensors at 0.5 mile spacing in I-80 work zone.

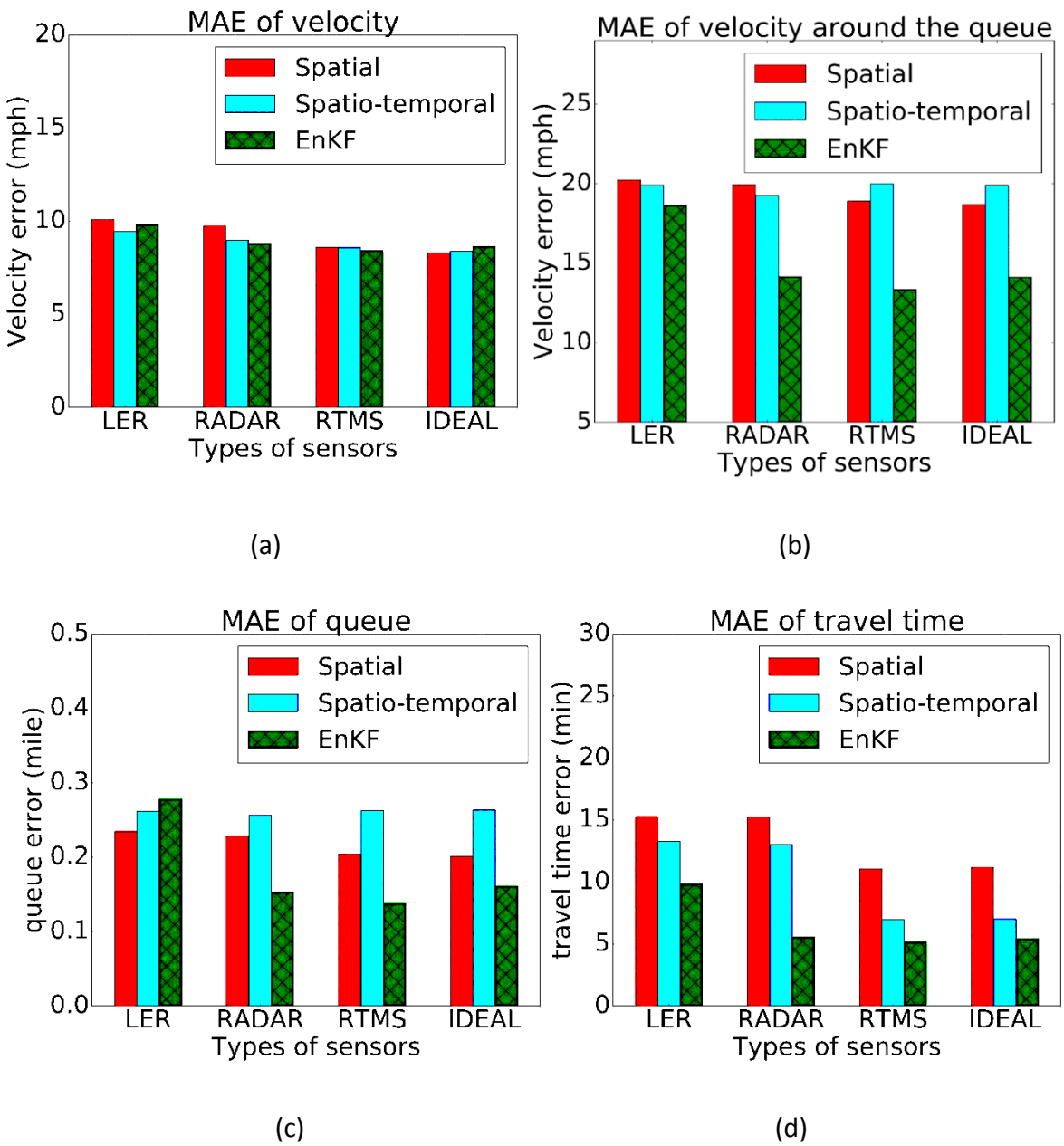

Figure D.22: MAE of the (a) velocity estimation over the entire spatio-temporal domain, (b) velocity estimation at ± 0.5 mile around the queue, (c) queue length estimation, and (d) travel time estimation using different types of sensors at 1 mile spacing in I-80 work zone.

D.1.3 Accuracy of Sensors

The subsection summarizes how the accuracy of individual sensors influences the estimation results. In this experiment, all sensors were assumed to have been properly calibrated to remove the measurement bias of individual vehicles and achieve the advertised accuracy in the product specification. Two scenarios were presented in this subsection: RTMS at 1 mile spacing and radar at 1 mile spacing.

RTMS at 1 Mile Spacing

The evaluation result is shown in Figure D.23. The improvements of the estimation accuracy for the velocity, queue length, and travel time were negligible. This finding indicated the quantization error was the dominating source of the measurement error, and the improvement of the accuracy of the existing RTMS could provide marginal benefits. It should be noted that the decreasing performance of the nonlinear Kalman filter when using improved sensors was caused by the selection of parameters for the Kalman filter, which was optimized for the existing RTMS.

Radar Sensors at 1 Mile Spacing

The evaluation result is shown in Figure D.24. The same finding for RTMS was confirmed to be valid also for radar sensors (i.e., improvement of the accuracy of radar sensors would provide negligible benefits).

D.1.4 Cost Accuracy Analysis

Please refer to Section 5.5 for the cost accuracy analysis.

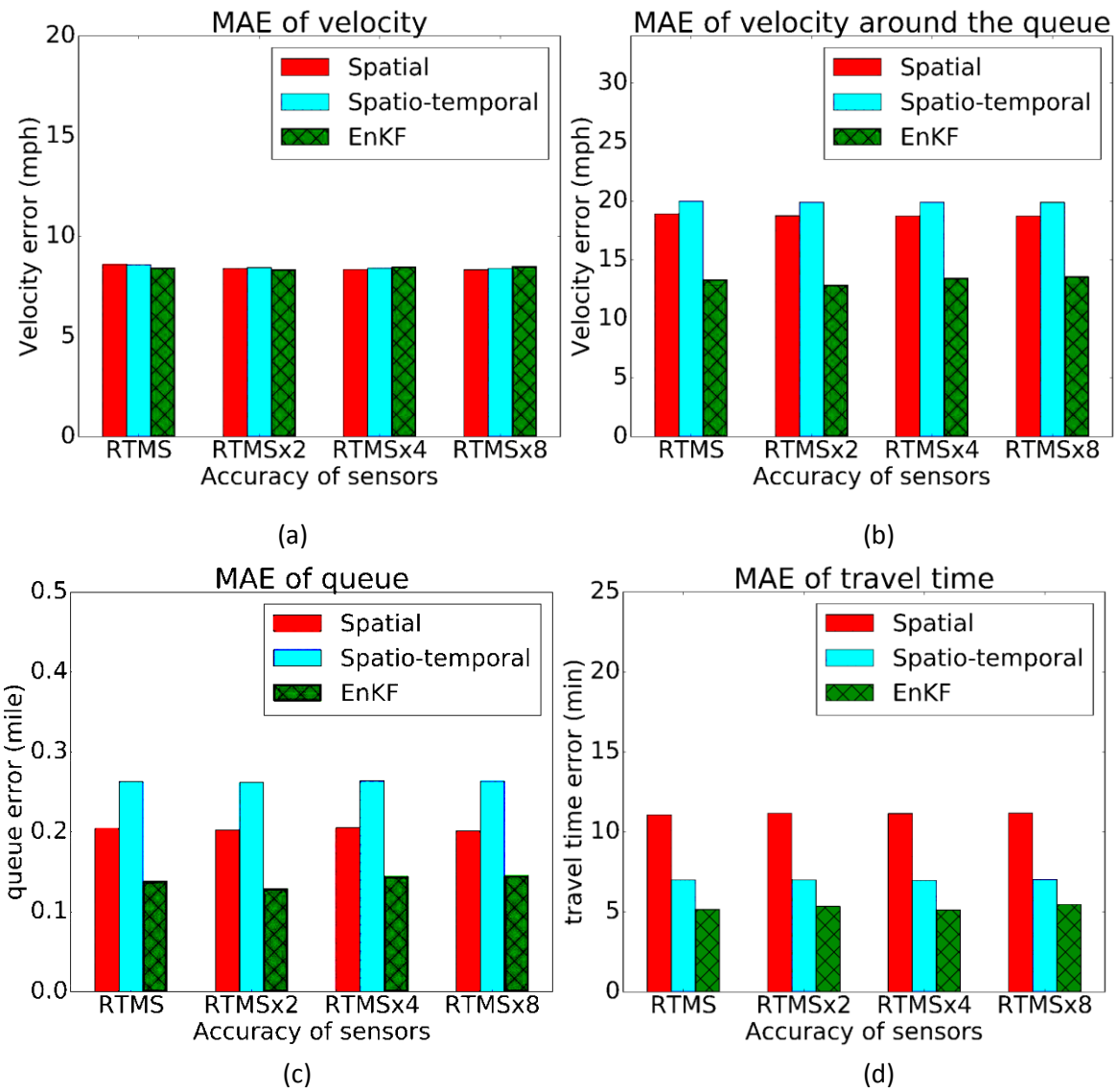

Figure D.23: MAE of the (a) velocity estimation over the entire spatio-temporal domain, (b) velocity estimation at ± 0.5 mile around the queue, (c) queue length estimation, and (d) travel time estimation using RTMS with different levels of accuracy at 1 mile spacing in I-80 work zone.

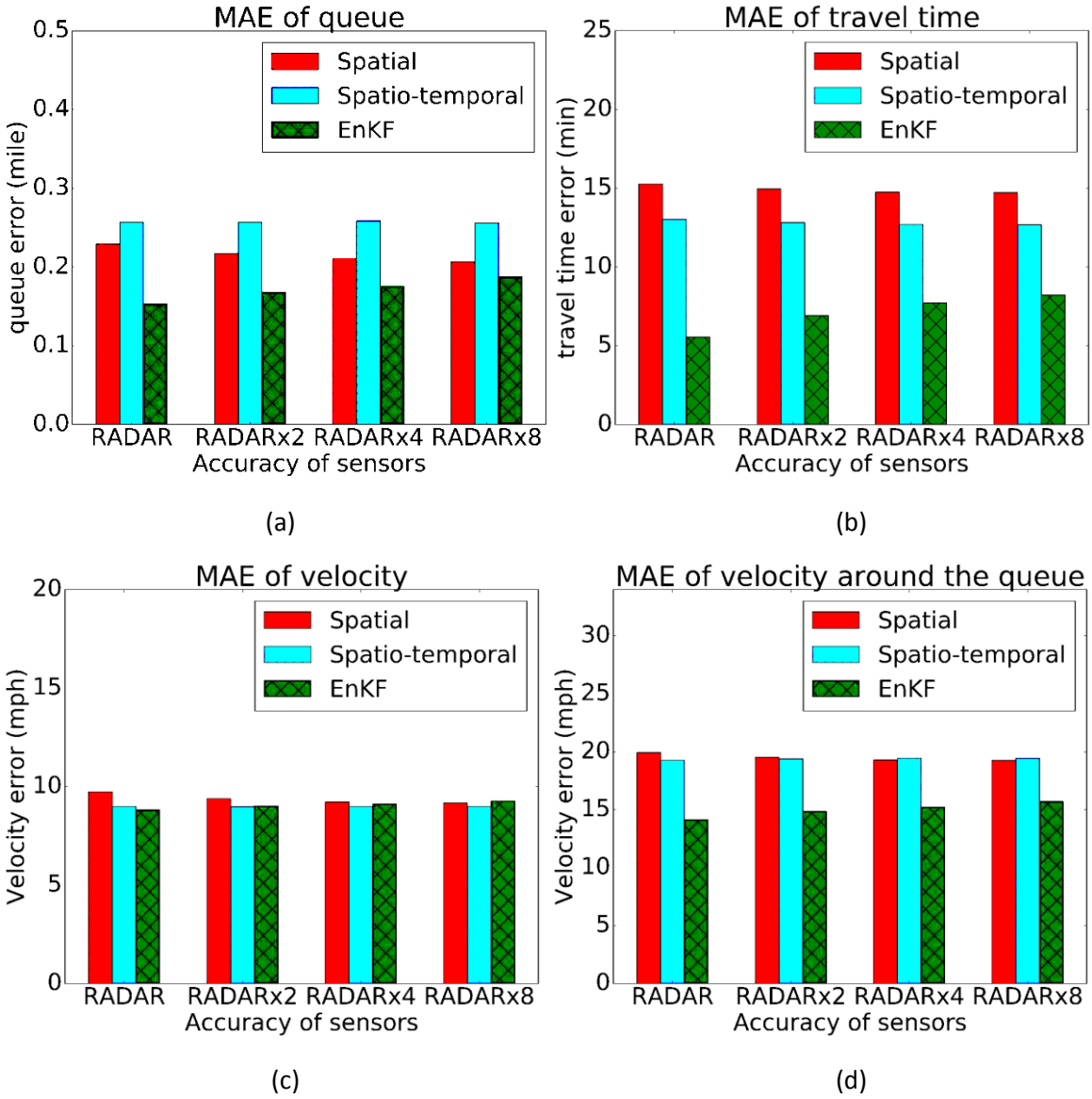

Figure D.24: MAE of the (a) velocity estimation over the entire spatio-temporal domain, (b) velocity estimation at ± 0.5 mile around the queue, (c) queue length estimation, and (d) travel time estimation using radar sensors with different levels of accuracy at 1 mile spacing in I-80 work zone.

D.2 I-57 WORK ZONE

For the I-57 work zone, only one replication was simulated for each sensor network configuration and traffic estimation algorithm since it was found the stochasticity in the micro simulation was negligible during the analysis for the I-80 work zone. For illustration, the true state is plotted in Figure D.25. The simulation successfully captured the formation of the congestion. However, the significantly amount of missing data as discussed in Section 3.2 caused challenges for a proper calibration of the micro simulation model. In addition, there lacked sufficient information in the work zone to justify the use of random fluctuating inflows to create a dissipation phase of the congestion. Therefore, the focus of the calibration was to capture the formation of the congestion (i.e., the backward propagation of the congestion).

An example of the velocity estimation using three algorithms with RTMS deployed at 0.5 mile spacing is depicted in Figure D.26. The periods of free-flow velocity estimates in the congested area showed the spatial interpolation was sensitive to missing data. The nonlinear Kalman filter algorithm produced unsatisfactory velocity estimation in the free-flow area, which again was due to the inaccurate fundamental diagram.

The corresponding queue length estimation is plotted in Figure D.27. The spatio-temporal filtering algorithm consistently overestimated the queue length due to the assumption of the influence domain of each measurement.

The typical travel time estimation for this example using RTMS at 0.5 mile spacing is plotted in Figure D.28. Both the spatial interpolation and the nonlinear Kalman filter underestimated the travel time due to the use of the instantaneous travel time computation scheme, which failed to capture the fast propagating congestion. Though the spatio-temporal filtering algorithm consistently overestimated the queue length, it produced the best travel time estimation.

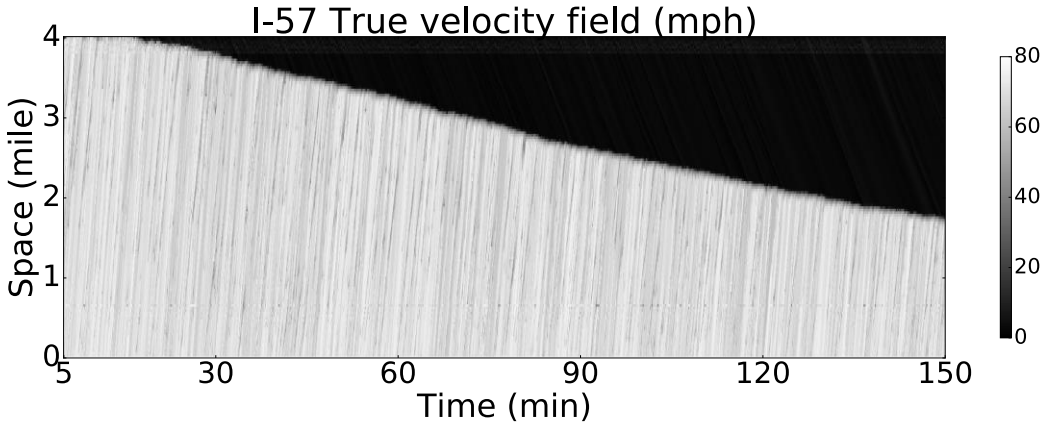

(a) True velocity field over 4 miles and 2.5 hourS

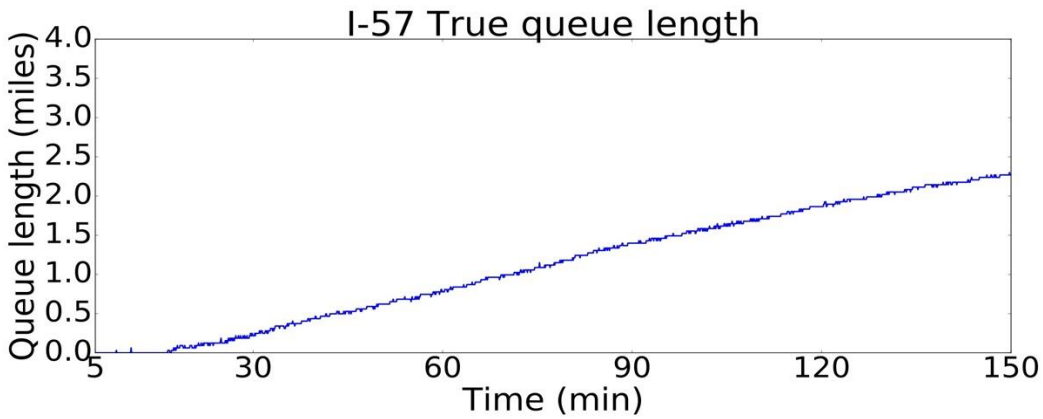

(b) True queue length over 2.5 hours

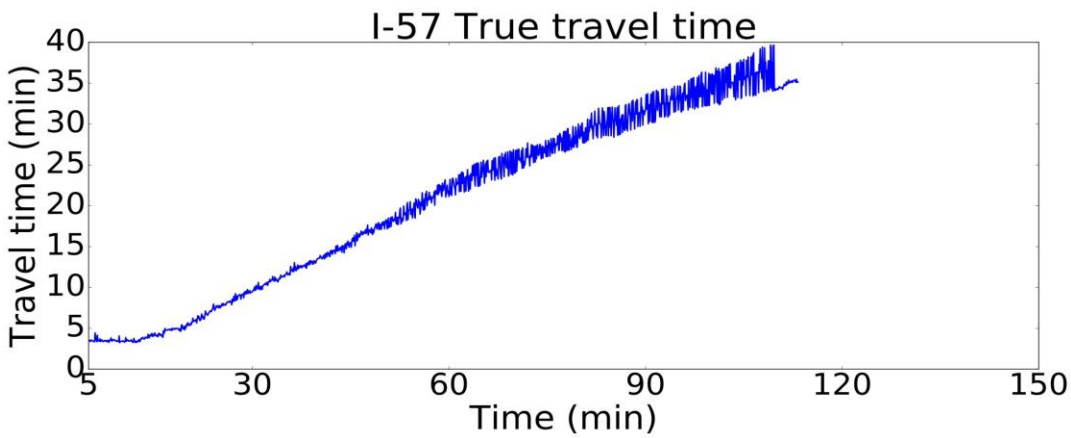

(c) True travel time over 2.5 hours; the true travel time was not obtained in the last period because vehicles that entered the road after approximately 2 hours did not exit before the simulation stopped

Figure D.25: True state of the (a) velocity field, (b) queue length, and (c) travel time obtained in simulation for the I-57 work zone over 4 miles during 1530 to 1800 hours on November 26, 2014.

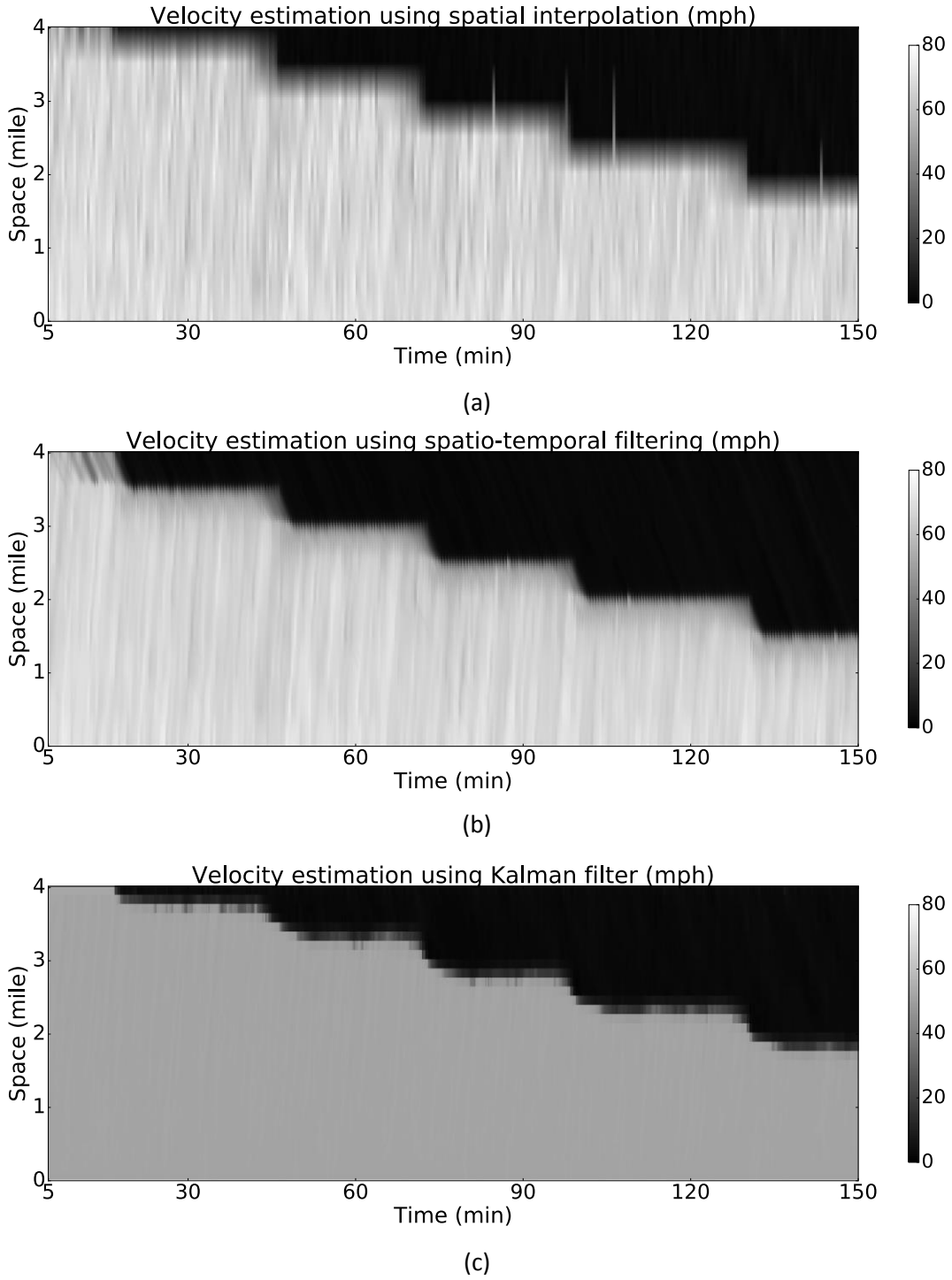

Figure D.26: An example of estimated velocity field using (a) spatial interpolation, (b) spatio-temporal filtering, and (c) nonlinear Kalman filter, with RTMS at 0.5 mile spacing in the I-57 work zone.

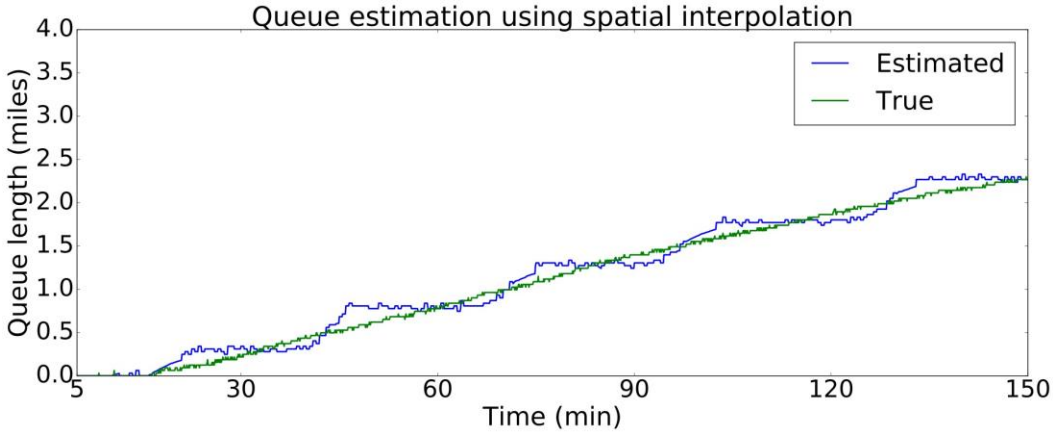

(a)

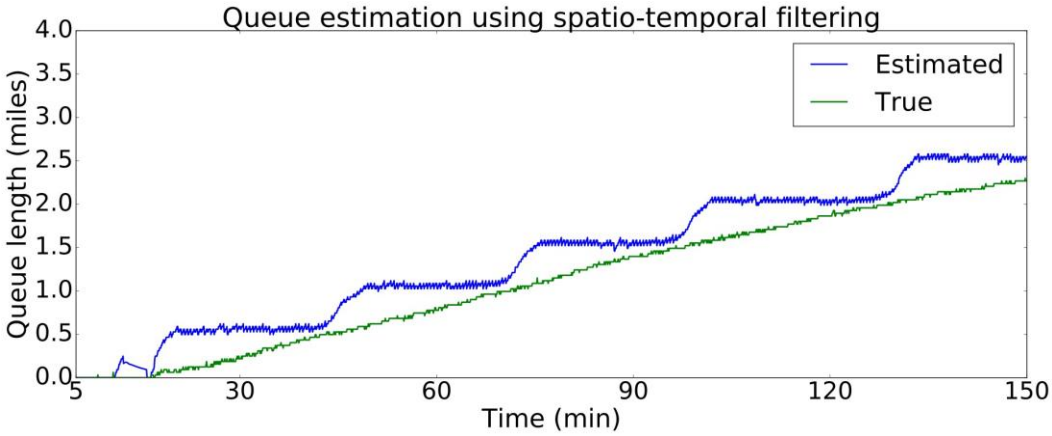

(b)

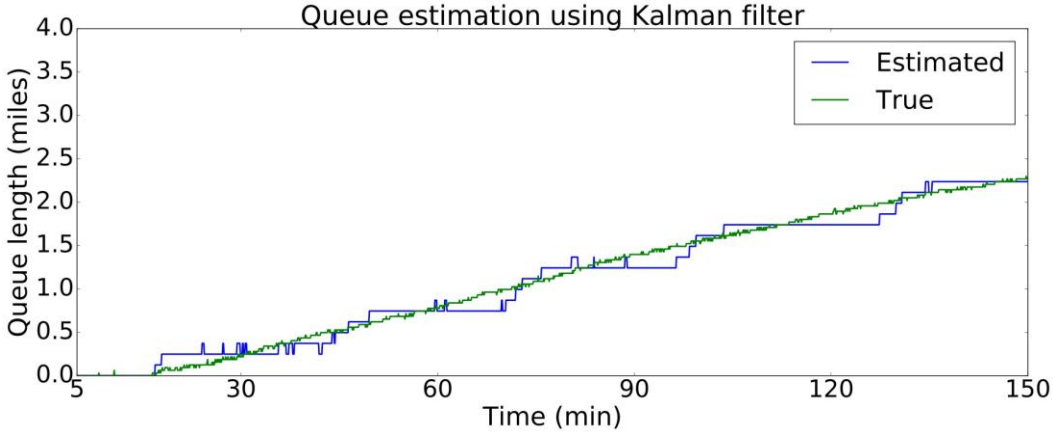

(c)

Figure D.27: An example of estimated queue length using (a) spatial interpolation, (b) spatio-temporal filtering, and (c) nonlinear Kalman filter, with RTMS at 0.5 mile spacing in I-57 work zone. The estimated and true queue lengths are plotted respectively in blue and green lines.

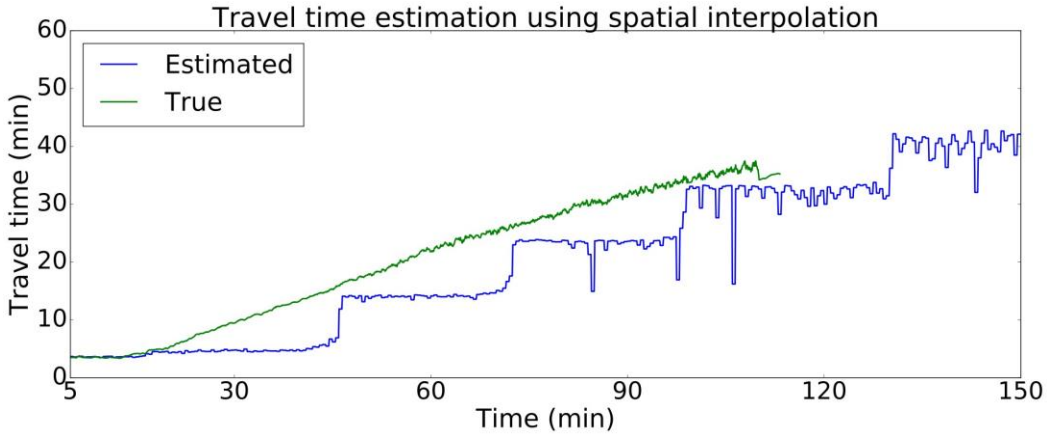

(a)

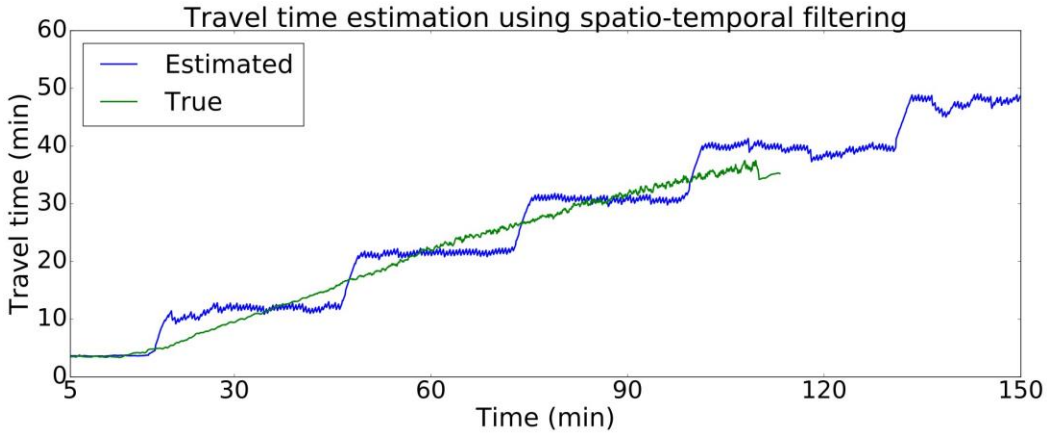

(b)

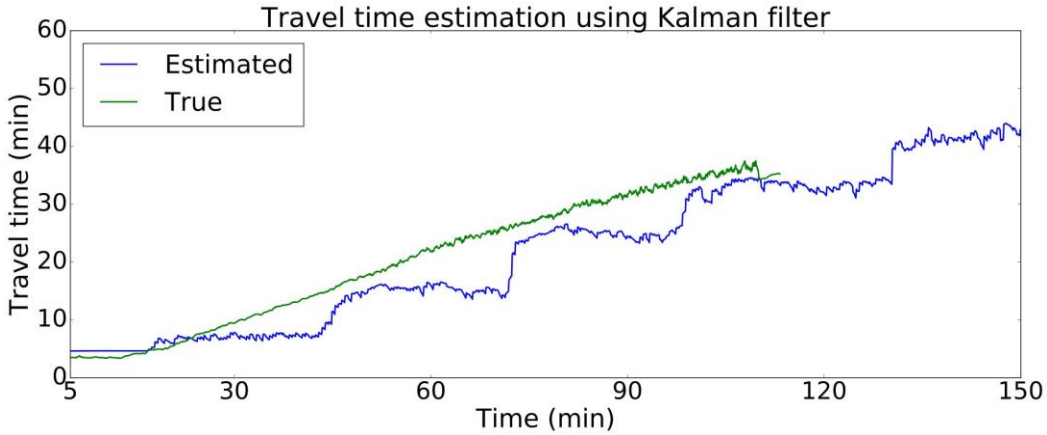

(c)

Figure D.28: An example of estimated travel time using (a) spatial interpolation, (b) spatio-temporal filtering, and (c) nonlinear Kalman filter, with RTMS at 0.5 mile spacing in the I-57 work zone. The estimated and true travel times are plotted respectively in blue and green lines.

D.2.1 Algorithms and Sensor Spacing

The algorithms and spacing were evaluated in three scenarios in the I-57 work zone, respectively using RTMS, radar, and LER. The findings in I-80 work zone were confirmed.

RTMS

The estimation results when using RTMS at different combinations of algorithms and spacings in I-57 are summarized in Figure D.29, Figure D.30, Figure D.31, and Figure D.32. The velocity estimation error for the nonlinear Kalman filter was significantly higher than using other algorithms for most of the spacings. The main reason was the large estimation error in the free-flow area as illustrated in Figure D.25a. Due to the inaccurate fundamental diagram calibrated for the I-57, the nonlinear Kalman filter showed less advantages on the estimation accuracy compared to other algorithms.

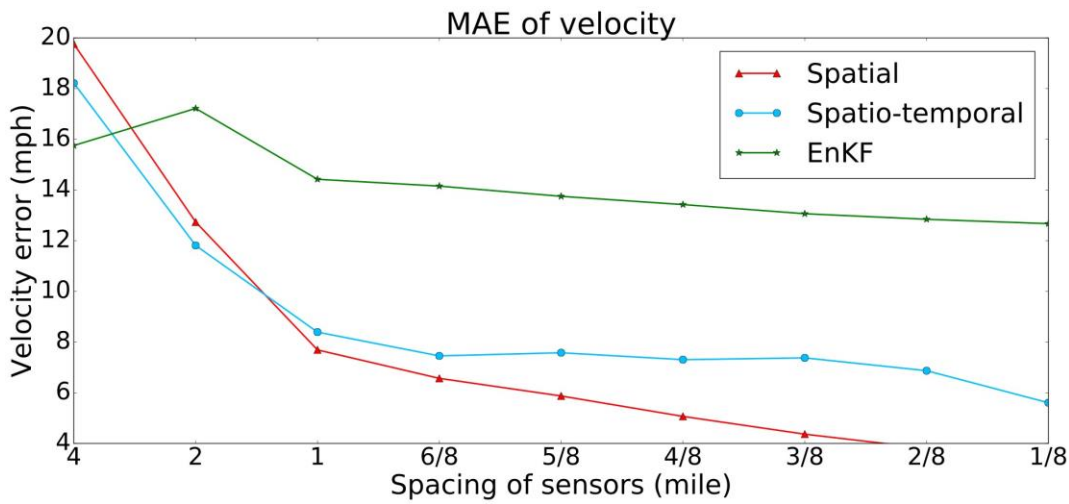

Figure D.29: MAE of the velocity field over the entire spatio-temporal domain using RTMS across a range of spacings in the I-57 work zone.

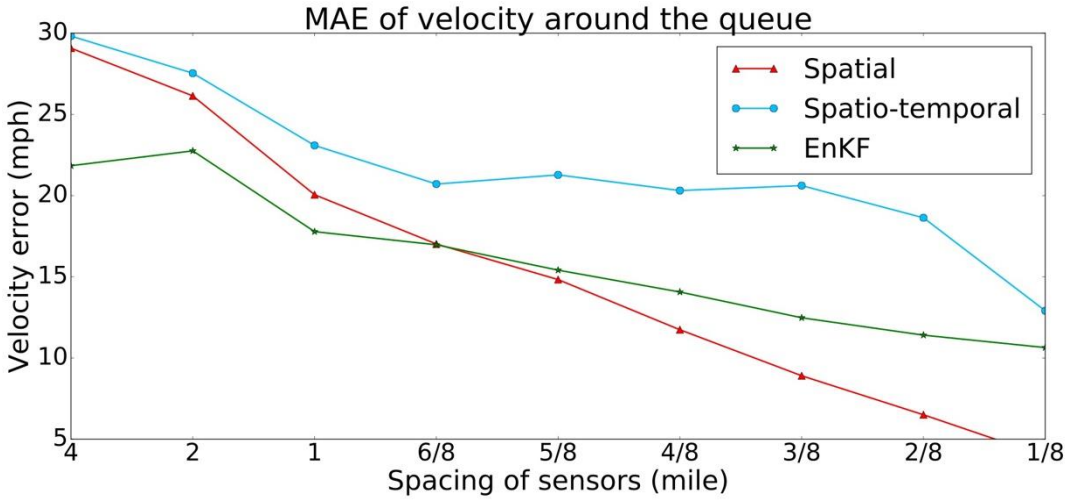

Figure D.30: MAE of the velocity field ± 0.5 mile around the queue using RTMS across a range of spacings in I-57 work zone.

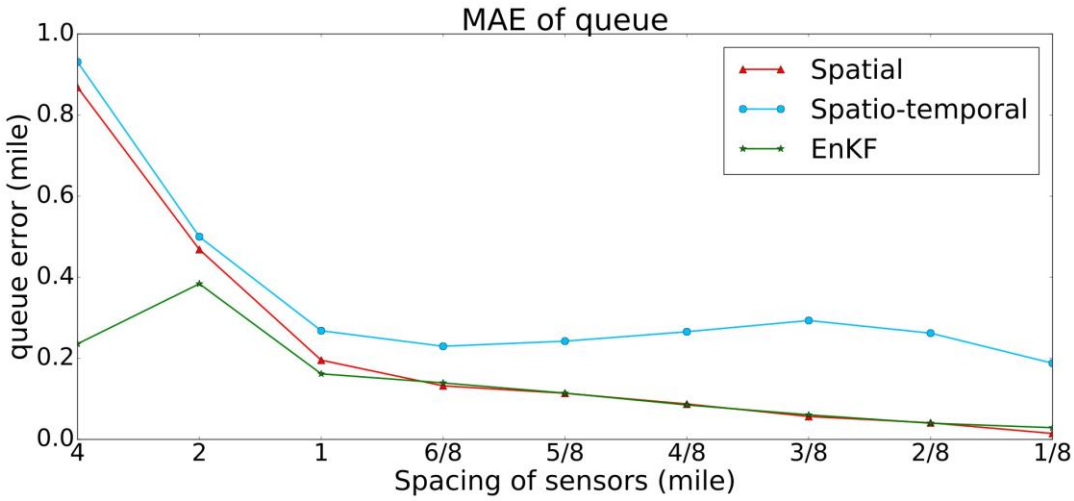

Figure D.31: MAE of the queue length using RTMS across a range of spacings in I-57 work zone.

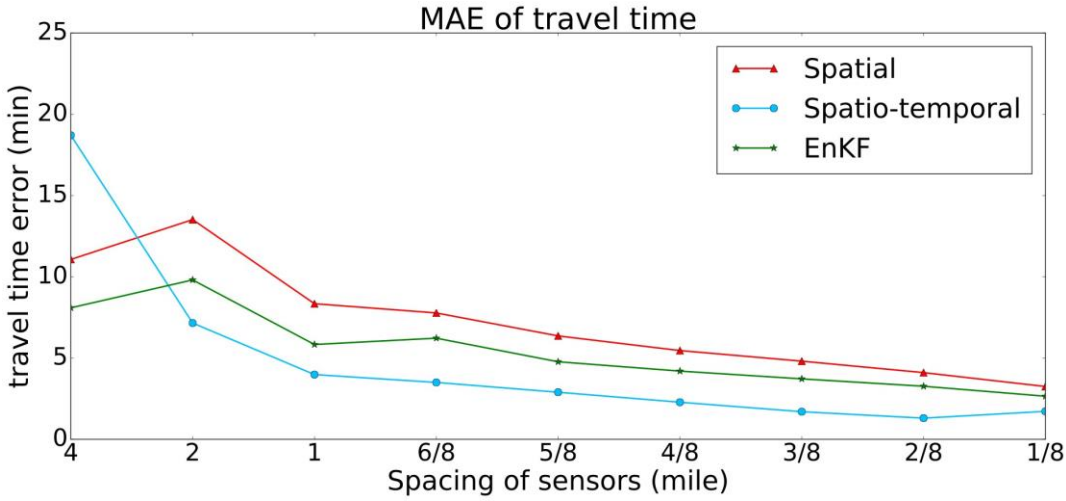

Figure D.32: MAE of the travel time using RTMS across a range of spacings in I-57 work zone.

Radar Sensors

The estimation results when using radar sensors at different combinations of algorithms and spacings in I-57 are visualized in Figure D.33, Figure D.34, Figure D.35, and Figure D.36. The findings were similar to the RTMS scenarios.

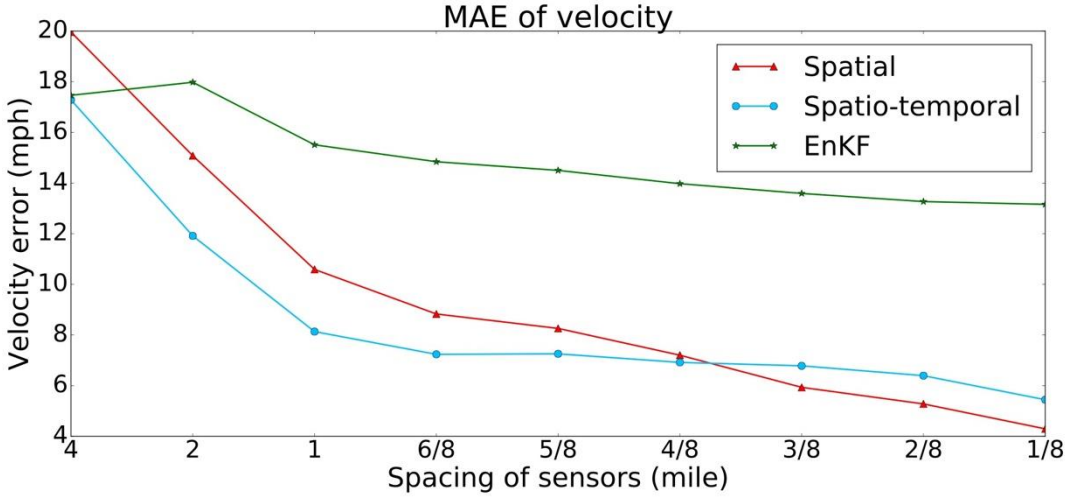

Figure D.33: MAE of the velocity field over the entire spatio-temporal domain using radar sensors across a range of spacings in the I-57 work zone.

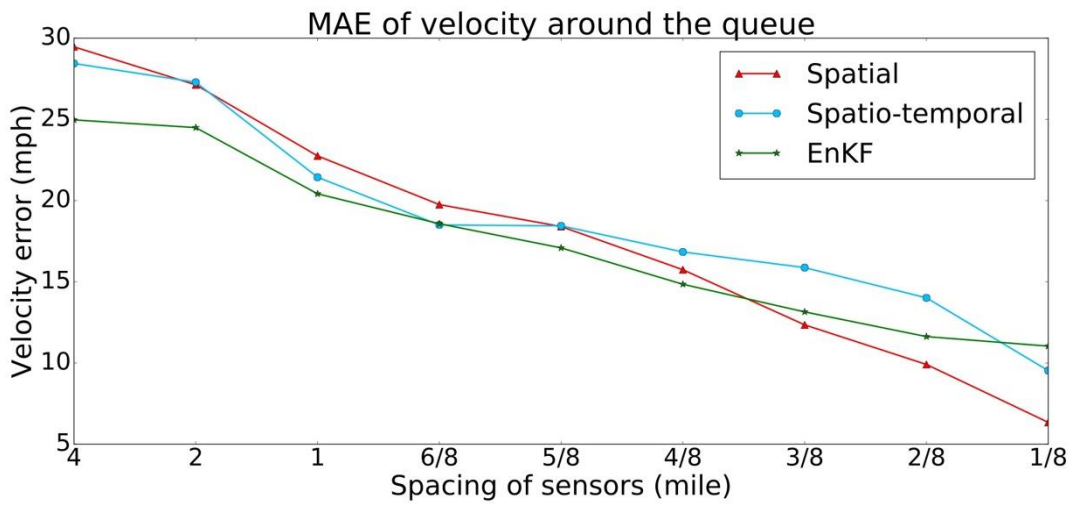

Figure D.34: MAE of the velocity field ± 0.5 mile around the queue using radar sensors across a range of spacings in the I-57 work zone.

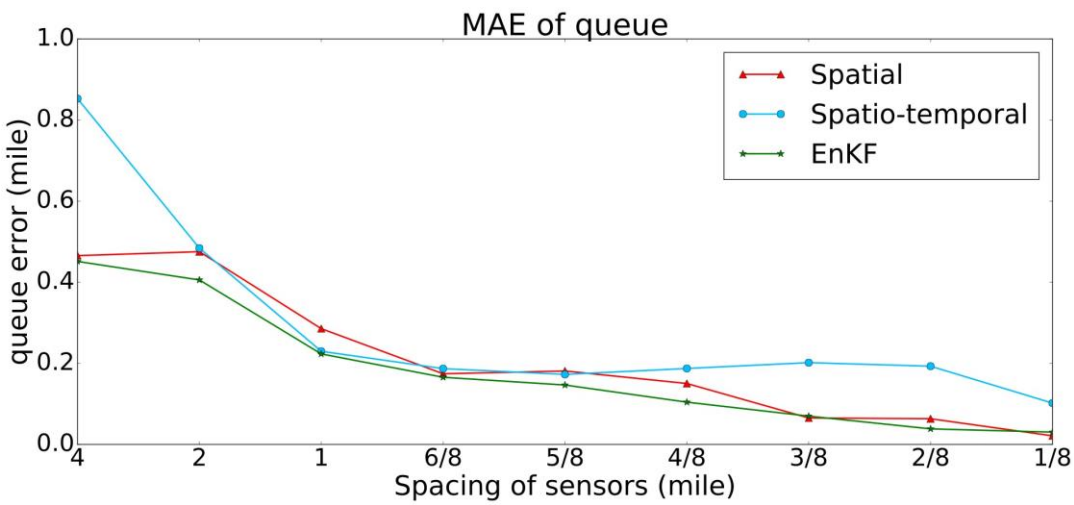

Figure D.35: MAE of the queue length using radar sensors across a range of spacings in the I-57 work zone.

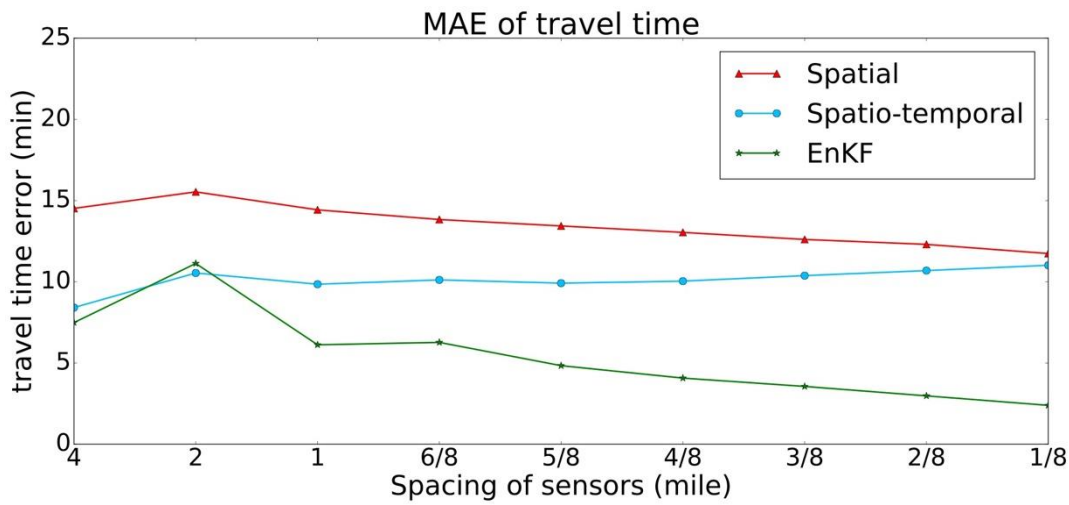

Figure D.36: MAE of the travel time using radar sensors across a range of spacings in the I-57 work zone.

LER Sensors

The estimation results when using LER sensors at different combinations of algorithms and spacings in the I-57 work zone are visualized in Figure D.37, Figure D.38, Figure D.39, and Figure D.40. The increased flow measurement error from LER sensors further degraded the performance of the nonlinear Kalman filter algorithm.

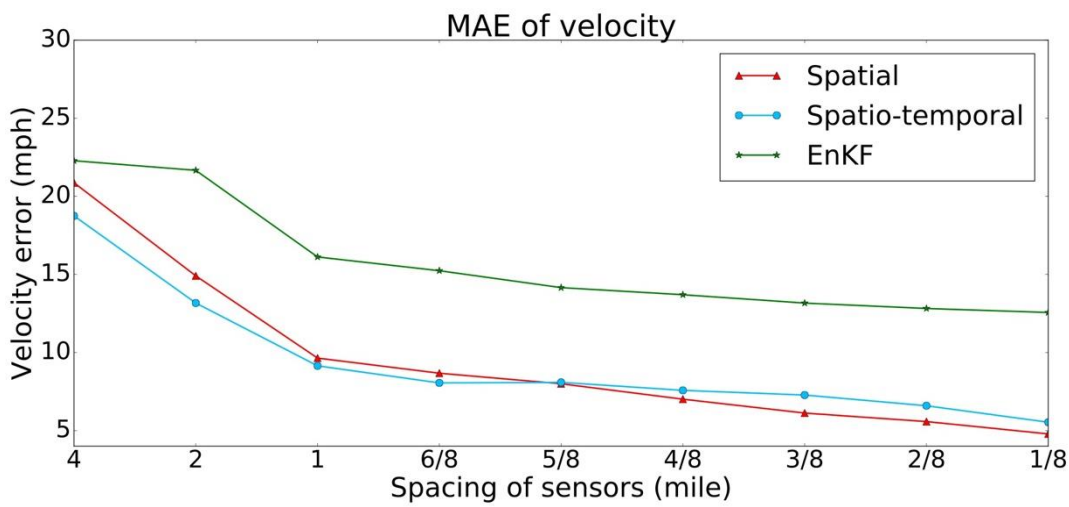

Figure D.37: MAE of the velocity field over the entire spatio-temporal domain using LER sensors across a range of spacings in the I-57 work zone.

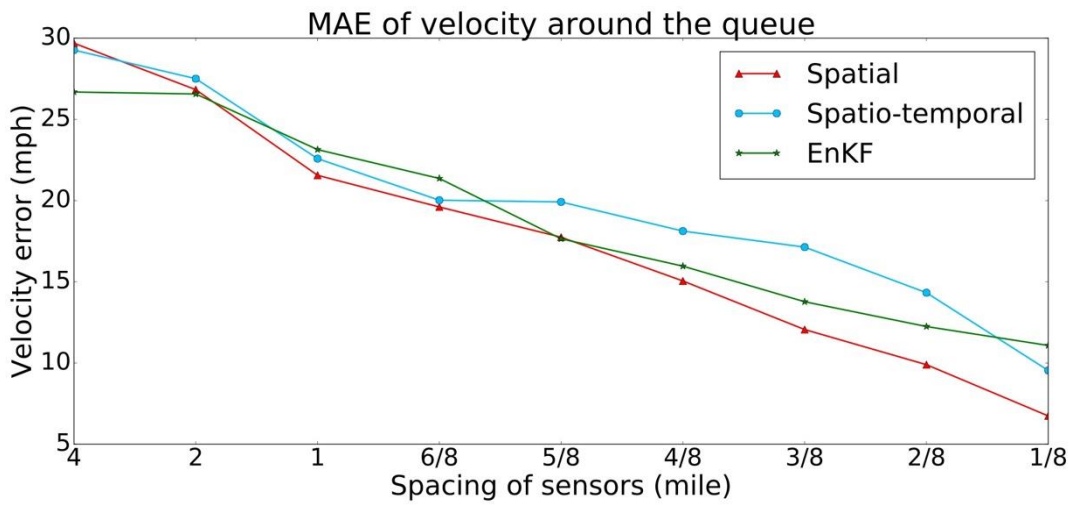

Figure D.38: MAE of the velocity field ± 0.5 mile around the queue using LER sensors across a range of spacings in the I-57 work zone.

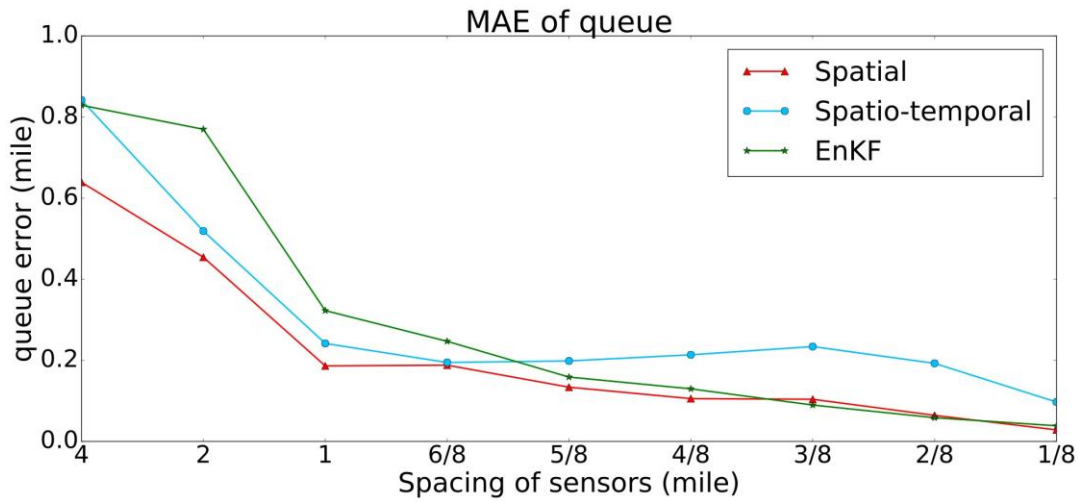

Figure D.39: MAE of the queue length using LER sensors across a range of spacings in the I-57 work zone.

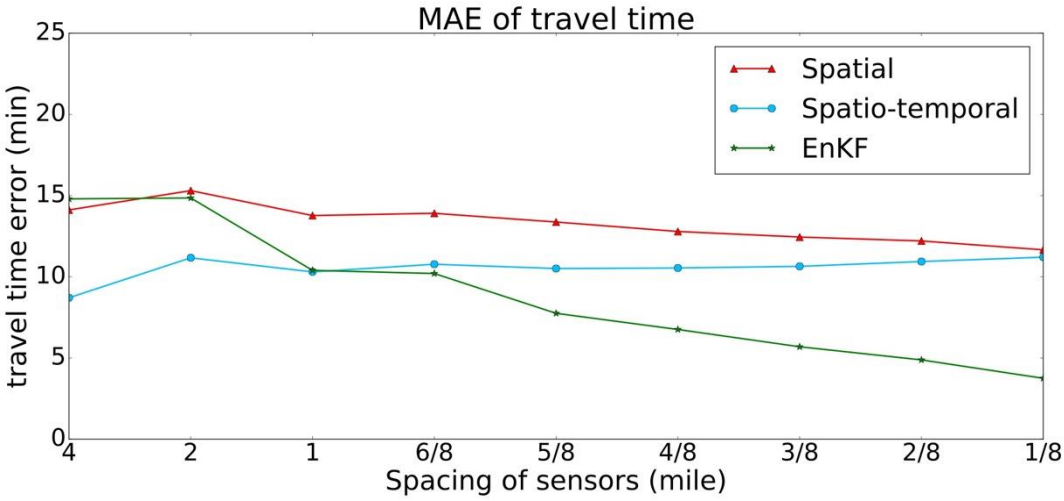

Figure D.40: MAE of the travel time using LER sensors across a range of spacings in the I-57 work zone.

D.2.2 Type of Sensors

This subsection presents two scenarios where the influence of the type of sensors was evaluated, respectively at 0.5 mile spacing (Figure D.41) and at 1 mile spacing (Figure D.42).

At 0.5 Mile Spacing

The evaluation result is shown in Figure D.41. The findings from I-80 were confirmed.

At 1 Mile Spacing

The evaluation result is shown in Figure D.42. The findings from I-80 were confirmed.

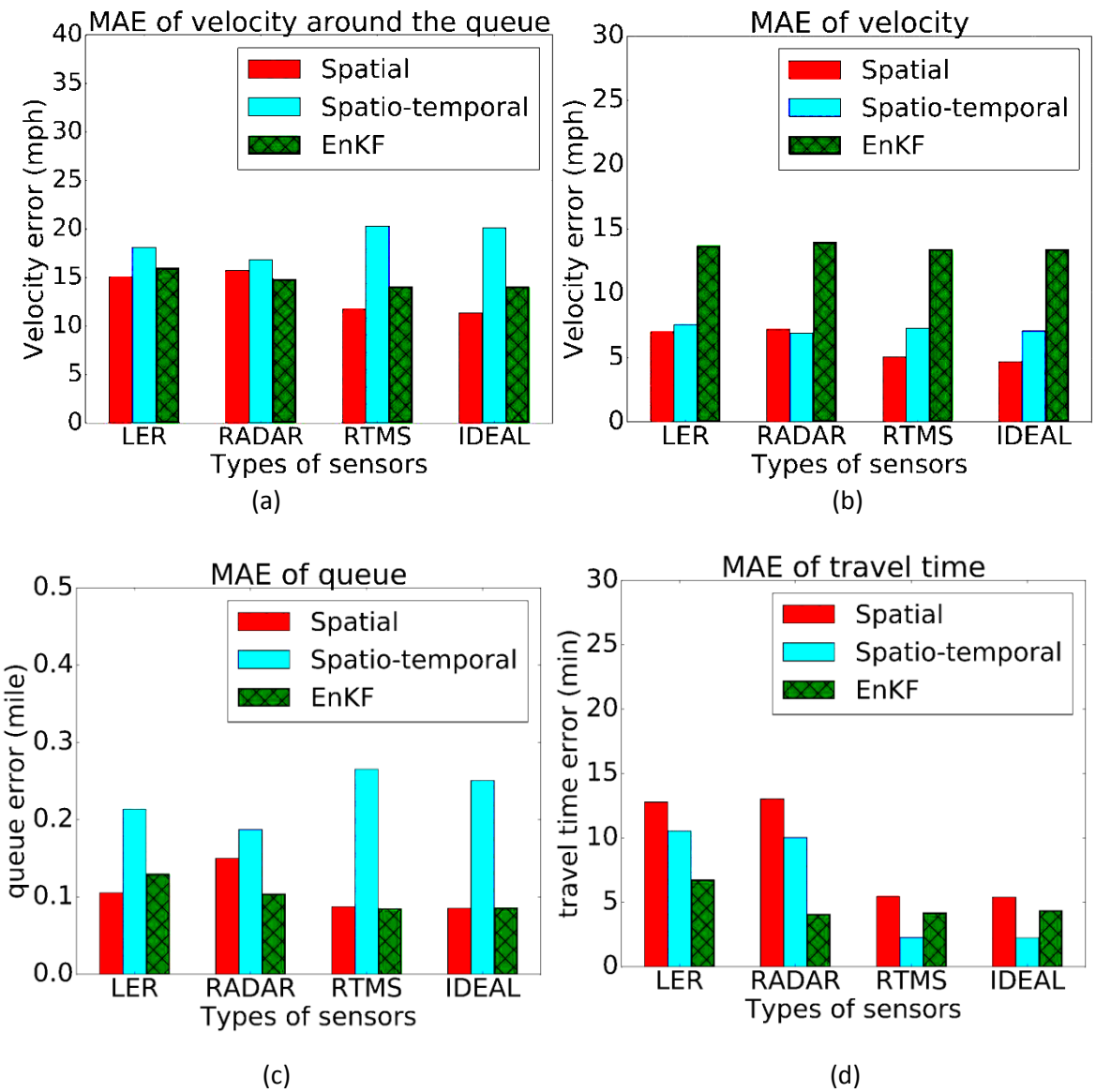

Figure D.41: MAE of the (a) velocity estimation over the entire spatio-temporal domain, (b) velocity estimation at ± 0.5 mile around the queue, (c) queue length estimation, and (d) travel time estimation using different types of sensors at 0.5 mile spacing in I-57 work zone.

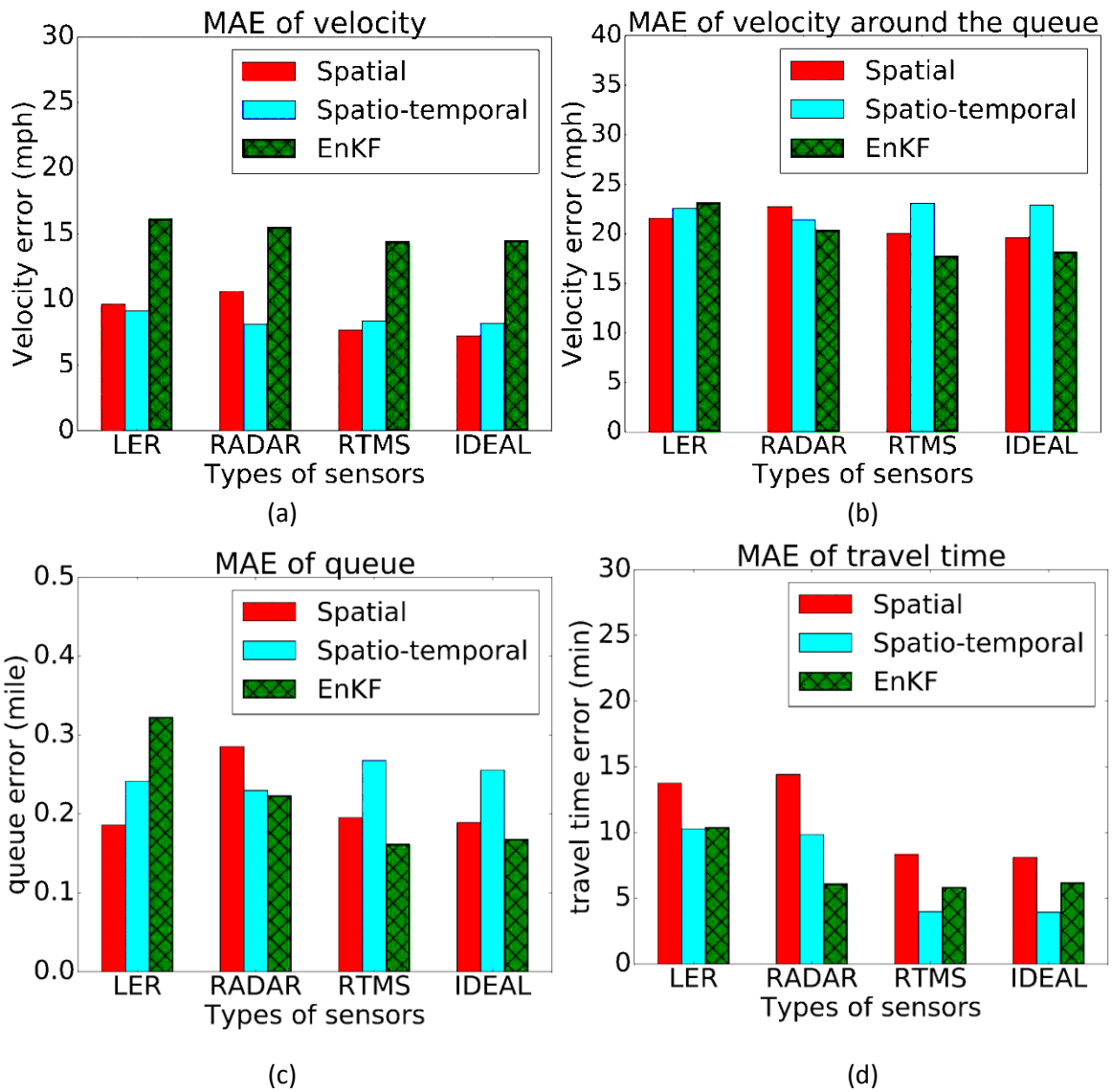

Figure D.42: MAE of the (a) velocity estimation over the entire spatio-temporal domain, (b) velocity estimation at ± 0.5 mile around the queue, (c) queue length estimation, and (d) travel time estimation using different types of sensors at 1 mile spacing in I-57 work zone.

D.2.3 Accuracy of Sensors

The subsection summarizes how the accuracy of individual sensors influences the estimation accuracy in the I-57 work zone. In this experiment, all sensors were assumed to have been properly calibrated to remove the measurement bias of individual vehicles and achieve the advertised accuracy in the product specification. In this analysis, RTMS with different levels of accuracy were placed at 1 mile spacing.

The evaluation result is shown in Figure D.43. The same finding in I-80 was confirmed (i.e., improvement of the accuracy of radar sensors would provide negligible benefits).

D.2.4 Cost Accuracy Analysis

Please refer to Section 5.5 for the methodology of the cost accuracy analysis. The cost accuracy analysis for the I-57 work zone is plotted in Figure D.44, Figure D.45, Figure D.46, and Figure D.47. Due to the inaccurate fundamental diagram calibration, the nonlinear Kalman filter did not show compelling evidence to be more cost effective compared to the simple spatial interpolation algorithm.

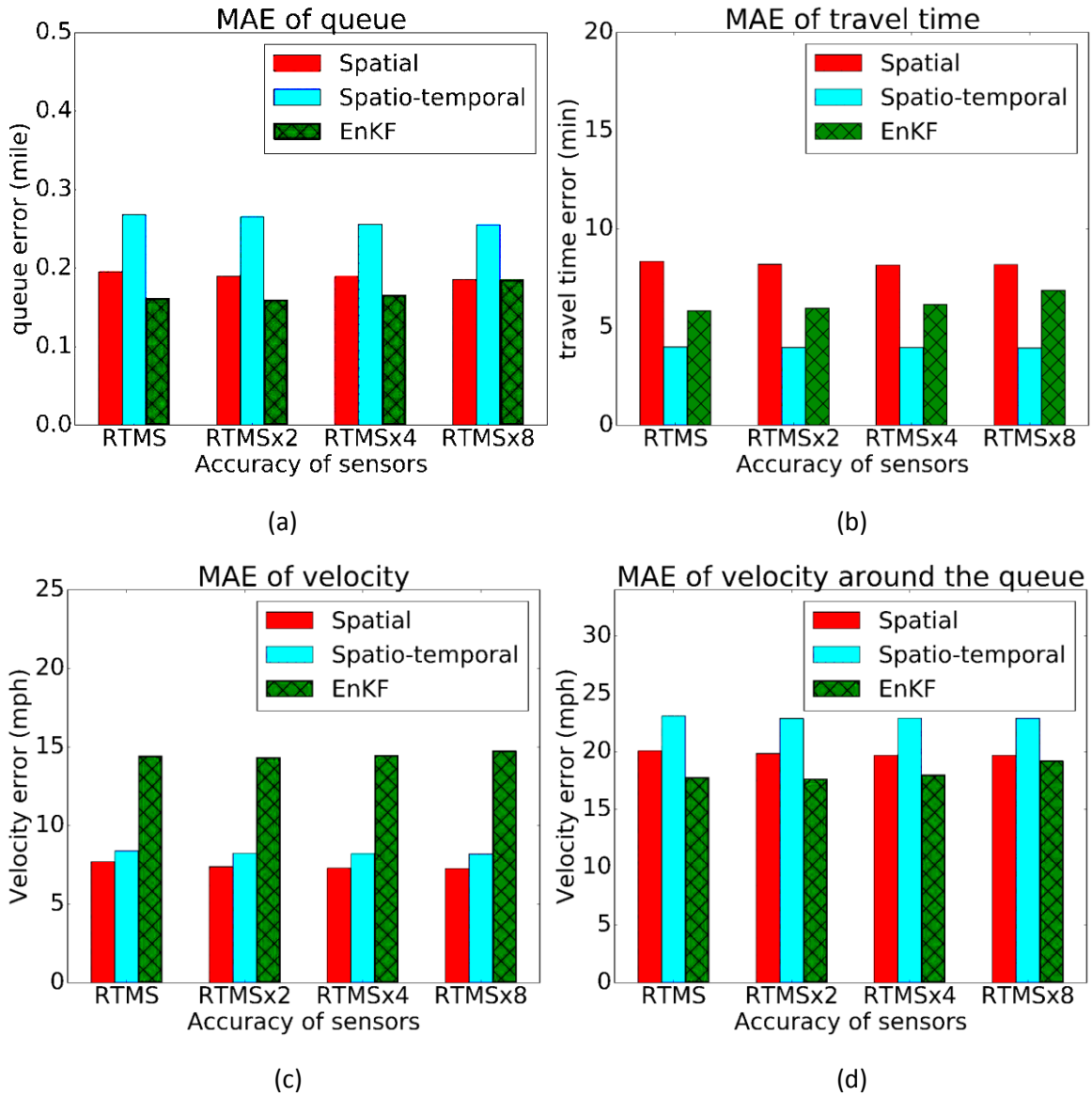

Figure D.43: MAE of the (a) velocity estimation over the entire spatio-temporal domain, (b) velocity estimation at ± 0.5 mile around the queue, (c) queue length estimation, and (d) travel time estimation using RTMS with different levels of accuracy at 1 mile spacing in the I-57 work zone.

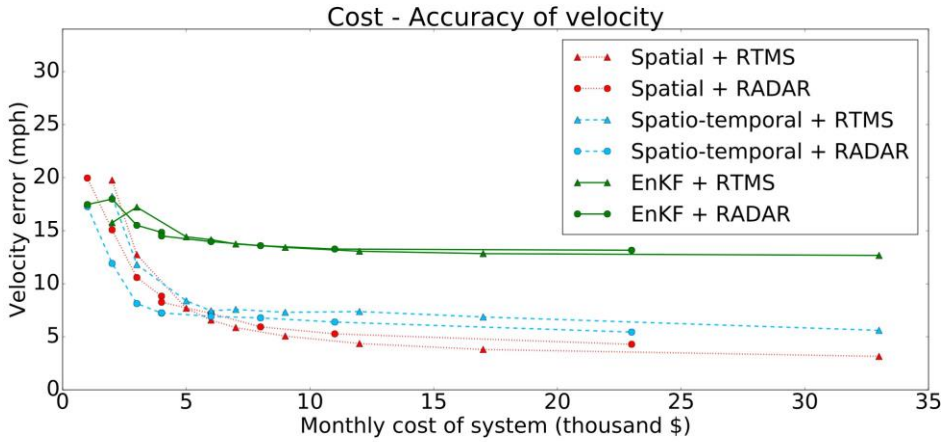

Figure D.44: Cost accuracy for the velocity estimation over the entire spatio-temporal domain in the I-57 work zone.

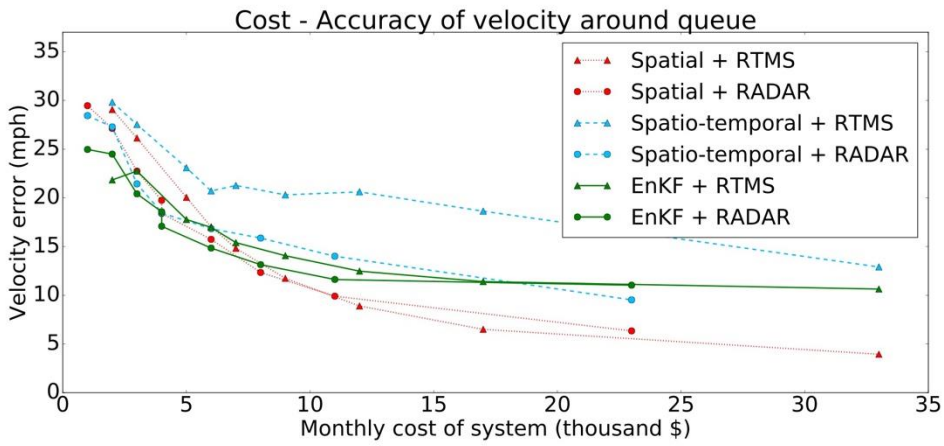

Figure D.45: Cost accuracy for the velocity estimation ± 0.5 mile around the queue in the I-57 work zone.

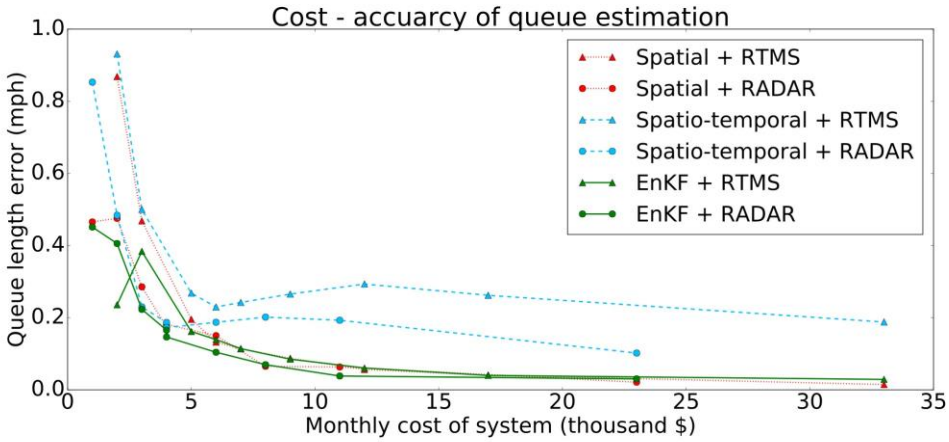

Figure D.46: Cost accuracy for the queue length estimation in the I-57 work zone.

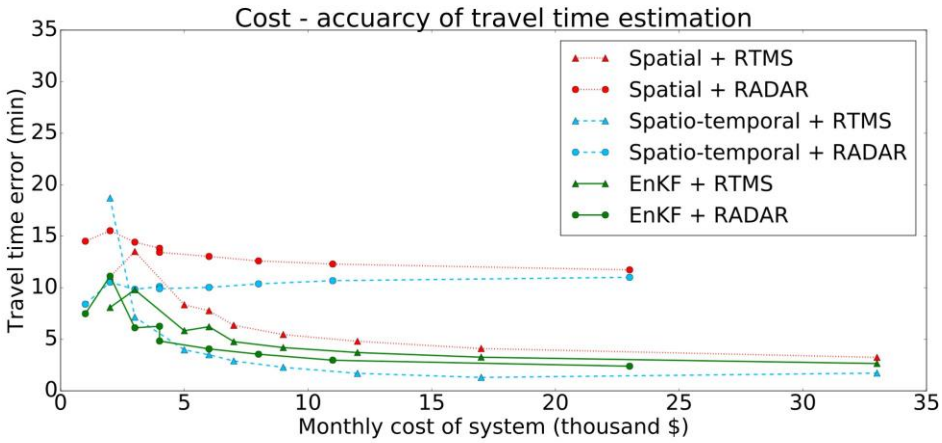

Figure D.47: Cost accuracy for the travel time estimation in the I-57 work zone.

Illinois Department of Transportation

ILLINOIS
UNIVERSITY OF ILLINOIS AT URBANA-CHAMPAIGN